NOVEL ROLES OF THE CILIARY GENES, *THM1* AND *THM2,* IN ADIPOGENESIS, SKELETAL DEVELOPMENT, AND SPERMATOGENESIS

By
© 2017
Bailey Ann Allard
M.A. Teaching, Learning and Teacher Education, University of Nebraska at Lincoln, 2011
B.S. Biology, Nebraska Wesleyan University, 2010

Submitted to the graduate degree program in Anatomy and Cell Biology and the Graduate Faculty of the University of Kansas in partial fulfillment of the requirements for the degree of Doctor of Philosophy.

_____
Chair: Dr. Pamela Tran

_____
Dr. James Calvet

_____
Dr. Dianne Durham

_____
Dr. Xiaogang Li

_____
Dr. Irfan Saadi

Date Defended: April 14, 2017

The dissertation committee for Bailey Ann Allard
certifies that this is the approved version of the following dissertation:

NOVEL ROLES OF THE CILIARY GENES, *THM1* AND *THM2,* IN ADIPOGENESIS, SKELETAL DEVELOPMENT, AND SPERMATOGENESIS

_____

Chair: Dr. Pamela Tran

Date Approved: May 8, 2017

Abstract

Primary cilia are non-motile sensory organelles, which extend from the surface of most vertebrate cells. Mutations in ciliary genes result in a group of pleiotropic disorders termed ciliopathies, which can manifest obesity, skeletal abnormalities, and infertility. Previously, we identified THM1 as an intraflagellar transport Complex A protein essential for embryogenesis and post-natal tissue development and homeostasis. Here, we investigate novel roles for *Thm1* and its uncharacterized paralog, *Thm2*. shRNA-mediated *Thm1* knockdown in 3T3-L1 mouse pre-adipocytes reveals *Thm1* deficiency increases adipogenesis and insulin sensitivity, providing an additional mechanism underlying *Thm1*-deficient obesity. Like THM1, THM2 localizes punctately along the ciliary axoneme, establishing THM2 as a ciliary protein. To determine a role for THM2, we generated two *Thm2*-null mouse lines - one using a construct from the knockout mouse project (KOMP) consortium, which has been backcrossed 5 generations onto a C57BL6/J background, and the other, using CRISPR/Cas9 genome editing which has been maintained on a mixed FVB/C57BL6/J background. Unexpectedly, *Thm2*-null mice on both backgrounds survive into adulthood with seemingly normal health. However, *Thm2* deletion with an additional loss of one *Thm1* allele on a C57BL6/J background at the 5th generation causes skeletal defects resulting in markedly smaller mice by post-natal day 14. On a mixed FVB/C57BL6/J background, $Thm2^{-/-}$; $Thm1^{aln/+}$ male mice appear healthy, but show a 44% decrease in fertility, accompanied by low sperm count, abnormal sperm flagella and sperm motility, and abnormal testis morphology, indicating defects in early sperm development. Thus, our studies establish novel roles for *Thm1* and *Thm2* in adipogenesis, skeletal development, and spermatogenesis and provide novel models to study molecular mechanisms underlying ciliopathies. These studies also establish functional interactions between *Thm1* and *Thm2*.

Acknowledgements

When I decided to continue my education at the University of Kansas Medical Center, I could not have imagined the immense support, encouragement, and friendship I would be lucky enough to find. For this, I have many individuals to thank.

To my friends – Thank you for your constant support and encouragement. Whether I have known you for as long as ten years, or as little as two, you have all made an invaluable impact on my life. The phone calls, weekend visits, and lunchtime discussions are just some of the things that made my graduate experience so enjoyable. My journey would not be as complete or, most importantly, nearly as fun without each and every one of you.

To my committee members – Dr. James Calvet, Dr. Dianne Durham, Dr. Xiaogang Li, Dr. Pamela Tran and Dr. Irfan Saadi, thank you for the valuable insights and time spent driving my project forward. Your guidance, support, and enthusiasm kept me going throughout the past four years. I appreciate not only the work you have put into my project, but also the work you have put into developing me as a scientist – it is this aspect that I am most grateful. Your dedication to students and your profession is something I hope to carry forward in my career.

To our collaborators – Dr. Jinxi Wang, Dr. Gustavo Blanco, Dr. Gladis Sanchez, and Dr. Jay Vivian, thank you for your guidance on the *Thm2* project. When we first made the *Thm2* mouse, I can confidently say neither Pam nor myself could have imagined the unexpected directions it would take us. Thank you for contributing your time to provide valuable insight and help with experiments to move the project forward. It has truly been a joy to have had the opportunity to work with all of you, thank you for your support.

To the members of the Anatomy and Cell Biology Department and Kidney Institute – Thank you for your constant support of graduate students. In particular, thank you to the

Anatomy and Cell Biology Department graduate education directors, previously Dr. Peggy Petroff and currently Dr. Julie Christianson. Both of you have been essential to my growth as a graduate student. Whether it was helping me find opportunities to teach on campus after you discovered my interest in education, or ensuring I was making adequate progress towards my degree, you both have made my time at the University of Kansas Medical Center rewarding and enjoyable.

To my lab friends – It has been a privilege to work alongside each of you for the past four years. You are all so much more than co-workers, you are my friends and supporters. Wei – as the newest graduate student in the lab, I am excited to hand over the *Thm2* project to you. Your positivity, critical thinking, and hard work are just what this project needs to keep it moving forward. Damon – whether it was helping me with an experiment, troubleshooting, or reassuring me that *Thm2* really did have a role, thank you for your support. Luci – My graduate student partner and friend, thank you for the early morning talks we often had to critically think about our projects. You were always there to offer suggestions, a helping hand, or simply to listen, thank you for your support and friendship. I can confidently say I am a better person because of each of you. You were all such an integral part of my life, and I could not be more thankful to have had (and hopefully continue to have) all of you in it.

To my mentor and friend, Dr. Pamela Tran – I am not sure where to begin when thanking you for all you have done. Not only did you take the time to teach me the techniques needed to succeed, you taught me to critically think about results and experiments – an invaluable skill that has transformed me into a budding new scientist. You have become more than a mentor to me, you have become a friend. Thank you for the countless hours you helped me with my project and

for the constant support. Most importantly, thank you for all of the smiles and laughter shared along the way.

To my family, Mom (Kay), Dad (Floyd), Sister (Sarah) and Brother-in-law (Adam) - Thank you for cultivating my curiosity and encouraging me to always follow my dreams. From a young age, you taught me the value of kindness, hard work, and dedication, all which have been invaluable during my graduate school career. Although you did not always understand why I was happy, excited, or confused about an experiment, you always supported me, reassured me things would work out, and told me how proud you were. I am so lucky to have you as family, thank you from the bottom of my heart.

Finally, to my husband, Corey –Thank you for believing in me, often times, more than I believed in myself. Even while in medical school and residency, you always found time to listen to detailed explanations of experiments, results, and further questions regarding my projects. You willingly and, at times, unwillingly I would guess, watched all of my seminars before I presented them and assured me my projects would work out with enough hard work and dedication. You always celebrated with me in my successes, encouraged me through the setbacks, and ultimately, supported me every step of the way. For that, I am forever grateful.

Table of Contents

Chapter One: Introduction

1.1 Primary Cilia Structure

Cilia and flagella are evolutionarily conserved organelles found in nearly all eukaryotic organisms ranging from the unicellular alga, *Chlamydomonas reinhardtii* and single-celled protozoan, *Tetetrahymena thermophila,* to complex, multicellular vertebrates such as humans[1]. Two different types of cilia have been characterized based on their microtubule structure: motile cilia and sensory (primary) cilia[2]. Our studies focus on non-motile primary cilia, whose presence was first documented in multiple tissues by Zimmerman, over a century ago, in 1898[3]. Primary cilia appear as antenna-like appendages extending from the surface of nearly all cell types[4]. For more than 100 years after their discovery, these structures were thought to be vestigial organelles[4]. However, in the early 2000's, evidence accumulated revealing that primary cilia are essential for the proper development and function of many tissue types[5].

Primary cilia are found at the apical surface of vertebrate cells and begin assembly during the G0/G1 stage of the cell cycle, when cells become quiescent[6]. The assembly of the primary cilium is highly controlled, creating a complex structure with three major compartments: the basal body, the transition zone, and the axoneme (Figure 1.1)[5]. When cells enter G0/G1, the mother centriole matures and differentiates into the basal body of the primary cilium, attaching to the apical plasma membrane through distal and subdistal appendages[5]. The basal body functions as the microtubule-organizing center (MTOC)[2], which serves as the microtubule nucleation site during the construction of the ciliary axoneme[6]. Located at the basal body is a subset of ciliary proteins including BBS1, BBS2, BBS4, BBS5, BBS7, BBS8, BBS10, and BBIP10 that comprise a complex known as the BBsome[7]. Although generally not required for cilia formation[6], the BBsome is thought to function in trafficking vesicles and signaling molecules to the cilium[7] and is essential for human health[8].

Positioned adjacent to the basal body is the second compartment of the primary cilium, the transition zone[5]. A characteristic of the transition zone is the presence of Y-shaped links. These links connect the microtubules of the axoneme to the ciliary membrane[9]. This region is responsible for regulating protein trafficking into and out of the primary cilium thereby acting as a barrier and gate between the cytoplasm and cilium[10]. The "ciliary gate" is comprised of the transition zone and the transition fibers of the basal body, and establishes and maintains the unique protein composition of the cilium[5]. The transition fibers are thought to form a ciliary pore complex that functions similarly to the nuclear pore complex[5], regulating the entry and exit of proteins into and out of the primary cilium. Recent studies in *Chlamydomonas reinhardtii* have proposed that the ciliary necklace, a structure found within the transition zone, may participate in the active transport of certain proteins into the cilium[10]. Proteins localizing to the transition zone contribute different functions to the trafficking of select proteins into and out of the cilium[9], with defects leading to human disease[6].

The most distal region of the primary cilium consists of a microtubule-based ciliary axoneme that nucleates from the basal body in a 9+0 organization, making the primary cilium non-motile[5]. The axoneme is surrounded by a ciliary membrane which contains a distinct subset of signaling proteins and is attached to the plasma membrane[4]. The extension of the ciliary axoneme is dependent on intraflagellar transport (IFT) proteins and only occurs at the plus-end of the microtubules[11]. IFT proteins can be divided into two complexes: IFT Complex B and IFT Complex A. IFT Complex B proteins utilize the plus-end directed kinesin-2 motor to facilitate anterograde transport, moving cargo from the base to the tip of the primary cilium. The IFT B complex consists of 11 IFT proteins including IFT172, IFT88, IFT81, IFT80, IFT74, IFT57, IFT54, IFT52, IFT46, IFT27, and IFT20. IFT Complex A proteins utilize the minus-end directed

dynein motor and largely mediate retrograde transport, returning cargo from the tip to the base of the primary cilium. The IFT-A complex consists of 6 IFT proteins including IFT144, IFT140, IFT139, IFT122, IFTA-1, and IFT43[12]. IFT-A and IFT-B proteins form IFT trains, which transports cargo (structural and signaling proteins) throughout the primary cilium[8]. Cargo is thought to be loaded onto the IFT-B trains near the basal body and carried to the ciliary tip where it is released[8]. IFT-B components are then loaded onto IFT-A trains, and brought to the base of the primary cilium[8]. Aberrant trafficking leads to defects in cilia structure and signaling, affecting overall health[12,13]. In this dissertation, we focus on the roles of two ciliary genes, *Thm1 (Ttc21b)* and *Thm2 (Ttc21a)* in vertebrate cells and tissues.

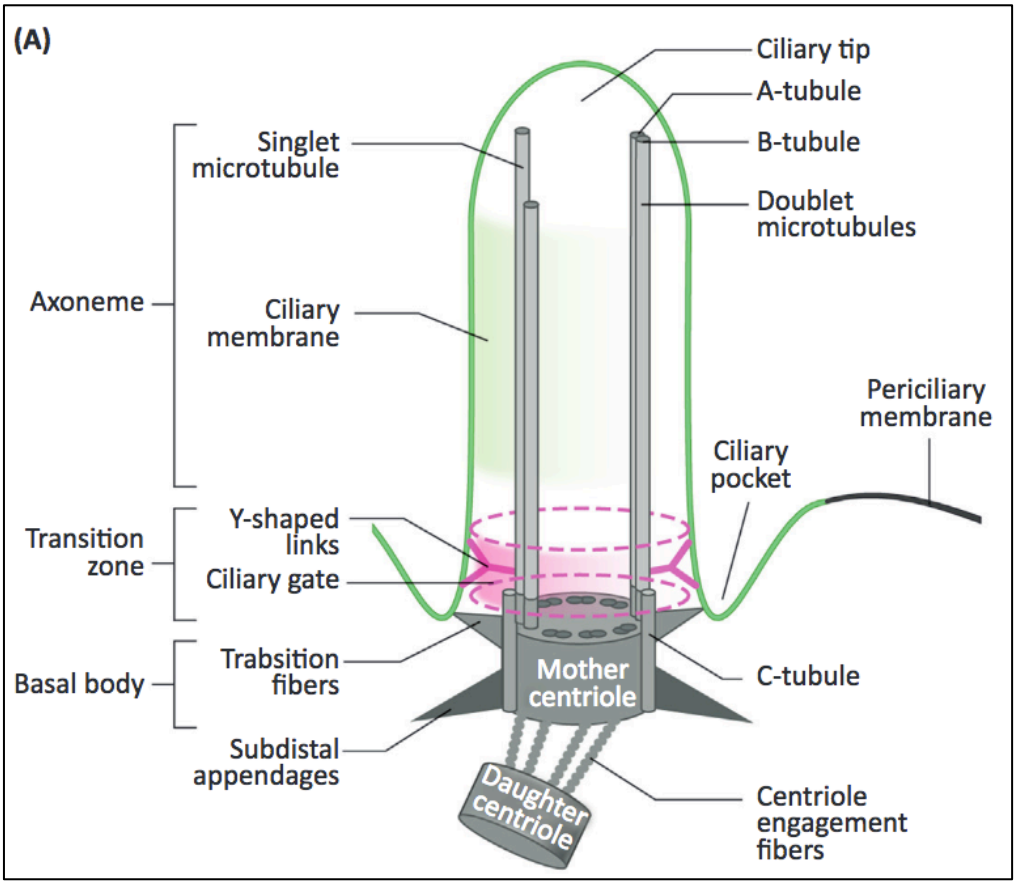

Figure 1.1. Primary Cilia Structure. Image (Schematic of Primary Cilia Structure) was originally published in Malicki, J.J. & Johnson, C.A. The Cilium: Cellular Antenna and Central Processing Unit. *Trends Cell Biol* (2016)[5], located at http://www.cell.com/trends/cell-biology/fulltext/S0962-8924(16)30104-0. Copyright 2016 The Authors. This article is licensed under the Creative Commons Attribution is an open access article under the CC BY license 4.0, http://creativecommons.org/licenses/by/4.0/. Diagram of the primary cilium extending from the surface of a cell. Three major regions are identified as the basal body, transition zone and axoneme and include associated structures. Ciliary membrane is highlighted in green with the cell membrane in black.

1.2 Primary Cilia Function

Primary cilia function as sensory organelles, which receive extracellular signals[5] and translate them into intracellular signals. The mammalian Hedgehog (Hh) signaling pathway is recognized as a cilia-dependent pathway important in development and tissue patterning[14]. Interestingly, the Hh signaling pathway was first identified in *Drosophila melanogaster*[15], in cells without primary cilia[14]. Although these findings suggest differences between *Drosophila* and mammalian Hh signaling, the pathways share several basic tenants. In both pathways, when the Hh ligand is absent, the transmembrane receptor Smoothened (SMO) is held in a repressed state by another transmembrane receptor, Patched (PTCH). Once the Hh ligand binds to PTCH, SMO inhibition is released and the Hh signal is transduced into the activation of transcription factors[14,15]. In *Drosophila,* SMO is released from cytoplasmic vesicles once the Hh ligand binds to PTCH. SMO is then phosphorylated and accumulates at the plasma membrane, which results in the activation of Cubitus interruptus (Ci), a transcription factor[15]. This activation is caused by a series of phosphorylation events which disassemble an inhibition complex, allowing Ci to be converted from its repressed form to its active form, which activates downstream target genes[15].

In the mammalian Hh signaling pathway, one of three Hh ligands, Sonic Hedgehog (SHH), Indian Hedgehog (IHH), or Desert Hedgehog (DHH), are able to bind to PTCH[14]. Each of the Hh genes are thought to play specific roles in different tissue types with *Shh* usually being associated with embryonic development and post-natal tissue homeostasis, *Ihh* with bone development and *Dhh* with spermatogenesis[15]. Once one of the Hh ligands binds to PTCH, which is located on the primary cilium, PTCH delocalizes from the primary cilium, releasing the inhibition of SMO. SMO then translocates to the primary cilium, a step which is associated with Hh pathway activation[14]. Once in the primary cilium, SMO activates GLI transcription factors,

GLI2 and GLI3, which translocate from the cilium to the nucleus to activate different Hh target genes, including *Gli1*[14] (Figure 1.2). Although both GLI2 and GLI3 can be processed to function as activators or repressors, GLI2 is primarily thought of as a positive regulator while GLI3 functions mainly as a repressor of the Hh pathway[14]. Experiments investigating GLI2 and GLI3 have shown their functional states are controlled by phosphorylation and dephosphorylation events at specific sites within the proteins[16]. Interestingly, the contribution of *Gli* transcription factors to Hh signaling differs in various tissue types[15]. Neural tube patterning is thought to be largely dependent on *Gli2*, with lesser involvement from *Gli1* and *Gli3*, while limb patterning is thought to be dependent on *Gli3*, with *Gli2* mutants exhibiting normal digit numbers[15]. Furthermore, all key components of mammalian Hh signaling are found in the primary cilium, underscoring the importance of the primary cilium in the regulation of the Hh signaling pathway[14].

Studies investigating roles for IFT proteins have revealed valuable insights into the functions of IFT trafficking in Hh signaling. Epistatic experiments have shown *Ift* genes function downstream of *Smo*, but upstream of *Gli* genes[15]. Analysis of neural tube patterning, a process dependent on a SHH gradient[15], revealed that mutations in both IFT- B and IFT-A proteins result in Hh signaling abnormalities. Null or severe mutations in IFT Complex B proteins such as IFT172[17], IFT88[17], IFT52[18], and IFT57[19] cause failure of primary cilium formation and decreased Hh signaling with a loss of caudal neural tube ventral markers[14], which are dependent on the highest levels of Hh ligand[20]. In contrast, mutations in IFT Complex A proteins, such as THM1[20] and IFT122[21], cause shortened cilia with an accumulation of proteins in a swollen, bulb-like distal tip, and upregulation of Hh signaling, with expansion of ventral-specific markers in the caudal neural tube[14]. However, differences in the roles of IFT-A proteins in trafficking Hh

signaling components into the primary cilium have recently been discovered. Although SMO localized to the primary cilium in THM1 null nodal cilia[20], deficiency of another IFT Complex A protein, IFT121, in retinal pigment epithelial 1 (RPE) cells caused a significant decrease in SMO ciliary localization, even when treated with a Hh pathway activator[22]. Similarly, treatment of IFT144-null mouse embryonic fibroblasts (MEFs) with a Hh pathway activator, did not result in SMO localization to the primary cilia[23]. In an IFT144 hypomorphic model, SMO localized to the primary cilium[23]. These differing results indicate that certain IFT Complex A proteins can regulate entry of signaling proteins or membrane receptors into the primary cilium, and that the roles of IFT proteins individually, and as a complex, in Hh signaling are still not completely understood.

In contrast to the widely accepted evidence linking Hh signaling to the primary cilium, associations between primary cilia and the Wnt signaling pathway are still debated due to conflicting experimental results[12]. In canonical Wnt signaling, β-catenin is phosphorylated and held in an inhibition complex in the absence of Wnt ligand[24]. In response to ligand stimulus, the inhibition complex is demolished, allowing β-catenin to travel to the nucleus and activate β-catenin-TCF responsive elements, activating the Wnt signaling pathway[24]. Evidence supporting a role for ciliary proteins in Wnt signaling has been found both *in vitro* and *in vivo*. *BBS4*, *BBS1, MKKS,* and *KIF3A* knockdown in human epithelial kidney (HEK) 293T cell lines[24], and mouse embryonic fibroblasts (MEF) derived from *Kif3a*$^{-/-}$ [25], *IFT88*$^{orpk/orpk}$ [25] and *Thm1*$^{aln/aln}$ [26] embryos harboring a Bat-gal Wnt reporter showed an increase in Wnt signaling when treated with WNT3a ligand compared to a control cell line[24-26]. Additionally, conditional deletion *of Ift20* in the kidney collecting ducts of mice resulted in cystic kidneys, and Western blot analysis revealed an increase in the active nuclear β-catenin levels in cystic kidneys, at p (post-natal day) 31[27].

Transcriptional analysis of downstream Wnt target genes revealed an increase in *Myc, Jun, Tcf3, Tcf7*, and *Wisp1* in *Ift20* conditional knockout mouse kidneys[27]. Conversely, extensive analysis of *Kif3a, IFT88, Dync2h1,* and *Thm1* mutant embryos *in vivo* revealed normal amounts of Wnt activity when compared to control littermates[28,29]. Supporting this observation, mouse embryonic IFT mutants do not show abnormalities associated with Wnt signaling such as gastrulation and axis duplications[12]. Taken together, these results suggest cilia are likely not necessary for Wnt signaling during the early stages of embryogenesis[12], but may facilitate Wnt signaling later in life, or in certain tissue types. Future studies are needed to examine the links between Wnt signaling and the primary cilium.

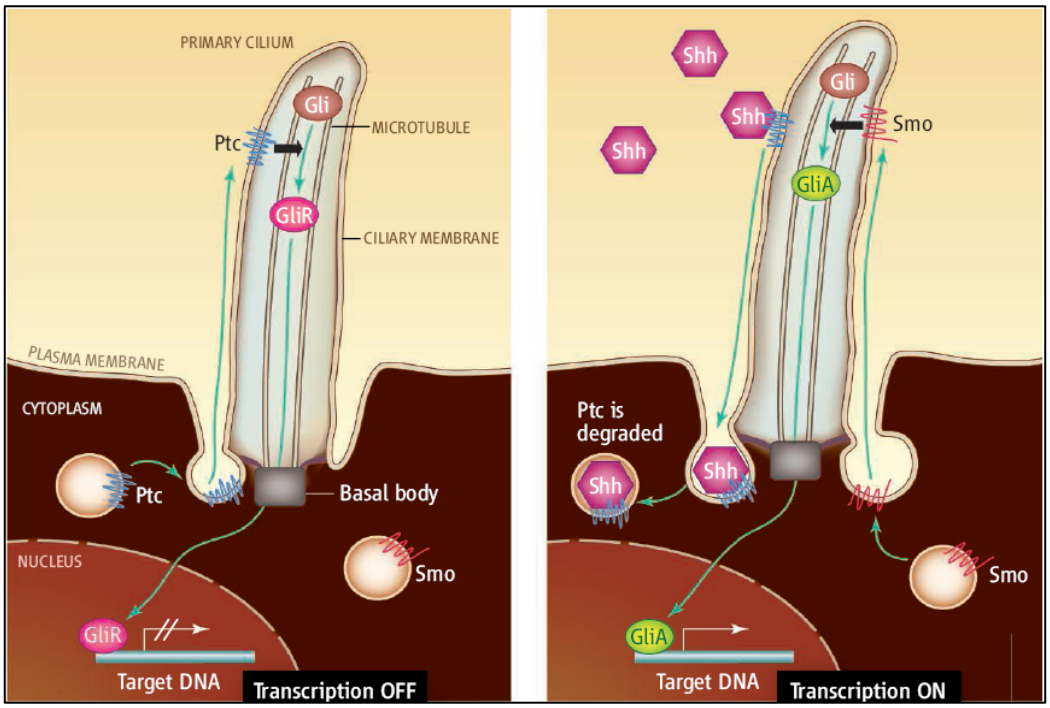

Figure 1.2. Hedgehog Signaling Pathway. Image from Christensen, S.T. & Ott, C.M. Cell signaling. A ciliary signaling switch. *Science* **317**, 330-1 (2007)[30]. Image reprinted with permission from AAAS. http://science.sciencemag.org/content/317/5836/330.full?rss=1. Schematic diagram of Hh signaling in the absence of Hh ligand (left) and the presence (right) of Hh ligand. In the absence of Hh ligand, PTCH localizes to the primary cilium and excludes SMO. In the presence of Hh ligand, Hh ligand binds to PTCH and PTCH delocalizes from the cilium. This allows SMO to localize to the primary cilium where GLI transcription factors are activated and translocate to the nucleus to activate Hh target genes.

1.3 THM1 and THM2

The importance of *Thm1* in mammalian embryonic development was first revealed in a N-ethyl-N-nitrosourea (ENU) mouse mutagenesis screen for late developmental phenotypes to generate models of autosomal recessive congenital defects[20,31]. As a result of the screen, multiple mutants showing late embryonic lethality were identified, including *alien (aln)*[31]. The *aln* mutation was mapped to mouse chromosome two and found to encode a missense mutation that converts a glutamine to a proline residue of the *Ttc21b/Thm1* (tetratricopeptide repeat-containing hedgehog modulator 1) gene product[20,31].

Recessive inheritance of the *aln* mutation results in a mutant lacking THM1[20]. Loss of THM1 causes peri-natal lethality, polydactyly, split and fused ribs, abnormal forebrain structure, craniofacial abnormalities, and neural tube defects[20,31]. THM1 localizes punctately throughout the ciliary axoneme[20], suggesting that it functions in primary cilia. Further investigation of the limbs of *Thm1*-null embryonic mice (*aln)* revealed shortened primary cilia with a bulb-like structure at the distal portion of the cilium[20]. Immunofluorescence staining showed accumulation of IFT88, an IFT-B protein at the tip of the cilium, a hallmark of impaired retrograde trafficking[20]. Using a *Thm1* knockdown cell line, live imaging analysis of IFT88 ciliary trafficking confirmed a role for THM1 in retrograde trafficking, as measured by a decrease in transport velocity of IFT88 particles from the tip to the base of the primary cilium[20].

Molecular evidence supports a role for *Thm1* as a negative regulator of Hh signaling. In *Thm1*-null mouse embryos, Hh signaling transcriptional targets were upregulated and ectopically expressed, indicating increased Hh signaling[20]. Specifically, *in situ* hybridization for *Ptch1*, a transcriptional target of Hh signaling, showed increased staining in the maxilla, first branchial arches, somites, and limbs in *aln* mutant embryos at embryonic day (E) 9.5 relative to control

embryos[20]. *In situ* hybridization for *Gli3* in E10.5 THM1 null embryos revealed an increased expression in the branchial arches and limbs, and Western blot analysis for GLI3 in anterior limb buds revealed a significant increase in the GLI3 activator: Gli3 repressor ratio[20]. Additionally, *aln* mutants exhibit abnormal neural tube patterning, a process dependent on a Hh signaling gradient[20]. In *Thm1*-null mice, neural tube ventral domain markers, HNF3β, NKX2.2, NKX6.1, OLIG2, were expanded dorsally while a dorsal domain marker, MSX2, was decreased, consistent with increased Hh signaling[20]. Epistatic genetic analysis revealed that THM1 is positioned downstream of SMO and the SHH ligand, but upstream of GLI2 in the Hh signaling cascade[20]. Taken together, these experiments highlight the importance of THM1 in cilia structure and function in mammalian development.

Further studies suggest a critical role for *Thm1* in embryonic brain development[28]. THM1 null embryos exhibit signs of abnormal forebrain architecture as early as E9.5, with a lack of distinct separation between the telencephalon and the diencephalon[28]. Measurements at E12.5, E14.5, E18.5, and post-natal day (P) 0 show significantly smaller telencephalons in *aln* mutants compared to control littermates[28]. Molecular analysis of dorsal-ventral patterning of the embryonic forebrain at E12.5 indicated an increase in the ventral neuronal subpopulations, marked by *Mash1* or *Dlx2* and a decrease in dorsal domain markers such as *Wnt3a, Lhx,* and *Ngn2*[28]. *In situ* hybridization experiments revealed an increase in *Shh* and Hh target genes such as *Foxa2* and *Ptch1* in the brain suggesting a potential mechanism for the forebrain abnormalities observed[28]. Rescue experiments were performed by genetically down-regulating levels of the *Shh* ligand[28]. When *aln* mutant mice also harbored one null allele of *Shh*, brain abnormalities were partially rescued[28], underscoring the functional significance of *Thm1* as a negative regulator of Hh signaling in the developing brain.

In addition to a role for THM1 in embryonic development, evidence supports a role for *Thm1* in multiple tissue types during post-natal development[26,32]. Using a ubiquitous tamoxifen inducible Cre recombinase, deletion of THM1 at E17.5 resulted in cystic kidneys at six weeks of age[26]. Cystic kidneys of the *Thm1* conditional knockout mice were accompanied by higher blood urea nitrogen (BUN) levels, increased kidney weight to body weight ratios, and higher levels of cAMP compared to control littermates[26]. Molecular studies in *ex vivo* embryonic kidney cultures revealed an increased cystogenic potential of *aln* embryonic kidneys at E13.5 which was attenuated by disrupting the Hh signaling cascade[26]. Loss of *Thm1* combined with genetic loss of *Gli2,* decreased cystogenesis of *ex vivo* cultured *Thm1*-null kidneys[26]. Additionally, pharmacological inhibition of the Hh signaling pathway using Gant61 or Sant2, targeting GLI2 and SMO, respectively, was also effective in decreasing the cystogenesis of *Thm1*-null cultured embryonic kidneys[26]. These results were supported by *in vivo* studies of *Thm1* and *Gli2* double mutant conditional knockout mice. Conditional deletion of *Gli2* in addition to *Thm1* at E17.5 decreased renal cystogenesis at 6 weeks of age compared to *Thm1* deletion alone[26]. These studies established a role for THM1 and Hh signaling in post-natal kidney development.

Furthermore, post-natal loss of *Thm1* at five weeks of age resulted in significantly higher body weights of *Thm1* conditional knockout mice compared to wild-type (WT) littermate controls at eight weeks of age[32]. Pair-feeding experiments largely maintained the weights of *Thm1* conditional knockout mice similar to control mice, indicating hyperphagia as a predominant mechanism of increased weight gain[32]. Further experiments provide evidence of metabolic dysfunction in the *Thm1* conditional knockout mice including increased levels of leptin and blood glucose at 18 weeks of age[32]. Interestingly, a glucose tolerance test revealed sex differences in the *Thm1* conditional knockout mice. While female *Thm1* conditional knockout

mice responded to an intraperitoneal injection of glucose similarly to controls, male *Thm1* conditional knockout mice lagged in clearing the glucose, resulting in significantly higher levels of blood glucose at 60, 90, and 120 minutes post-glucose injection[32]. These results suggest that *Thm1* conditional knockout male mice have impaired glucose metabolism, a sign of type 2 diabetes[32]. Molecular analysis of the arcuate nucleus in the hypothalamus, a central regulating center of appetite and energy expenditure[33], revealed a decrease in pro-opiomelanocortin (POMC) RNA transcript levels in pre-obese *Thm1* conditional knockout mice, and lack the alternation of these transcripts in response to fasting, in contrast to control littermates[32]. This suggests that the *Thm1* ciliary defect impairs the response to appetite-controlling stimuli, resulting in hyperphagia and obesity[32].

Interestingly, a separate study revealed an extra-ciliary role for THM1 in focal segmental glomerulosclerosis (FSGS). Genetic analysis of 46 families with FSGS revealed 7 families with an autosomal recessive mutation in *Thm1,* p.P209L, which was later determined to be a hypomorphic mutation[34]. Histological analysis of patient kidney tissue biopsies with the p.P209L mutation revealed both glomerular and tubulointerstitial lesions[34]. Although undifferentiated podocytes have a primary cilium, mature podocytes lack this structure[34]. Studies examining the localization of THM1 found THM1 at the base of the primary cilium in undifferentiated podocytes. However, THM1 rearranges and localizes along the microtubule network in mature podocytes[34]. Loss of THM1 led to abnormal actin and microtubule cytoskeleton organization[34] revealing importance of Thm1 in the cytoskeleton of mature podocytes. These data were the first to identify a role for a ciliary protein in hereditary glomerulopathy and shows THM1 is able to function in areas of the cell outside of the primary cilium[34].

A BLAST search revealed *Ttc21a*/*Thm2* as a paralog of *Thm1*[20]. *Thm2* is found on mouse

chromosome nine and is predicted to encode a protein 49% identical to THM1[20]. Comparable to THM1, THM2 is expected to have a similar protein structure including 10 tetratricopeptide repeat (TPR) domains[20]. Furthermore, *Thm2* and *Thm1* share ubiquitous RNA developmental expression patterns at E10.5, with increases in the branchial arches, maxillary prominence, limb buds, somites, and spinal cord (Figure 1.3A)[20]. In contrast to *Thm1,* the role of *Thm2* has not yet been studied.

BLAST searches revealed *Thm1* and *Thm2* are orthologous to *FLA17* in *Chlamydomonas reinhardtii*[20]. This gene is known to encode an IFT Complex A protein, IFT139[35]. Analysis of IFT Complex A proteins in *Chlamydomonas reinhardtii* revealed IFT139 is linked to the core IFT-A complex (IFT144, IFT140, and IFT122) through IFT121 (Figure 1.3B)[36]. Loss of IFT139 in *Chlamydomonas reinhardtii* resulted in a flagellar bulge and a decrease in retrograde trafficking velocity[37]. Thus, the findings of *Thm1* loss in mammalian cells are consistent with these data. This project focuses on expanding our knowledge of *Thm1* in adipogenesis and establishing a role for *Thm2* in tissue development and maintenance.

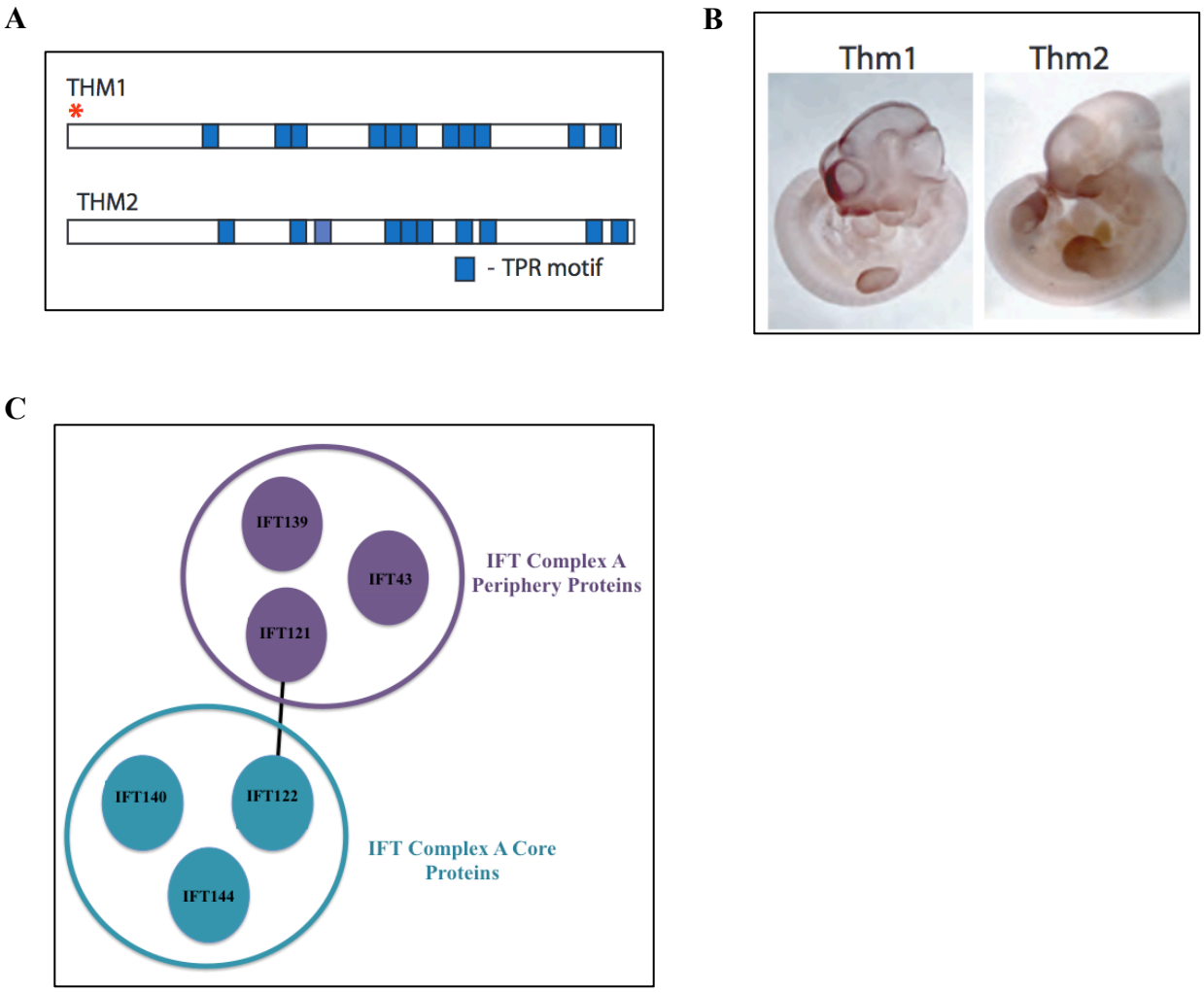

Figure 1.3. Comparison of THM1 and THM2. Image (A, B) reprinted by permission from Macmillan Publishers Ltd: Nature Genetics, Tran, P.V. *et al.* THM1 negatively modulates mouse sonic hedgehog signal transduction and affects retrograde intraflagellar transport in cilia. *Nat Genet* **40**, 403-10 (2008)[20], copyright 2008. Image (C) adapted from Behal, R.H. *et al.* This research was originally published in the Journal of Biological Chemistry. Behal, R.H. *et al*, Subunit interactions and organization of the Chlamydomonas reinhardtii intraflagellar transport complex A proteins. *J Biol Chem* (2012) **287**, 11689-703, Copyright the American Society for Biochemistry and Molecular Biology. (A) Predicted protein structures of THM1 and THM2 including the presence of TPR motifs. Protein structures predicted by Pfam (http://pfam.wustl.edu/). (B) *In situ* hybridization at E10.5 shows similar developmental expression patterns of *Thm1* and *Thm2*. (C) Schematic diagram of core and peripheral IFT Complex A proteins. IFT121 is thought to connect core and peripheral proteins.

1.4 Ciliopathies

Mutations in genes which cause dysfunctional cilia result in a collection of inherited disorders termed "ciliopathies"[38]. Ciliopathies are a heterogeneous group of diseases[39] with an incidence of 1:1,000 to 1:150,000[38]. These diseases share broad-ranging clinical abnormalities including obesity, cystic kidney disease, skeletal dysplasia, retinal degeneration, and male infertility[40]. (Figure 1.4). Treatment options for ciliopathies are limited to managing the symptoms of disease, with no curative options available[4]. Importantly, these clinical features are also prevalent in the general population, including obesity (1:3)[38], cystic kidney disease (1:500)[38], skeletal dysplasia (1:5,000)[41], retinal degeneration (1:3,000)[38] and male infertility (7:100)[42]. Thus, the study of ciliary genes allows unique insight into potential shared molecular mechanisms between ciliopathies and abnormalities in the general population.

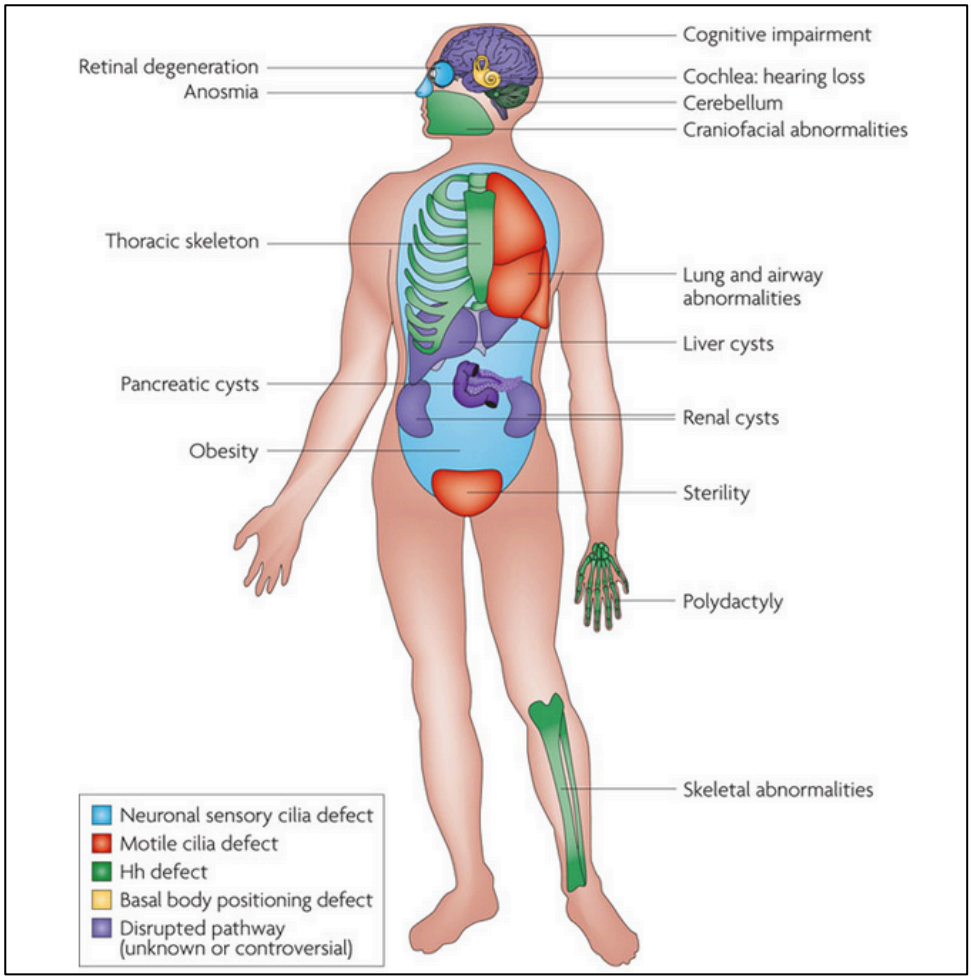

Figure 1.4. Clinical Manifestations of Ciliopathies. Image reprinted by permission from Macmillan Publishers Ltd: Nature Reviews Genetics. Goetz, S.C. & Anderson, K.V. The primary cilium: a signalling centre during vertebrate development. *Nat Rev Genet* **11**, 331-44 (2010)[12], copyright 2010. Diagram showing the multiple organ systems affected by ciliopathies due to the nearly ubiquitous presence of cilia on the cells in our body. In particular, we focus on obesity, skeletal, and sterility abnormalities.

1.4.1 THM1 and THM2

Mutations in *THM1* have been found in patients with ciliopathies. Genetic analysis of 753 ciliopathy patients revealed *THM1* mutations in five ciliopathies, including Jeune Asphyxiating Thoracic Disorder Syndrome (JATD), Meckel Syndrome (MKS), Joubert Syndrome (JBTS), Bardet-Biedl Syndrome (BBS), and Nephronophthesis (NPHP)[43]. In total, pathogenic *THM1* mutations were found in approximately 5% of ciliopathy patients[43]. Interestingly, one-third of patients with a homozygous mutation in another ciliary gene also harbored a heterozygote *THM1* mutation, suggesting that mutations in *THM1* may be both causal and modifying factors in human ciliopathies[43]. The mutational load of *THM2* in ciliopathies has not been published. Based on these human genetic studies and our experimental findings, we are interested in the roles of THM1 and THM2 in obesity, skeletal dysplasia, and male infertility.

1.4.2 Obesity

Obesity has become a worldwide epidemic, with an estimated 1.4 billion people affected globally[44]. Patients with obesity often develop metabolic syndrome, which is estimated to affect between 10-84% of the general population, varying with the demographics of the population examined[44]. Individuals with metabolic syndrome are two times more susceptible to cardiovascular disease and five times more susceptible to type 2 diabetes, due to the presence of abdominal obesity, insulin resistance, dyslipidemia, and hypertension[45]. Obesity and its associated chronic conditions cost the United States alone an estimated $209 billion[46], reinforcing the need to understand and elucidate novel mechanisms underlying this disease.

Primary cilia have been proposed to play a role in leptin and insulin signaling cascades which function in metabolic homeostasis. Insulin is produced by the β-cells of the pancreas and

promotes the uptake of glucose in tissues including skeletal and cardiac muscle, and adipose tissue, while leptin is a hormone produced in white adipose tissue and acts on the hypothalamus as a satiety signal[33]. Evidence suggests primary cilia are essential in the hypothalamus, a key regulatory center of food intake, energy expenditure, and homeostasis[33]. Furthermore, cilia have been shown to function in tissues outside of the central nervous system, including in skeletal muscle, cardiac muscle, liver, and adipose tissue[33]. Defects in primary cilia have been linked to obesity and metabolic syndrome[33] with two ciliopathies, Bardet-Biedl Syndrome (BBS) and Alström Syndrome (ALMS), holding remarkably high rates of obesity, at 72-91% and 95%, respectively[38].

Bardet-Biedl Syndrome is a genetically inherited disorder with an autosomal recessive mode of inheritance[47]. Populations from around the world have vastly different occurrence rates with the incidence in North America below 1:100,000 individuals, while the incidence rate in an isolated group of residents living on the Faroe Islands of Denmark is strikingly higher at 1:3,700[48]. ALMS is also a recessively inherited disorder, but is found in the population much less frequently with only 500 cases reported globally. Both patients with BBS and ALMS are affected by a broad spectrum of clinical abnormalities, including retinal abnormalities, obesity, kidney disease, liver disease, male hypogonadism, and diabetes[33,38,47]. Although BBS and ALMS share many clinical phenotypes, BBS patients are also affected with polydactyly, cognitive deficiencies, and situs invertus[33]. The onset age of obesity differs between BBS and ALMS with ALMS patients developing obesity as early as six months of age[49], while BBS patients develop obesity after two to three years of life[47].

Careful analysis of BBS patients has revealed a complex genetic basis for this disease, rooted in mutations of at least 21 *BBS* genes[50], all of which have a ciliary function[48]. Evidence

suggests that at least some BBS patients may have a triallelic inheritance pattern with three mutations at two different gene loci[47,51]. Furthermore, mutations in loci other than *BBS* genes have been identified in patients with BBS including *Thm1*[43] and *ALMS1*[47]. These findings suggest that BBS clinical outcomes may be modified based on mutations in interacting alleles[47] coding for proteins within the ciliary proteome. Genomic sequencing of ALMS patients has identified 239 mutations, all of which are found in the *ALMS1* gene[52]. Although it is known ALMS1 localizes to the primary ciliary base and centrosomes, the function of the protein is not completely understood[2], but is thought to play a role in ciliary trafficking[52]. The clinical phenotype of ALMS has been hypothesized to be modified by other genes, however, such genes have not yet been identified[49].

Mouse models of BBS and ALMS recapitulate many of the phenotypes in human diseases, including hyperphagia, obesity, retinal degeneration, and male sterility[33,38,53]. In particular, mouse models have provided valuable insights into leptin and insulin signaling and the mechanisms by which aberrant cilia function results in obesity and metabolic dysfunction. BBS1 has been shown to interact with the leptin receptor, and loss of BBS proteins is thought to lead to abnormal leptin trafficking[54]. Underscoring the importance of BBS proteins in leptin signaling, *Bbs2, Bbs4, and Bbs6* knockout mice did not reduce their food intake or lose weight after receiving an intracerebroventricular leptin injection, suggesting that these mice are unable to respond to leptin. Analysis revealed a decrease in STAT3 phosphorylation, a downstream target of leptin signaling, providing a molecular basis for the observed abnormalities in response to leptin injection[54]. In contrast, another group used an *Ift88* conditional knockout mouse model and a *Bbs4* knockout mouse model. Interestingly, after these mice were intraperitoneally injected with leptin, the mice decreased their food intake, suggesting that they are able to respond to

leptin signals. On a molecular level, these mice also showed a response to leptin with an increase in STAT3 phosphorylation[55]. These conflicting results suggest that the role of primary cilia in leptin signaling is complex and still relatively unknown[33].

Conflicting results regarding insulin signaling have also been reported in different *Bbs* mouse models. Associations between primary cilia and insulin signaling components have been established with the insulin receptor localizing to primary cilia of insulin-activated β cells of the pancreas[56]. *Bbs*4 pre-obese null mice were injected with glucose and, compared to their littermate controls, had impaired glucose clearing as measured by higher levels of glucose in the blood. This was accompanied by a decrease in first-phase insulin secretion by the *Bbs4* null pancreatic islets[56]. On the other hand, *Bbs12* knockout mice, although obese, did not show impaired glucose handling when administered a glucose tolerance test. Surprisingly, these mice were more sensitive to injected glucose, with lower blood glucose levels when compared to control littermates. Pathway analysis reveals this response is specific to adipose tissue, with a significant increase in PAKT levels, a known downstream target of insulin signaling[57]. Although direct comparisons between these two studies are difficult, due to the differing weights of the knockout mice compared to controls[33], opposing results indicate that the roles of ciliary proteins in insulin signaling are likely complex and warrant further investigation.

In vitro studies utilizing mutations in *BBS* genes have also provided important molecular insight into adipocyte biology. Although differentiating pre-adipocytes have a primary cilium, mature adipocytes lack this organelle[58]. The presence of a cilium on differentiating pre-adipocytes raises questions regarding the function of cilia in adipocyte differentiation. Throughout the differentiation process, many pathways and regulators work in concert to determine the extent of adipogenesis. Key pathways known to antagonize adipogenesis include

Hedgehog (Hh) and Wnt signaling, while PPARγ and C/EBPα are transcription factors known to promote adipogenesis[58].

In a study of human white pre-adipocytes, knockdown of either *BBS10* or *BBS12* decreased the percentage of ciliated cells and increased PPARγ expression, indicative of pro-adipogenic signaling[58]. In a separate experiment, similar pro-adipogenic observations were verified with an experiment using fibroblasts of patients with mutations in *BBS10* and *BBS12*[58]. Fibroblasts were differentiated into mature adipocytes and, compared to control cells, cells with mutations in *BBS10* or *BBS12* had greater lipid accumulation[58]. Other models of the adipocyte differentiation process involve the use of a mouse pre-adipocyte line, 3T3-L1 cells. Knockdown of *Ift88* in 3T3-L1 cells led to an inability of the cells to produce primary cilia[59]. Interestingly, these cells exhibited a decrease in adipocyte differentiation with corresponding decreases in PPARγ and C/EBPα[59]. Furthermore, knockdown of ALMS1 in 3T3-L1 cells led to a decrease in adipogenesis and PPARγ expression[60]. These contradictory results suggest that although ciliary proteins regulate adipogenesis, the extent and mechanism of regulation is unclear. Individual ciliary proteins or complexes likely have unique, differing roles in regulating adipogenesis, and future studies are needed to further investigate this possibility.

1.4.3 Skeletal Dysplasias

In the general population, skeletal dysplasias affect nearly 1:5,000 individuals and cause short stature due to defects in skeletal development and maintenance[41]. Mutations in ciliary genes can result in skeletal abnormalities, underscoring the importance of primary cilia in signal transduction, mechanosensation and orientation within developing bone and cartilage[61]. In particular, several ciliopathies are characterized by skeletal abnormalities including Jeune

Asphyxiating Thoracic Disorder Syndrome (JATD), Oro-facial-digital syndrome type 1 (OFD1), Ellis van Creveld syndrome (EVC)[38], and Short-Rib Polydactyly Syndromes (I-IV)[62]. Here I focus on JATD because mutations in *THM1* have been identified in patients with this ciliopathy[43], as noted above.

JATD is an autosomal recessive genetic disorder affecting approximately 1:100,000-1:130,000 individuals[63]. Major skeletal manifestations of JATD include polydactyly, shortened long bones and the presence of a small, narrow thoracic cavity, which often leads to respiratory insufficiency[64]. In 60-80% of JATD cases, respiratory insufficiency results in death during the neonatal-infantile period of life[64]. However, some patients with JATD survive this timespan with little to no respiratory distress and can develop kidney, liver, and pancreas abnormalities, and retinal degeneration, later in life[38,64]. Of JATD patients three to ten years old, kidney failure is the leading cause of death[63]. A case review of 13 individuals with JATD revealed a wide spectrum of clinical abnormalities in patients with this disease[65] which may be attributed, in part, to the genetic heterogeneity of JATD. Genetic analysis of individuals with this disease has revealed mutations in multiple cilia-related genes including *WDR19 (IFT144)*[64,66], *DYNC2H1*[64], *IFT140*[64,67], and *IFT80*[68], in addition to *THM1*[43], which all function in trafficking cargo throughout the primary cilium. Moreover, sequencing analysis of some patients diagnosed with JATD did not reveal mutations in any known genes, implying other loci may contribute to this disease[64].

In a case study analysis, researchers noted as JATD patients grew older, respiratory problems and thoracic abnormalities seemed to lessen[65]. These data suggest that if patients survive the critical early years of life, respiratory distress may subside[65], increasing the likelihood of survival. Although some surgical techniques have been successfully used to

improve the constricted thoracic cavity in patients with JATD, the results are not guaranteed[63]. Many of these procedures involve using invasive techniques to place bars or plates in the sternum which expand the space within the thoracic cavity[63]. Due to the unknown success of surgical procedures and lack of curative option[63], further research is needed to uncover novel genetic contributors and molecular mechanisms underlying this disease.

Endochondral and intramembranous ossification are two types of bone development that give rise to the skeleton[69]. Intramembranous ossification is responsible for the development of craniofacial bones while endochondral ossification is responsible for a large part of the remaining skeleton[69]. The ossification process for both endochondral and intramembranous derived bones begin with mesenchymal progenitor cells[69]. In endochondral ossification, these cells differentiate into chondrocytes and go through a maturation process before they are replaced by osteoblasts[69]. In contrast, mesenchymal progenitor cells mature straight into osteoblasts during intramembranous ossification[69]. Since skeletal abnormalities in JATD arise from irregular endochondrial bone development[70], here we focus on the role of primary cilia in endochondral ossification.

Endochondral ossification is a highly regulated process dependent on a variety of signaling pathways[71]. In particular, Hh signaling in the developing growth plate of long bones, such as the tibia, is important during the process of chondrocyte maturation[71]. In the growth plate, chondrocytes mature through three major zones: the proliferation, prehypertrophic, and hypertrophic zones[71]. IHH and Parathyroid hormone-related peptide (PTHrP) are two factors essential in maintaining the organization of the endochondral growth plate[72]. PTHrP is a hormone secreted by the periarticular cartilage, found near the growth plate[72], and IHH is secreted by prehypertrophic chondrocytes[71]. PTHrP diffuses through the growth plate, keeping

cells in a proliferative state. Once the expression falls below a certain level, chondrocytes begin expressing IHH, which also promotes chondrocyte proliferation[72]. This relationship forms a feedback loop where PTHrP inhibits IHH expression and IHH stimulates the expression of PTHrP[72] (Figure 1.5). Suppressor of fused (*Sufu)* is a known negative regulator of Hh signaling and conditional deletion of *Sufu* in chondrocytes resulted in an increase in the proliferation zone and a decrease in the hypertrophic zone of tibia explants when compared to control mice at E16.5[73]. In contrast, absence of, or decreased, Hh signaling, promotes premature hypertrophy of chondrocytes[69]. A study of *Ihh*-null mice revealed a decrease in long bone and rib length, indicating abnormalities in endochondral ossification[74] and providing further evidence of Hh signaling in bone development.

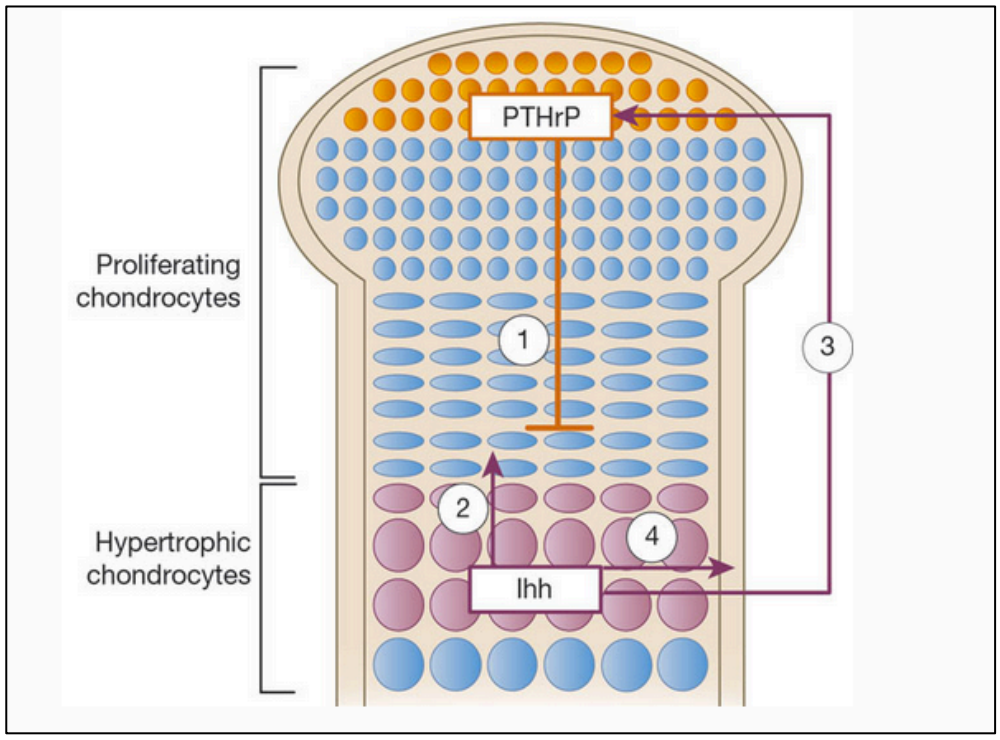

Figure 1.5. Growth Plate Signaling. Image reprinted by permission from Macmillan Publishers Ltd: Nature, Kronenberg, H.M. Developmental regulation of the growth plate. *Nature* **423**, 332-6 (2003)[72], copyright 2003. Schematic diagram showing the feedback mechanisms of IHH and PTHrP in the endochondral growth plate. (1) PTHrP inhibits the expression of IHH in the proliferating chondrocytes. (2) Once PTHrP levels fall below a certain level, IHH is expressed and promotes proliferation while (3) driving the expression of PTHrP from the articular cartilage. (4) IHH stimulates perichondral cells to mature into the bone collar.

Ciliary-mediated Hh signaling in chondrocytes has also been shown to be mechanosensitive[75]. Using primary bovine chondrocytes, the effects of cyclical tensile strength (CTS) on the Hh signaling pathway were assessed[75]. When chondrocytes were exposed to 10% CTS, transcript levels of *Ihh, Gli1* and *Ptch1* increased compared to unstrained cell lines, suggesting Hh pathway activation in response to mechanical stimulation[75]. In order to determine the role of the primary cilium in this response, further studies were conducted using chondrocytes derived from the *Tg737*^{ORPK} mouse, harboring a hypomorphic mutation of *Ift88*[75]. Immunofluorescence analysis of cilia from this cell line revealed the majority of chondrocytes lacked a cilium in the *Tg737*^{ORPK} line[75]. Interestingly, when the Tg737^{ORPK} and control cell lines were exposed to 10% CTS, *Ihh* transcript levels increased[75]. However, *Gli1* and *Ptch1* transcript levels only increased in the control cell line, suggesting IHH ligand expression is mediated by mechanosensation in a primary cilium-independent manner, however, primary cilia are needed to transduce IHH signaling[75].

Further evidence supporting a role for primary cilia in mechanotransduction of the Hh signaling pathway was elucidated using hydrostatic loading[76]. Chondrocytes isolated from Sprague Dawley rats at P2 were exposed to hydrostatic loading for one or two days[76]. After one day, *Ihh* transcription levels were increased by seven-fold, and after two days were further increased, up to 20-fold[76]. Additional pathway analysis after exposure to hydrostatic loading for two days revealed *Gli1* luciferase activity was increased three-fold compared to non-treated control chondrocytes[76]. Interestingly, this increase in *Gli1* activity was repressed when cells were treated with cyclopamine, a Hh antagonist, or chloral hydrate, which causes cilia loss, indicating an essential role for primary cilia in the Hh response triggered by hydrostatic loading[76]. Taken

together, these data indicate a role for primary cilia in mechanosensation and Hh transduction in models of cyclical tensile strength and hydrostatic loading.

Additionally, primary cilia are involved in the maintenance of growth plate organization[77]. Chondrocytes in the growth plate arrange into ordered columns through a process known as "chondrocyte rotation"[77]. In this process, once cells undergo proliferation, the daughter cell initially resides next to the mother cell[77]. The daughter cell then rotates in line with the established stacked columns[77]. Interestingly, primary cilia in the growth plate maintain a specific orientation, and changes in primary cilia orientation are thought to result in growth plate disorganization[77]. Ablation of *Kif3a,* a subunit of the ciliary anterograde motor, in the chondrocytes of mice resulted in loss of primary cilia on chondrocytes and a disorganized growth plate[77,78]. Interestingly, hypomorphic loss of *Ift80* resulted in a disorganized growth plate, even in the presence of primary cilia[79]. Together, these data indicate a role for cilia function, likely signaling, in growth plate organization.

Ciliary mouse models of genes mutated in JATD have provided valuable insights into the role of individual proteins in skeletal development. Hypomorphic loss of *Ift140*, an IFT Complex A gene, resulted in embryonic lethality at E13.5[67]. Interestingly, two *Ift140* mutants survived past E13.5, allowing skeletal formation to be assessed at E16.5[67]. Skeletal preparations revealed severe malformations involving abnormal development of the ribs and polydactyly[67]. Close examination revealed *Ift140* mutant ribs were characterized by branching, thickened protuberances, and abnormal joint architecture between the vertebrae and the heads of the ribs[67]. Analysis of primary cilia structure using scanning electron microscopy (SEM) showed irregular cilia morphology, including a bulb-like structure at the distal tip[67]. Furthermore, molecular analysis using *in situ* hybridization at E11.5 revealed disordered somites of the body plan, and

abnormalities in Hh signaling including an expansion of *Ptch1* and a restriction of *Gli3* domains in the developing limb bud, indicating an increase in Hh signaling[67]. The authors of this study acknowledge that, although more severe than the human disorder JATD, the *Ift140* hypomorphic mouse mutations highlight a role for IFT Complex A proteins in skeletal abnormalities[67].

The *Ift144*^{twt} mouse mutant is another hypomorphic IFT Complex A mouse model[66]. *Ift144* mutants also die during embryogenesis, but survive close to birth[66]. Similar to *Ift140* mutations, loss of IFT144 resulted in multiple skeletal abnormalities as assessed by skeletal preparations at E18.5. Skeletal staining revealed *Ift144* mutants with polydactyly and smaller thoracic cavities with abnormal rib architecture, including rib fusion and branching, and decreased hind limb length[66]. Although SEM of primary cilia revealed no overt abnormalities in cilia structure, whole embryo *in situ* hybridization at E10.5 revealed an increase in *Ptch1* staining in the face and limbs, and disorganized somites of *Ift144* mutant embryos[66]. This study adds to the body of evidence implicating IFT Complex A proteins in skeletal development.

In addition to mouse models investigating the role of IFT-A proteins in skeletal development, hypomorphic mutation of *Ift80*, an IFT-B gene, resulted in post-natal skeletal deformities[79]. Although many of the *Ift80* mutant mice did not survive embryogenesis, those that did were characterized by severe skeletal defects[79]. Skeletal stains of *Ift80* mutant mice at P21 show abnormalities of the thoracic cavity including abnormal boundaries between the bone and cartilage and constriction of the rib cage[79]. Additional analysis of skeletal stains revealed polydactyly and shortening of the long bones and skull in the *Ift80* mutant mice[79]. Furthermore, histological analysis of the humerus of post-natal day 2 mice revealed disorganization of the growth plate in the *Ift80* mutant compared to control littermates[79], providing a potential mechanism for the observed skeletal defects. Although immunofluorescence analysis showed the

presence of structurally normal cilia on E14.5 *Ift80* mutant derived MEFs, these cells showed a decreased response to Hh agonist, as shown by lower levels of Hh target transcripts including *Ptch1* and *Gli1* compared to littermate controls[79].

More specifically, the role of *Ift80* in chondrocyte differentiation has been investigated using an inducible, chondrocyte-specific Cre-recombinase[80]. Three week cultures of isolated mouse chondrocytes from *Ift80* conditional knockout mice revealed a decrease in sulfated proteoglycan deposits in IFT80-deficient chondrocytes, compared to control chondrocytes, indicating a decrease in chondrocyte differentiation[80]. Transcriptional analysis revealed a decrease in levels of chondrocyte markers *Sox9, Aggrecan,* and *type X collagen*[80]. Further molecular analysis of isolated chondrocytes revealed a decrease in Hh signaling in response to SHH ligand and an increase in Wnt signaling in response to WNT3A ligand, suggesting IFT80 mediates chondrocyte differentiation through regulation of Hh and Wnt signaling[80]. These experiments provide a molecular basis for the cellular abnormalities of the reduced growth plate observed in *Ift80* conditional knockout mice. In addition, conditional deletion of *Ift88,* another IFT-B gene, resulted in skeletal abnormalities including polydactyly, and shortening of the long bones which could be detected during embryogenesis and post-natally[81]. Molecular analysis of the forelimbs revealed a decrease in *Gli1* levels, indicating a decrease in Hh signaling[81]. Taken together, these results suggest further studies are needed to determine the precise contributions of IFT Complex A and Complex B proteins in skeletal development.

1.4.4 Infertility

Approximately 48.5 million couples are estimated to struggle with infertility worldwide[82]. Although both male and female factors can contribute to this health concern, male

factors are thought to cause infertility 20-30% of the time and to contribute to infertility in 50% of cases[82]. Based on population approximations, almost 11 million men are predicted to be infertile in North America alone[82]. The vast majority of male infertility cases can be attributed to poor sperm quality or amount, which result from abnormal events before, during, or after sperm development in the testis[42]. These abnormalities can result from environmental[83] or genetic factors[84], such as the male infertility observed in ciliopathies.

Interestingly, ciliopathies resulting in issues related to male fertility have been attributed to abnormal mechanisms in both motile and primary cilia[47,85]. Motile cilia utilize mechanisms similar to primary cilia, including IFT[40], but are present on specific cells throughout the body with multiple cilia per cell[39]. Instead of the 9+0 microtubule arrangement of primary cilia, motile cilia contain a 9+2 arrangement with two microtubules located in the center of the axoneme[40]. In addition, motile cilia contain dynein motor proteins, which utilize ATP to facilitate the beating movement of motile cilia[39]. The sperm flagella (tail) shares the 9+2 microtubule organization and presence of dynein motors with motile cilia, allowing for sperm motility[39].

Primary Ciliary Dyskinesia (PCD) is a motile cilia disorder with an autosomal recessive mode of inheritance and is thought to affect approximately 1:10,000 individuals[85]. Mutations in genes causing PCD result in defective ciliary beating patterns, leading to different clinical abnormalities including male infertility, hearing and respiratory defects, and *situs inversus*[85]. Male infertility is generally the last abnormality characterized in patients with PCD, while approximately 80% of newborns exhibit signs of severe respiratory abnormalities[86] which lead to recurrent infections[85]. Genetic analysis of patients with PCD uncovered mutations in approximately 25 genes, most of which result in structural abnormalities of the motile cilia or flagella[86]. Although mutations in most genes do not correlate with specific clinical outcomes, a

mutation in the gene *CCDC114,* has been identified in patients with PCD, who exhibit normal fertility[85]. Future studies are necessary to determine the roles of individual proteins and their contributions to the development of diverse clinical manifestations observed in patients with PCD.

Furthermore, patients with BBS, described above in section 1.4, are affected by hypogonadism[47]. Male hypogonadism is characterized by a decrease in gametogenesis and/or gonadal hormones[87]. The hypogonadism observed in male BBS patients results from testes which fail to undergo puberty, causing infertility the vast majority of the time[88]. Underscoring the importance of BBS proteins in sperm development, *Bbs4* mutant mice develop primary and motile cilia throughout the body, but fail to generate a sperm flagellum, resulting in infertility[89]. By studying male infertility in models of ciliary mutants, I aim to uncover novel proteins and mechanisms underlying male infertility in ciliopathies and the general population.

The testis is the major male reproductive organ responsible for spermatogenesis, or sperm development[90]. Of interest, *in situ hybridization* revealed Hh-related signaling transcripts in cells within the testis, including in germ cells and Sertoli cells found within the seminiferous tubules[91], and Leydig cells located in the interstitial tissue[92]. Germ cells undergo a highly organized, step-wise process to mature into functional sperm and Sertoli cells form the blood-testis barrier and aid in spermatogenesis and Leydig cell function[90]. Leydig cells produce male sex hormones, such as testosterone, which plays an integral role in the hypophyseal-testicular axis, affecting the development of male reproductive organs and spermatogenesis[90]. In the hypothalamus-pituitary-gonadal (HPG) signaling axis, the hypothalamus produces gonadotrophin releasing hormone (GnRH) which acts on cells in the pituitary[93]. The pituitary then releases follicular stimulating hormone (FSH) and luteinizing hormone (LH), which reach

the testis, and regulate the development of gametes through the production of steroid hormones in the gonads, such as testosterone[90,93]. The steroid hormones form part of a negative feedback loop and act on the hypothalamus and pituitary to control levels of GnRH, FSH, and LH[87].

Most sperm development occurs within the germinal epithelium of the seminiferous tubules and can be divided into three stages: spermatogoniogeneisis, maturation of spermatocytes, and spermiogenesis[90]. Spermatogoniogenesis is a process that involves the development of B type spermatogonia for the beginning of germ cell development[90]. Spermatogonia develop into spermatocytes that are classified based the number of meiotic rounds the cell has completed[90]. Spermatocytes that have not yet undergone a round of meiosis are called primary spermatocytes while cells that have undergone the first round of meiosis are called secondary spermatocytes[90]. The secondary spermatocytes undergo another round of meiosis to become haploid cells called spermatids[90]. Spermatids then undergo spermiogenesis where a variety of changes take place, including the growth of the flagella[90]. The Sertoli cells then mediate a process known as spermiation where the spermatids leave the germinal epithelium and become spermatozoa[90]. During this process, residual bodies can also be released and digested by Sertoli cells (Figure 1.6)[90].

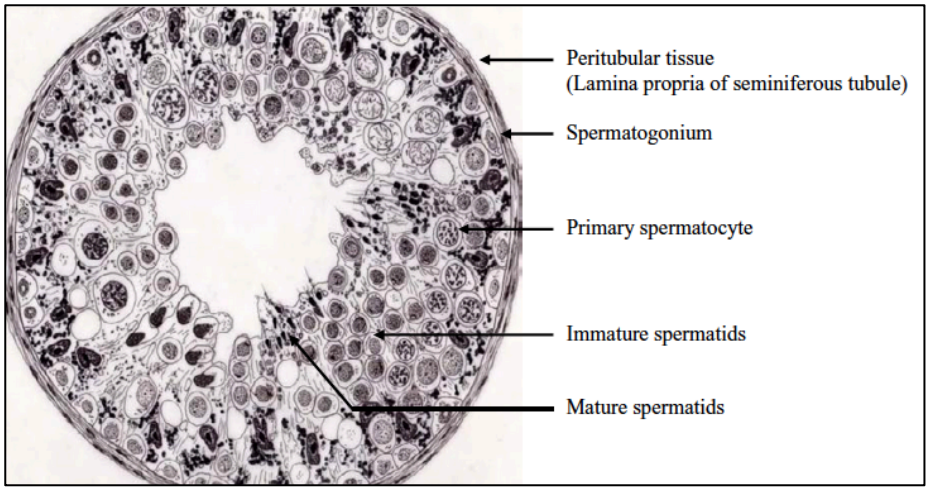

Figure 1.6. Process of Spermatogenesis. Image from Holstein, A.F., Schulze, W. & Davidoff, M. Understanding spermatogenesis is a prerequisite for treatment. *Reprod Biol Endocrinol* **1**, 107 (2003)[90]. Copyright Holstein et al; licensee BioMed Central Ltd. 2003. This is an Open Access article: verbatim copying and redistribution of this article are permitted in all media for any purpose, https://www.ncbi.nlm.nih.gov/pmc/articles/PMC293421/. Drawing of a cross section of a seminiferous tubule containing progressively more developed sperm towards the center (lumen) of the tubule. Once spermatids are released from the germinal epithelium, they are called spermatozoa.

Interestingly, it appears as though Hh signaling may be regulated in a developmentally appropriate manner throughout the process of spermatogenesis[91]. *In situ* hybridization in adult mouse testis revealed the Hh signaling transcripts, *Gli1, Gli2, Gli3, Ptch2,* and *Smo* are expressed at the beginning stages of spermatogenesis, in spermatogonia and spermatocytes, with *Gli1, Gli3, Ptch2,* and *Smo* showing less intense staining in round spermatids[91]. Complementarily, transcripts of a negative regulator of Hh signaling, *Sufu*, were found to be expressed in round spermatids and immunohistochemistry revealed SUFU expression in round and elongating spermatids, proposing SUFU works to downregulate Hh signaling towards the end of spermatogenesis[91]. These observations suggest Hh signaling functions in the process of spermatogenesis[91].

In addition to the germ cells, there are other cell types within the testis involved in Hh signaling[92]. The Sertoli cell precursors are the first known cell type of the testis to exhibit transcription of *Dhh,* at E11.5, just one day after the earliest indicator of male determination, *Sry,* is expressed[92]. The expression of *Dhh* in the Sertoli cells continues into adulthood[92]. In the testis, Sertoli cells are closely intertwined with germ cells in the seminiferous epithelium, and co-culture experiments showed that when mouse P9 testicular cells were cultured with a mouse Sertoli cell-derived line (15P-1), testicular cells were able to undergo meiosis[94]. These results suggest that signaling molecules from Sertoli cells may affect spermatogenesis[92,94]. Furthermore, Leydig cells in the testis are shown to exhibit *Ptch* expression, a target of Hh signaling[92]. Supporting a role for Hh signaling in Leydig cells, immunofluorescence experiments have identified primary cilia on immature Leydig cells[95]. *In vitro* experiments utilizing an immature mouse Leydig cell line (TM_3), confirmed the ability of these cells to transduce the Hh signal[95]. When TM_3 cells were stimulated with a Hh agonist, SAG, cells were capable of transducing Hh

signaling exhibited by increased SMO localization to the primary cilium and increased RNA expression of *Gli1* and *Ptch1*[95]. Taken together, these data provide evidence for Hh signaling in Sertoli and Leydig cells of the testis.

Underscoring the importance of Hh signaling in the testis, *Dhh* null mice are infertile and are characterized by a 60% decrease in testis weight at P10[92]. Histological analysis of pure *129/Sv Dhh*-null mice revealed the presence of primary spermatocytes, but the absence of spermatids[92]. However, on a 129/Sv-C57BL/6J mixed background, some developing sperm underwent meiosis, but failed to mature into sperm[92]. In *Dhh* mutant testis, Sertoli and Leydig cells were present, but Leydig cells lacked *Ptch* expression, suggesting Leydig cells may be targets for *Dhh* in the developing testis[92]. Interestingly, on a 129/Sv-C57BL/6J mixed background, a separate group revealed that fetal Leydig cells failed to undergo differentiation, suggesting a role for Hh signaling in this process[96]. Since Hh signaling plays an essential role in multiple cells of the testis, sperm development can be affected by abnormalities in germ cell Hh signaling, or by abnormalities in Sertoli and Leydig cell Hh signaling[92].

Several mouse models highlighting proteins primarily involved in anterograde trafficking have elucidated roles for ciliary proteins in spermatogenesis[97-99]. Hypomorphic loss of *Ift88* resulted in infertile male mice with significantly lower sperm counts compared to control male mice at eight weeks of age or more[97]. Close examination of sperm morphology showed abnormally shaped sperm heads[97]. While many sperm heads lacked tails, the few tails present were shorter and irregularly shaped compared to control sperm tails[97]. Localization analysis of IFT88 revealed presence in the Golgi apparatus[100], and head and tail of developing spermatids[97]. Despite localization of IFT88 in the tail of developing sperm, immunofluorescence analysis revealed the absence of IFT88 in mature sperm, suggesting IFT88 may only be required in the

flagellum of developing sperm[97]. Furthermore, histological staining of testis architecture showed a decrease and scattered organization of sperm heads surrounding the lumen, and abnormal morphology of some spermatid heads, underlying the importance of *Ift88* in sperm development[97].

Another IFT Complex B protein, IFT20, has been associated with male fertility[98]. IFT20 is expressed in the testis of male mice and increases in expression from P30-P42, when the first wave of spermatogenesis occurs, suggesting this protein functions in sperm development[98]. Conditional deletion of *Ift20* specifically in male germ cells of mice showed that loss of IFT20 resulted in infertility when male mice are mated at two to three months of age[98]. Interestingly, approximately 1/3 of *Ift20* conditional knockout male mice mated with females at six weeks of age were able to father litters that were reduced in size compared to control litters, and were unable to father future litters[98].

Using scanning electron microscopy (SEM), the structure of *Ift20* mutant sperm was investigated[98]. Analysis revealed a variety of phenotypes in the *Ift20* conditional knock out mice including some sperm heads without a tail, other sperm heads with a bent tail, and irregularly, round-shaped sperm heads[98]. Interestingly, residual cytoplasm was also observed in the bent portions of tails of *Ift20* mutant mice[98]. Additionally, histological analysis characterized abnormal features of sperm within the *Ift20* mutant testis at different stages including the presence of abnormal elongating spermatids, residual bodies in the lumen, and the absence of sperm tails in the lumen[98]. Live imaging analysis revealed that while most *Ift20* mutant sperm failed to move, some flagella exhibited defective beating patterns[98]. Further, immunofluorescence staining revealed the absence of two proteins normally found in mature

sperm flagella, ODF2 and SPAG16L, in *Ift20* mutant mice[98]. These data indicate that the IFTB gene, *Ift20* is essential in sperm development and trafficking of proteins to the flagella.

Additional studies investigated a role for a subunit of the anterograde molecular motor, KIF3a, in spermatogenesis[99]. Immunofluorescence of sperm at different stages of development showed distinctive localization patterns[99]. KIF3A was found to localize to the cytoplasm in a variety of stages of sperm development, including the spermatocytes, round spermatids, and elongating spermatids[99]. Specifically, immunofluorescence analysis of round and elongating spermatids showed KIF3A localization at the basal body and axoneme, with additional presence in the manchette, in elongating spermatids[99]. However, in mature spermatids, staining for KIF3A was only found in the principal piece, suggesting KIF3A localizes to different regions of the sperm during the maturation process[99].

To study the role of KIF3A in spermatogenesis, a male germ cell-specific conditional knockout mouse was used[99]. *Kif3a* conditional knockout males mated with females were unable to father litters, suggesting loss of *Kif3a* renders male mice infertile[99]. Histological analysis of the epididymis revealed cellular remains and very few sperm in the *KIF3A* mutant mice, while the control epididymis was filled with sperm[99]. The little sperm present in the *KIF3a* mutant epididymis were characterized by abnormal head and tail morphology, with transmission electron microscopy showing complete loss of axonemal and accessory structure organization[99]. Despite a decrease in total testis weight, histological analysis revealed normal morphology of the *Kif3a* mutant testis[99]. Although spermatogonia, spermatocytes and spermatids were unaffected by loss of KIF3A, irregularities were seen in elongating spermatids[99]. Specifically, elongating spermatids did not have tails and exhibited unusual head shapes[99]. Studies investigating the mechanisms underlying abnormal sperm head shape in *Kif3a* mutant mice centered on the

manchette, a structure known to function in sperm head shaping[99]. Taken together, these data reveal a role for the IFT Complex B proteins and motor in sperm development[97-99]. Future studies are needed to expand our knowledge of IFT Complex B proteins, and establish a role for IFT Complex A proteins in spermatogenesis.

1.5 Study Significance

An abundance of evidence suggests primary cilia are important signaling organelles, essential for proper development of many tissue types throughout the body. Since mutations in ciliary genes result in human diseases known as ciliopathies, which are characterized by clinical manifestations found also in the general population, expanding our knowledge of ciliary proteins and their roles within the body has broad clinical relevance. In particular, this dissertation investigates the role of *Thm1* and of the novel ciliary gene, *Thm2,* in obesity, skeletal abnormalities, and male infertility.

In chapter two, a novel *in vitro* model of *Thm1* deficiency was used to determine a role for *Thm1* in adipogenesis. The data show deficiency of *Thm1* increases adipogenesis, adipogenic promoting pathways, and insulin sensitivity. In chapter three, we investigate the role of the novel ciliary gene, *Thm2,* together with *Thm1* in skeletal development. Using the first *Thm2* knockout mouse model, and combining with a null allele of *Thm1,* the results show that loss of *Thm2* and one allele of *Thm1* results in decreased body weight and length accompanied by a trend of abnormal growth plate morphology when backcrossed five generations onto a C57BL6/J background. In chapter four, a second mouse model of *Thm2* loss was created using CRISPR/Cas9 genome editing. Loss of *Thm2,* and one allele of *Thm1,* results in decreased male fertility, low sperm count, impaired sperm motility, and abnormal testis morphology on a mixed

FVB/C57BL6/J background. Taken together, these studies have established novel roles for *Thm1* in adipogenesis and for the novel gene, *Thm2,* in post-natal skeletal development and male infertility, expanding the ciliome. These studies also have revealed functional interaction between *Thm1* and *Thm2*. Further, these investigations provide novel *in vitro* and *in vivo* models of *Thm1* and *Thm2* deficiency that will be instrumental in elucidating molecular mechanisms underlying multiple clinical manifestations of ciliopathies.

Chapter Two: Novel Role of *Thm1* in Adipogenesis

2.1 Abstract

Ciliopathies are genetic disease syndromes that can manifest obesity and are caused by underlying primary cilia dysfunction. Mutations in *THM1*, an intraflagellar complex A component which facilitates ciliary protein transport, have been reported in patients with Bardet-Biedl Syndrome, which presents obesity as a cardinal clinical feature. Previously, we have shown that global deletion of *Thm1* in adult mice causes hyperphagia and obesity. Here, we show that *Thm1* deficiency markedly enhances adipogenesis. shRNA-mediated *Thm1* knock-down of 3T3-L1 pre-adipocytes resulted in decreased ciliary length and increased lipid accumulation. When pre-adipocytes are differentiated into mature adipocytes, *Thm1* loss results in earlier AKT and ERK signaling activation, and nuclear expression of adipogenesis transcriptional regulators, C/EBPα and PPARγ. Further, insulin treatment caused greater AKT and ERK phosphorylation in *Thm1*-deficient pre-adipocytes, suggesting increased insulin sensitivity. Together, these data indicate that *Thm1* deficiency in pre-adipocytes promotes differentiation and insulin signaling.

2.2 Introduction

Obesity has become a significant global health concern. Obesity affects almost 1 in 3 individuals worldwide[38] and associates with insulin resistance that can lead to Type II diabetes, cardiovascular disease and non-alcoholic fatty liver disease, placing individuals at heightened health risk. In light of this obesity epidemic, adipose tissue biology has garnered much interest. Adipose tissue plays a critical role in insulin sensitivity, and serves both as an energy depot and an endocrine organ[101]. In the latter role, adipose tissue secretes adipokines that are received by multiple organs, including the brain, liver, skeletal muscle, and pancreas, regulating systemic energy homeostasis. Expansion of adipose tissue results largely from hypertrophy or the enlargement of adipocytes in adult-onset obesity, or from a combination of hypertrophy and hyperplasia, which is the increased formation of adipocytes from precursor cells, in early-onset obesity[101]. Hypertrophy without hyperplasia is associated with adipocytes with metabolic dysfunction, while formation of new adipocytes from pre-adipocytes may promote healthy metabolism[101-103].

Genetic disorders which manifest obesity can provide valuable insight into cellular and molecular mechanisms. Such genetic disorders include ciliopathies, which are caused by an underlying primary cilia defect[104]. Primary cilia are singular, appendage-like organelles that transmit extracellular signals to the cell interior to regulate cellular processes, such as proliferation and differentiation, in a context-dependent manner. Since most vertebrate cells have a primary cilium, ciliopathies manifest multiple clinical features, which include renal, hepatic and pancreatic cystic diseases, retinal degeneration, as well as limb, neural, and craniofacial defects[12]. In two ciliopathies, Bardet-Biedl Syndrome (BBS) and Alström Syndrome, obesity presents as a central clinical feature, linking obesogenic processes to ciliary dysfunction[105,106].

Primary cilia extend from a modified centrosome known as the basal body, and are constructed and maintained via intraflagellar transport (IFT) or the bi-directional transport of protein cargo, which includes structural and signaling molecules, along a microtubular axoneme[12,107]. Protein complexes that mediate IFT can be classified as IFT-B or –A. IFT-B associates with the kinesin-2 motor to mediate anterograde IFT from the ciliary base to the tip, while IFT Complex A proteins and the cytoplasmic dynein motor mediate retrograde IFT from the ciliary tip to the base[12]. IFT-A proteins are also required for the ciliary entry of several membrane receptors in mammalian cells[22,108]. Eight proteins (BBS1, BBS2, BBS4, BBS5, BBS7, BBS8, BBS, and BBS18/BBIP1) conglomerate into a multi-protein complex, the BBSome[109,110], which transports signaling molecules to the cilium. Three other BBS proteins (BBS6, BBS10, and BBS12) form a BBS-chaperonin complex together with BBS7 to facilitate formation of the BBSome[111,112]. In *Chlamydomonas,* BBS proteins have also been shown to act as adaptors between IFT complexes and cargo, facilitating transport of signaling molecules within cilia[113]. In mammalian cells, evidence suggests BBS proteins may act in a similar fashion to enable ciliary trafficking of polycystin proteins[114,115], which are deficient in Autosomal Dominant Polycystic Kidney Disease.

While mutations of a single gene, *ALMS1,* cause Alstrom Syndrome[106], 21 *BBS* genes have been identified to date[116-119]; reviewed in[50]. Most BBS cases are autosomal recessive, but some also show evidence of tri-allelic inheritance[47,51]. In particular, heterozygous mutations of *THM1* (TPR-containing Hedgehog Modulator 1; also known as *TTC21B*), which encodes an IFT-A protein[20], have been identified in BBS patients who bear additional mutations in *BBS* genes[43].

In vitro adipogenesis studies have demonstrated that primary cilia present on confluent pre-adipocytes, lengthen during early differentiation stages, but shorten during later stages and are absent in mature, lipid-filled adipocytes[120]. *BBS10* and *BBS12*-patient derived fibroblasts and BBS12-deficient human primary mesenchymal stem cells showed enhanced adipogenesis[57,58]. In contrast, knock-down of *Ift88*, an IFT-B component, of *Kif3a*, a kinesin subunit, or of *Alms1,* whose gene product localizes to the basal body, inhibited adipocyte differentiation of 3T3-L1 mouse pre-adipocytes[60,121]. BBS10 and BBS12 deficiency reduced the number of ciliated cells *in vitro*[58]. *In vivo,* loss of IFT Complex B components results in short or absent cilia[17], while *Alms1*-mutant mice showed gradual loss of cilia[122]. The opposing effects on adipogenesis suggest differing roles of these ciliary proteins in regulating adipogenesis. Consistent with the notion that increased adipogenesis may benefit metabolism, obese *Bbs12* knockout mice showed enhanced glucose and insulin metabolism[57,58]. However, in contrast, lean, calorie-restricted *Bbs4* mice were insulin-resistant[123], indicating complexity in the roles of various BBS proteins in determining adipocyte metabolic health.

The role of an IFT-A protein in adipogenesis has not been reported. We have shown that THM1 loss impairs retrograde IFT, resulting in protein accumulation in swollen distal tips of shortened cilia[20], characteristic of an IFT Complex A mutant ciliary phenotype. Consistent with *THM1* mutations present in BBS patients, deletion of *Thm1* in adult mice causes hyperphagia and obesity, and the obese phenotype is preceded by misregulation of genes that encode neuropeptides that regulate appetite[32]. To determine additional underlying mechanisms of *Thm1*-deficient obesity, we have examined the role of *Thm1* deficiency in adipogenesis. Our findings suggest that diminished levels of this IFT Complex A protein promote adipogenesis and enhance insulin sensitivity.

2.3 Methods

2.3.1 Generation of 3T3-L1 Thm1kd cell line

3T3-L1 *Thm1* knockdown and empty vector (control) cell lines were generated using lentiviral transfection as described[20]. Briefly, viral particles were created by transfecting three plasmids, 4.2µg vector (pLKO.1 or pLKO.1-*Thm1* 5'-GTTCGTAGATGCCATTGAA-3', 7.4 µg delta 8.2 and 0.4 µg VSVG into 293T packaging cells using the Viafect Transfection Reagent (Promega, E4983) and incubated at room temperature for 20 minutes. The mixture was then incubated with 293T cells for 48 hours, after which supernatant was collected and filtered to obtain viral particles. Viral particles were placed onto 293T cells for 4 hours before media was changed. To obtain cells containing the construct, cells were selected with 1µg/ml puromycin. Individual clones were isolated using cloning disks (VWR) immersed in Trypsin, and expanded.

2.3.2 Differentiation Assay

3T3-L1 cells were maintained as pre-adipocytes in pre-adipocyte expansion media containing 90% Dulbecco's Modified Eagle's Medium DMEM (ATCC, 30-2002), 10% Bovine Calf Serum (ATCC, 30-2030) and 1% penicillin/streptomycin. To maintain in a pre-adipocyte state, cells were passaged at 70% confluency. Cells were maintained in the pre-adipocyte media until two days post-100% confluency. Two days post confluency was considered Differentiation Day 0 (DD0). At DD0, pre-adipocyte media was removed and re-placed with adipocyte expansion media containing DMEM (ATCC), 10% Fetal Bovine Serum (FBS) (Sigma), 1% penicillin/streptomycin, 1.0 µM dexamethasone (Sigma, D4902-25MG), 0.5 mM methylisobutylxanthine- IBMX (Sigma, I587-1G) and 1.0 µg insulin (Sigma, I0516-5ML) until Differentiation Day 2 (DD2) (48 hours). Adipocyte expansion media was then removed and

replaced with adipocyte maintenance media containing DMEM (ATCC), 10% FBS and 1.0µg insulin (Sigma, I0516-5ML) until differentiation day 8 (DD8).

2.3.3 Oil Red O Staining

3T3-L1 empty vector (EV) and *Thm1* knockdown cells were seeded on poly-l-lysine coated coverslips in a 24 well plate and differentiated according to the differentiation assay. At Differentiation Day 8 (DD8), cells were fixed with 4% PFA for 1 hour. Cells were then incubated with 60% isopropanol for 5 minutes and subsequently incubated with Oil-Red O (Sigma, O0625) stain for 20 minutes. After removing Oil Red O stain, cells were stained with Hematoxylin (Sigma, HHS32) for 20 seconds, rinsed, and then coverslips were inverted and mounted with fluoromount (Electron Microscopy Sciences, 17984-25) on a slide.

2.3.4 Immunofluorescence Staining

Cells were seeded on Poly-l-Lysine coated coverslips in 24 well plates. At experimental time points, cells were fixed with 4% PFA in PBST containing 0.1% Triton x-100 for 10 minutes at room temperature. Cells were then blocked in 2% Bovine Serum Albumin (BSA) (Sigma, A9647) overnight at 4°C. Primary antibodies were then added in blocking solution and incubated overnight at 4°C. Primary antibodies used include: PPARγ (Cell Signaling, 2435S, 1:200), CEBPα (Cell Signaling, 8178S, 1:100), ARL13b (Proteintech, 17711-1-AP, 1:300), γ-tubulin (Sigma, T6793, 1:4,000), IFT81 (Proteintech, 11744-1-AP). Cells were then incubated with secondary antibody (Life Technologies, 1008648, 1:500) for 1 hour at room temperature. Slides were incubated with BODIPY stain (Fisher, 1:1,000) for one hour at room temperature, inverted, and mounted on slides using fluoromount with DAPI (Electron Microscopy Services 17984-24).

Slides were visualized and captured using a Nikon80i microscope attached to a Nikon DS-Fi1 camera.

2.3.5 Western Blot

3T3-L1 EV and *Thm1kd* cells were collected and protein was extracted using passive lysis buffer (Promega, E1941) and protease/phosphatase inhibitor mini tablets, EDTA free (Thermo, 88669). Briefly, cells were resuspended and mixed in lysis buffer for 15 minutes. After which, cells were pelleted and protein was collected. Sample lysates were prepared and loaded onto a 4-20% SDS-gel (BioRad 456-1093 (10 well) or 456-1096 (15 well)). Membranes were probed for various antibodies: Thm1 (Sigma, HPA035495, 1:3,000), Phosphorylated AKT (Cell Signaling, 4060S, 1:2,000), Phosphorylated Erk (Cell Signaling, 9106S, 1:2,000), AKT (Cell Signaling, 4691S, 1:1,000), ERK (Cell Signaling, 9102, 1:2,000), B-Actin (Cell Signaling, 3700S, 1:1,000), PPARγ (Cell Signaling, 2435S), CEBPα (Cell Signaling 8178S).

2.4 Results

2.4.1 Thm1 deficiency promotes adipogenesis

To determine a role for *Thm1* deficiency in adipogenesis, 3T3-L1 mouse pre-adipocytes were infected with lentiviruses expressing *Thm1* shRNA. Following selection with puromycin, cells were clonally selected and expanded. Western blot analysis for THM1 showed that *Thm1* knockdown clone 3 had the greatest knockdown (Figure 2.1A). Therefore, this line was designated as *Thm1* knockdown and used for all subsequent analyses. We examined the capacity of *Thm1* knockdown pre-adipocytes to form mature adipocytes in an *in vitro* differentiation assay. Two days post-confluency, pre-adipocytes were induced by addition of dexamethasone, isobutylmethylxanthine, insulin, and fetal bovine serum to the cell culture medium for two days,

then maintained in media containing insulin and fetal bovine serum for six days. Differentiation into mature adipocytes was determined by assessing formation of lipid droplets that were stained by Oil Red O. In the experiment shown at higher magnification, 4.5% of empty vector (EV) cells and 89.2% of *Thm1* knockdown cells were lipid-laden, revealing that *Thm1* deficiency markedly enhances adipogenesis (Figure 2.1B).

We examined ciliary phenotype of *Thm1* knockdown pre-adipocytes. Post-confluent cells were immunostained for ciliary markers, acetylated alpha tubulin and IFT81, as well as for ARL13B and basal body marker, gamma tubulin. *Thm1* knockdown cells showed shorter ciliary length (Figures 2.1C and 2.1D).

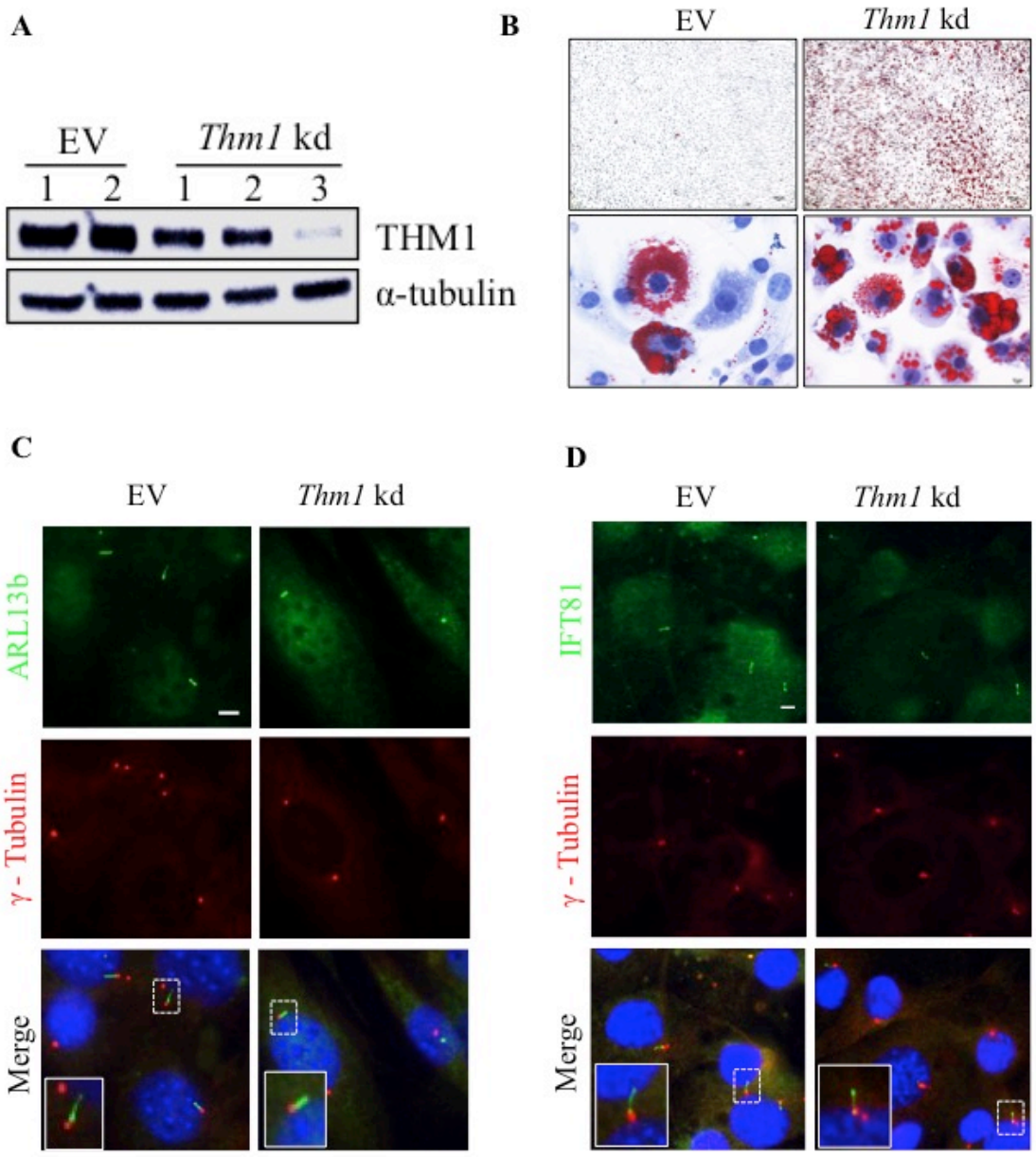

Figure 2.1. *Thm1* knockdown in pre-adipocytes enhances differentiation. (A) Western blot analysis of control and *Thm1* knockdown 3T3-L1 pre-adipocyte clonal lines shows decreased THM1 protein amounts. (B) Increased Oil red O staining at DD8 in *Thm1* kd cell lines. (C) Primary cilia of control and *Thm1* knockdown clonal lines are shorter than cilia in the EV cell line. (D) IFT81 localization in control and *Thm1* knockdown clonal lines shows an accumulation in *Thm1* kd cells.

2.4.2 Nuclear C/EBPα and PPARγ is increased in Thm1 deficient cells

Differentiation of pre-adipocytes into mature adipocytes is orchestrated by downregulation of Wnt and Hedgehog (Hh) signaling pathways, and activations of AKT and ERK pathways, leading to expression of adipocyte master transcriptional regulators, Caat/Enhancer Binding Protein alpha (C/EBPα) and Peroxisome proliferator-activated receptor gamma (PPARγ). Using Western blot, we examined levels of C/EBPα and PPARγ throughout the differentiation process, and observed that both of C/EBPα and PPARγ were markedly elevated in *Thm1* knockdown cells at differentiation day 5 (DD5) and DD8 relative to control cells (Figure 2.2A). To determine the subcellular localization of C/EBPα and PPARγ, we immunostained cells for of C/EBPα and PPARγ together with boron-dipyrromethene (BODIPY), a fluorescent dye with affinity to lipids. We observed that as early as DD1, *Thm1* knockdown cells showed increased nuclear localization of C/EBPα and PPARγ relative to control cells (Figure 2.2B). At this early differentiation stage, lipid droplets have not yet formed. At DD8, both control and *Thm1* knockdown cells showed lipid droplets as observed by BODIPY stain, and *Thm1* knockdown cells continued to show increased nuclear of C/EBPα and PPARγ expression.

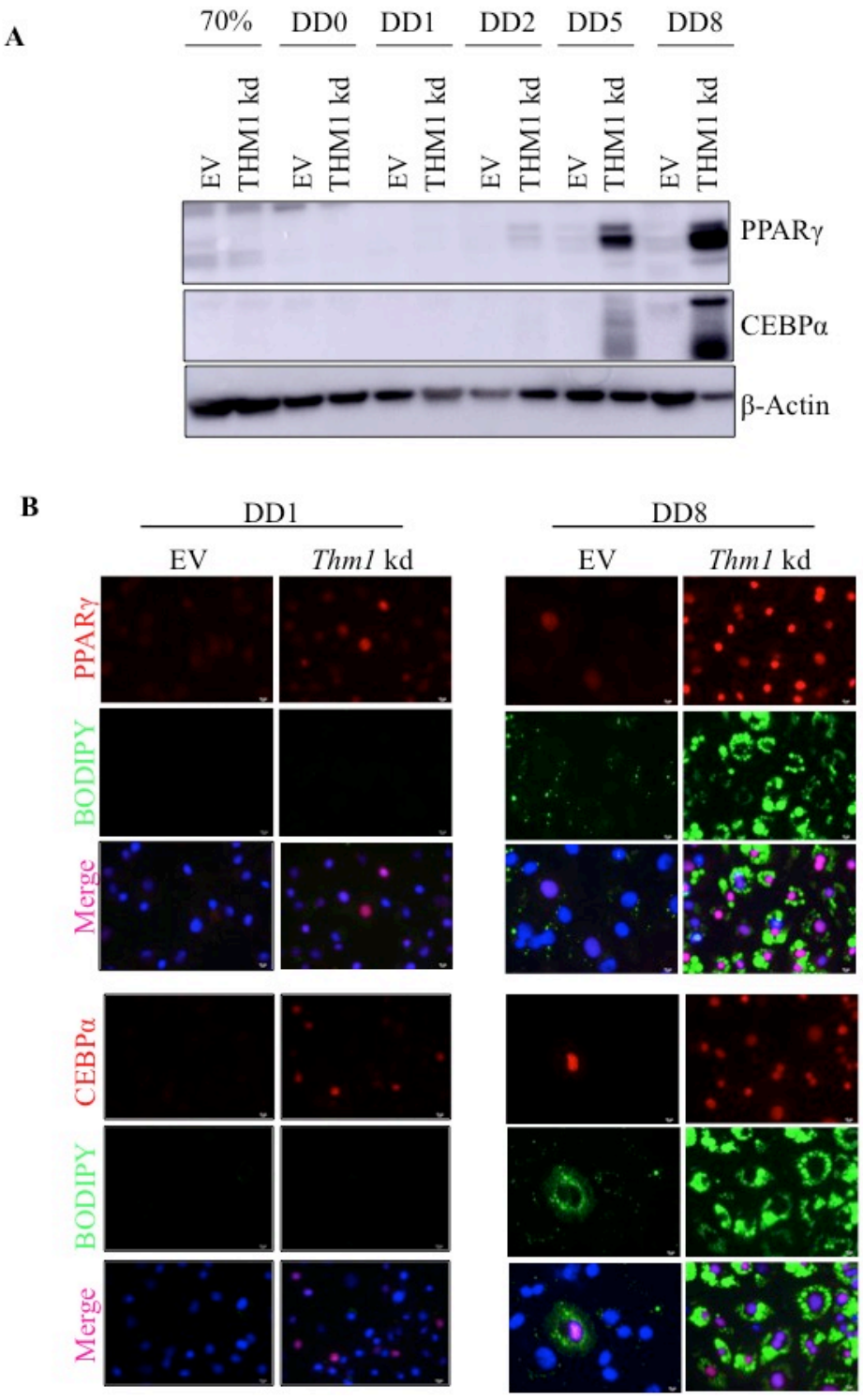

Figure 2.2. *Thm1* deficient 3T3-L1 cells show earlier upregulation of C/EBPα and PPARγ during differentiation. (A) Representative Western blot shows upregulation of C/EBP α and PPAR γ at DD5 and DD8 in the *Thm1* kd cell line. (B) Immunostaining for C/EBPα and PPARγ at DD1 and DD8 shows upregulation of C/EBP α and PPAR γ in *Thm1* kd cells at DD1 and DD8.

2.4.3 AKT and ERK signaling are increased in Thm1 knockdown cells

To determine which signaling pathways may promote differentiation of *Thm1* knockdown pre-adipocytes, we examined ERK and AKT signaling pathways throughout the differentiation process. Western blot analysis revealed a trend of elevated P-AKT/AKT ratios in *Thm1* knockdown pre-adipocytes at 70% confluency and at DD0, and a trend of increased P-ERK/ERK ratios in *Thm1* knockdown cells at DD1, suggesting the *Thm1* ciliary defect in pre-adipocytes may promote AKT and ERK signaling (Figure 2.3).

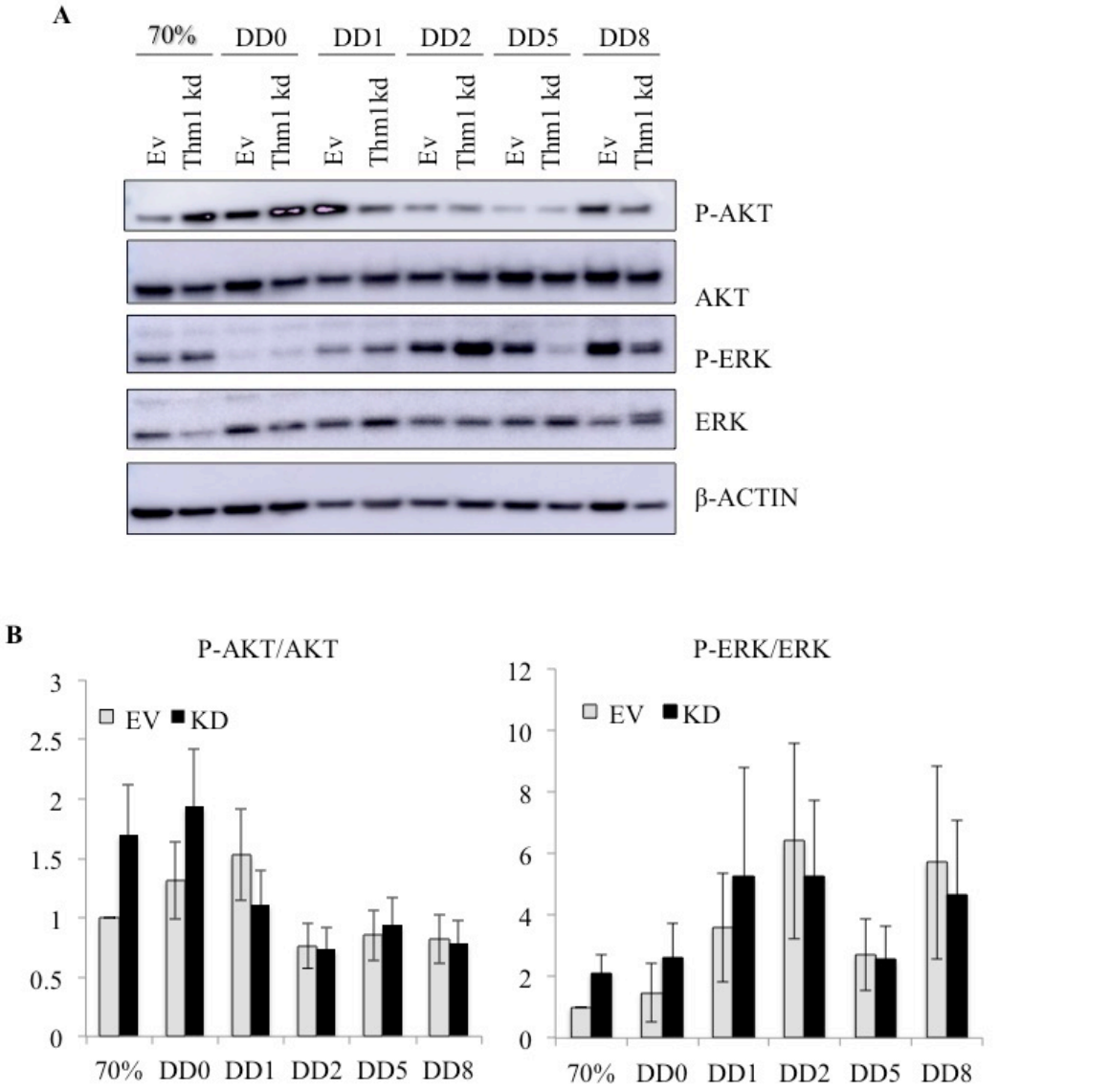

Figure 2.3. *Thm1* deficient 3T3-L1 cells exhibit earlier peak activation of AKT and ERK during differentiation. (A) Representative Western blot and (B) Quantification indicates a trend of earlier PAKT/AKT and PERK/ERK expression in the *Thm1* kd cell line. Bars represent mean ± standard error of the mean. N=4.

2.4.4 Thm1 knockdown pre-adipocytes are sensitized to insulin signaling

Insulin signaling is an important component in pre-adipocyte differentiation and activates AKT and ERK pathways. To examine insulin signaling in *Thm1* knockdown pre-adipocytes, cells at DD0 were treated with 100nM insulin for various durations. We observed that insulin treatment resulted in increased P-AKT/AKT and P-ERK/ERK ratios in *Thm1* knockdown cells relative to control cells (Figure 2.4), suggesting increased insulin sensitivity. These data suggest deficiency of *Thm1* sensitizes pre-adipocytes to insulin signaling.

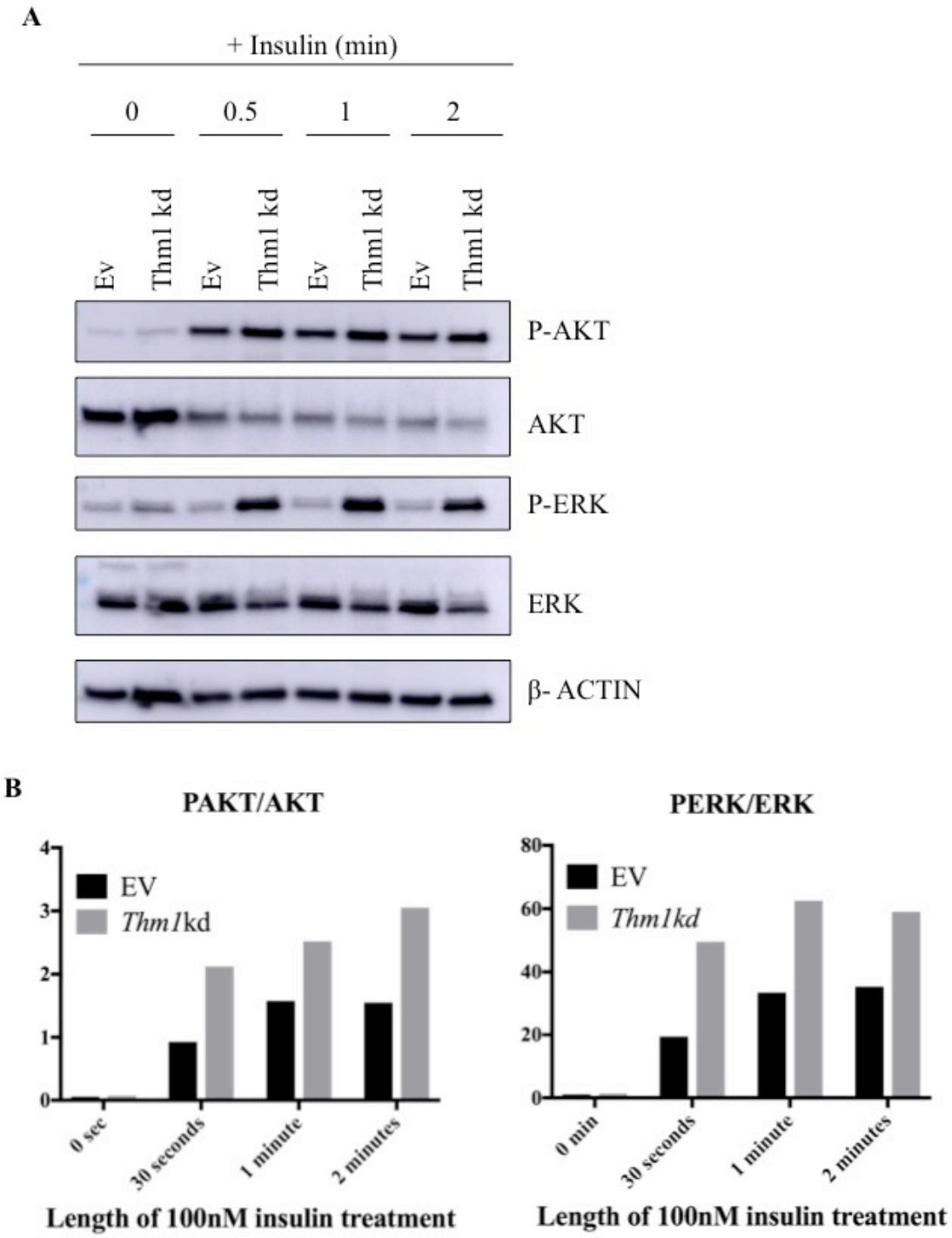

Figure 2.4. *Thm1* deficient 3T3-L1 cells are sensitized to insulin. (A) Western blot analysis of AKT and ERK activation in insulin-stimulated pre-adipocytes at DD0. (B) Quantification of western blot in A suggests an increase in PAKT/AKT and PERK/ERK ratios in the *Thm1* kd cell line in response to insulin treatment.

2.5 Discussion

Obesity results when caloric intake exceeds energy utilization[102]. Adipose tissue senses changes in energy intake by inducing hypertrophy and hyperplasia. When hypertrophy exceeds hyperplasia, this may result in overproduction of biologically active metabolites that may lead to inflammation and adipocytes that are metabolically unhealthy[101]. Conversely, hyperplasia may promote metabolically healthy adipocytes, and therefore, modulating hyperplasia may have therapeutic potential.

In this study, we provide the first demonstration of the role of an IFT Complex A protein in adipogenesis. We show that *Thm1* deficiency in 3T3-L1 pre-adipocytes markedly enhances adipogenesis. Expression trends indicated *Thm1* knockdown in 3T3-L1 pre-adipocytes showed a heightened response to insulin and earlier activation of AKT and ERK pathways during differentiation, culminating in elevated levels of C/EBPα and PPARγ compared to the EV cell line.

The differing roles of ciliary proteins in adipogenesis are increasingly apparent. Deficiency of *Thm1, BBS10* or *BBS12* promoted adipogenesis and insulin signaling, deficiency of *Ift88* or *Kif3a* suppressed adipogenesis and decreased insulin sensitivity[59], while deficiency of *Alms1* inhibited differentiation, but did not affect insulin response[60]. These differences may reflect that ciliary proteins work in concert to tune the signaling pathways that regulate adipogenesis. Indeed, the cilium has been shown to intricately regulate the Hh signaling pathway[12]. Similarly, pro-adipogenic pathways, in particular, insulin signaling, may be fine-tuned at the cilium. In support of this, insulin signaling components have been shown to enrich in primary cilia or basal bodies of pre-adipocytes in response to insulin, including IGF1Rβ, IRS, and P-AKT[59,124]. The insulin receptor has also been localized to primary cilia of insulin-

stimulated β cells of the pancreas[56]. Additionally, *Bbs1* or *Bbs2* deficiency in HEK293T cells or in mouse embryonic fibroblasts reduced levels of insulin receptor at the cell surface, suggesting a role for these BBS proteins or of the BBSome in intracellular trafficking of the insulin receptor[123].

Downregulation of anti-adipogenic pathways, Hh and Wnt, is essential for differentiation of preadipocytes[102,125]. Previously, we have shown that *Thm1* loss enhances Hh and Wnt activity in mouse embryonic tissues and cells[20]. Thus, prior to our experiments, we hypothesized loss of *Thm1* would result in inhibition of adipogenesis. Yet, in contrast to our expectations, *Thm1* deficiency promoted adipogenesis. The differing effects of *Thm1* deficiency in mouse embryonic tissues and in 3T3-L1 pre-adipocytes on Hh and Wnt signaling reflect that regulation of ciliary-mediated signaling pathways is context-dependent. Consistent with this notion, deletion of IFT Complex B gene, *Ift88* or of kinesin subunit, *Kif3a,* causes a loss of Hh signaling in early mouse embryos[17]. Yet instead of enhancing adipogenesis, *Ift88* or *Kif3a* knockdown in 3T3-L1 pre-adipocytes inhibited differentiation. To further delineate the mechanisms by which ciliary proteins regulate insulin signaling, determining which ciliary proteins mediate intracellular and ciliary trafficking of insulin signaling components, and determining the subcellular localization of insulin signaling components in the presence and absence of insulin and the possible mislocalization of insulin signaling components in various ciliary mutants are required.

Previously, we showed that *Thm1* conditional knockout mice are hyperphagic and that gene expression of appetite-controlling neuropeptides is misregulated prior to obesity onset[32]. Our present data suggest increased adipogenesis is an additional mechanism underlying *Thm1* deficient obesity.

In summary *Thm1* deficiency enhances adipogenesis and insulin signaling, contrasting with deficiency of IFT-B or BBSome proteins, and resembling deficiency of BBS-chaperonin proteins, BBS10 and BBS12. This suggests possible common mechanisms between THM1, BBS10 and BBS12 or between IFT Complex A and BBS-chaperonin complexes. Given that *THM1* mutations have been identified in combination with *BBS* mutant alleles in BBS patients[43], our data suggest that *THM1* mutations may modify insulin sensitivity in these patients. Further studies are required to elucidate the mechanisms underlying the differing roles of ciliary classes and proteins eg. IFT-B, IFT-A, BBS, Alström1, in adipogenesis and insulin signaling. Polymorphisms in *BBS* genes have been associated with obesity in a general population, suggesting a more widespread relevance for BBS-and cilia-mediated mechanisms[126]. Increasing our understanding of the cellular and molecular processes that drive hyperplasia of adipose tissue will enable identification of novel therapeutic targets and combinatorial strategies that may be most effective.

Chapter Three: Novel Role of *Thm2* and *Thm1* in Skeletal Development

3.1 Abstract

Ciliopathies are genetic disorders caused by mutations of genes that encode proteins that localize to the cilium. The clinical phenotypes of ciliopathies include obesity, cystic kidney disease, infertility, and skeletal abnormalities. Loss of *Thm1,* an intraflagellar complex A gene, results in a myriad of embryonic and post-natal abnormalities. Here, we study the role of a novel gene, *Thm2,* which is a paralog of *Thm1*. We have found *Thm2* localizes to the axoneme of the primary cilium, establishing THM2 as ciliary protein. Unlike loss of *Thm1,* which results in shortened primary cilia, *Thm2* knockdown in 293T cells results in normal cilia length, suggesting *Thm2* is dispensable for ciliogenesis. To determine a role for *Thm2 in vivo, Thm2* knockout mice were generated using a construct from the Knockout Mouse Project (KOMP) consortium. Unexpectedly, *Thm2*-null mice survive into adulthood with seemingly normal health. Since paralogs can have redundant functions, a null allele of *Thm1 (alien)* was used to determine a role for *Thm2*. At post-natal days 14 and 21, $Thm2^{-/-};Thm1^{aln/+}$ mice backcrossed five generations onto a C57BL6/J background are significantly smaller than control littermates and tibia growth plates show an increase in the length of the proliferation zone and a decrease in the length of the hypertrophic zone at P14. Together, these data establish THM2 as a ciliary protein necessary for skeletal development.

3.2 Introduction

Skeletal dysplasias affect 1:5,000 people and are often characterized by short stature leading to a wide range of clinical outcomes[41]. Many bones in the skeleton develop through a process known as endochondral ossification[69]. Endochondral ossification occurs when mesenchymal progenitor cells differentiate into chondrocytes which undergo a highly organized maturation process, resulting in apoptosis[69]. Osteoblasts then use the matrix secreted by chondrocytes as a template to form the bone[72]. Growth plates are found between primary and secondary ossification centers in long bones and contain chondrocytes which can be divided into different regions, such as the proliferating and hypertrophic zones[72]. Proliferating chondrocytes become hypertrophic chondrocytes before they undergo apoptosis and are replaced by osteoblasts[72]. One of the signaling pathways the growth plate is dependent on is a feedback loop established between parathyroid hormone-related peptide (PTHrP) and Indian hedgehog (*Ihh*) signaling which regulates the proliferation and maturation of chondrocytes[72].

Primary cilia are found on the surface of nearly all vertebrate cells[11] and are essential for Hedgehog (Hh) signal transduction[12]. The presence of Hh ligand triggers enrichment of Smoothened signal transducer in the primary cilium and culminates in activation of the *Gli* transcription factors[14]. The structure and function of primary cilia depend on two intraflagellar transport (IFT) protein complexes[11]. IFT Complex B proteins mediate anterograde trafficking, powered by the kinesin motor, along the ciliary axoneme, while IFT Complex A proteins, and the dynein motor, mediate retrograde trafficking[11]. Complex A proteins can also mediate the ciliary entry of membrane receptors[22]. Direct evidence connecting cilia dysfunction to skeletal abnormalities is found in patients with genetic disorders classified as ciliopathies[38]. Ciliopathies result in a broad range of clinical phenotypes including retinal degeneration, cystic kidney

disease, obesity, cognitive defects, and skeletal abnormalities[40]. Ciliopathies characterized by skeletal abnormalities include Short-Rib Polydactyly Syndromes (I-IV)[62], Jeune Asphyxiating Thoracic Disorder Syndrome (JATD), Oro-facial-digital syndrome type 1 (OFD1), and Ellis van Creveld syndrome (EVC)[38]. Of interest, mutations in *Thm1*[43] have been found in patients diagnosed with JATD, a disorder resulting in skeletal abnormalities, including a small thoracic cavity which often leads to respiratory insufficiency, shortened limbs, and polydactyly[64].

Previously, mouse models harboring mutations in *Ift* genes have revealed the importance of functioning primary cilia in skeletal development. While a mutation resulting in loss of the complex A protein, THM1, resulted in peri-natal lethality[20], hypomorphic mutations of *Ift144* and *Ift140* resulted in embryonic lethality[66,67]. Nonetheless, all IFT Complex A mutants were characterized by polydactyly, and abnormal development of the ribs of the thoracic cavity during embryonic development[31,66,67]. Hypomorphic mutation of the IFT Complex B gene, *Ift80,* resulted in the majority of mice exhibiting embryonic lethality[79]. However, the mice that did survive past birth exhibited skeletal abnormalities including shortened long bones, polydactyly, disorganization of the growth plate, and abnormal rib development[79]. Another IFT Complex B gene, *Ift88,* was conditionally deleted using a *Prx1 Cre recombinase,* which is expressed in the limb bud and some craniofacial mesenchyme and resulted in polydactyly, embryonic and post-natal shortening of the long bones and defects in growth plate organization[81]. Taken together, these data highlight an essential role for IFT proteins in skeletal development.

Although ciliary proteins are crucial to the proper development of the skeleton, the function of all proteins within the ciliary proteome is unknown. Previously, we identified *Thm1* as an IFT Complex A protein, and negative regulator of Hh signaling, important in embryonic development[20], and post-natal tissue maintenance[26,32]. To determine the role of a novel ciliary

gene and paralog of *Thm1, Thm2*[20], we created the first known *in vitro* and *in vivo* models of *Thm2* deficiency. Here, we establish a role for *Thm2,* together with *Thm1,* in post-natal skeletal development.

3.3 Methods

3.3.1 Generation of THM2 knockdown cell line

Lentiviral transfection was used to generate a 293T *Thm2* knockdown cell line. Briefly, viral particles were created by transfecting three plasmids, 4.2µg vector (*Thm2* shRNA sequence GACTTTGATTAATTACTAT), 7.4 µg delta 8.2 and 0.4 µg VSVG into 293T packaging cells using the Fugene transfection reagent (Promega, E2691) and incubated at room temperature for 20 minutes. The mixture was then incubated with 293T cells for 48 hours, after which supernatant was collected and filtered to obtain viral particles. Media was then placed onto 293T cells for 4 hours before media was changed. To obtain cells that had integrated the construct, cells were selected with 1µg/ml puromycin. Cells were seeded sparsely to allow growth and selection of cell clones using cloning disks immersed in Trypsin. Clones were then expanded.

3.3.2 Immunofluorescence Staining

Retinal pigment epithelial (RPE) or human embryonic kidney (293T) cells were seeded on Poly-L-Lysine coated coverslips and grown and serum starved overnight and fixed with 4% PFA in PBS containing 0.1% Triton x-100 for 10 minutes at room temperature. Fixed RPE or 293T cells were blocked in 2% Bovine Serum Albumin (Sigma, A9647) overnight at 4°C. THM2 (Custom-made Antibody, Proteintech S4132-2, 1:50) and acetylated α-tubulin (Sigma T6557, 1:4,000) were incubated with cells in 2% BSA overnight. Cells were incubated with

secondary antibody (Life Technologies, A11005 and A11008, 1:500) for 1 hour at room temperature, inverted, and mounted on slides using fluoromount with DAPI (Electron Microscopy Services 17984-24). RPE cells were imaged on a Leica confocal microscope (Leica TCS SPE) while 293T cells were imaged on a light microscope (Nikon 80i) attached to a camera (Nikon DS-Fi1).

3.3.3 Generation of THM2 knockout mouse

Thm2 knockout-first C57BL/6J embryonic stem cells were obtained from the NIH Knockout Mouse Project (KOMP) Repository (www.komp.org). These embryonic stem cells were confirmed to contain the correct *Thm2* knockout construct exhibiting evidence of homologous recombination and correct karyotype, and subsequently, were injected into C57BL/6J-*Tyr*$^{c\text{-}2J}$ (albino) blastocysts and implanted into female mice by Dr. Melissa Larson at the University of Kansas Medical Center Transgenic and Gene Targeting Facility. Resulting male chimeras were mated to multiple females. Genomic DNA from tails of resulting pups with black coat color was genotyped by polymerase chain reaction (PCR) and PCR amplicons were sequenced to confirm presence of the construct in the DNA. The KOMP allele contains a LacZ neo construct flanked by flippase recombinase (FLP) recombinase target (FRT) sites. Mice containing the KOMP construct were mated to a mouse carrying a FLP recombinase (Jackson Laboratories, 009086) to excise the LacZ-Neo cassette. Resulting mice were then mated to mice expressing cytomegalovirus (CMV) Cre recombinase (Jackson Laboratories, 006064) to excise exon 6, which created a premature stop codon, and *Thm2* null allele.

3.3.4 Genotyping of Thm2 knockout mouse

Genotyping primers were designed flanking the lox-P sites surrounding exon 6. Primer sequences used include: *Thm2*-KO-F- 5' CAG ATA TCT CCC CAC TTG TTA ACG 3', and *Thm2*-KO-R- 5' GTG TCA GAT ACC CTG GAA CCA GAG 3'. With these primers, a WT band is amplified at a size of 1,086bp while a knockout band is amplified at a size of approximately 400bp. At times, the PCR reaction favors the amplification of the knockout band, making the WT band difficult to see. Therefore, to confirm the presence or absence of a WT allele, an additional PCR reaction is performed using primers within exon 6, *Thm2*-WT-F-5'AAC TTC CTG CCC GCT TTA GT 3', and *Thm2*-WT-R-5' GTG TCA GAT ACC CTG GAA CCA GAG 3'. This PCR reaction results in a WT amplicon of approximately 461bp, indicating the presence of a WT allele. PCR products are run on a 0.7% agarose gel for the detection of the recombined band and a 2% agarose gel for detection of the WT band.

3.3.5 Generation of $Thm2^{-/-};Thm1^{aln/+}$ mice

$Thm2^{-/-};Thm1^{aln/+}$ mice were generated by intercrossing $Thm2^{-/+}$ mice on a C57BL/6 background with $Thm1^{aln/+}$ mice on an FVB background. $Thm2^{-/+};Thm1^{aln/+}$ mice were backcrossed five generations onto a C57BL6/J background and then intercrossed to generate $Thm2^{-/-};Thm1^{aln/+}$ mice.

3.3.6 Western Blot

293T cells and mouse tissues were collected and protein was extracted using passive lysis buffer (Promega, E1941) containing protease inhibitors (Thermo Scientific, 88669). Briefly, samples were resuspended and mixed in lysis buffer for 15 minutes (293T cells) or resuspended

in lysis buffer and homogenized (tissues). Cells and tissues were then pelleted and supernatants were collected. Sample lysates were prepared and loaded onto a 4-20% SDS-gel (BioRad, 456-8094). Gels were run for approximately 3.5 hours at 90V to allow for adequate separation between bands. Membranes were incubated with THM2 antibody using a Western blot procedure as described (Tran et al., 2008). THM2 antibody was targeted to N' Cys-RRQNYETAINLYHQVLEK, 963-980aa, in exon 22. (Proteintech S4132-2, 1:5,000).

3.3.7 Weight and Length Measurements

Total mouse body weight was measured in grams using a standard weighing scale. Crown to rump measurements in centimeters were taken manually using a standard ruler, measuring the length from the tip of the nose to the end of the rump. Total body weights and crown to rump measurements were recorded at post-natal days (P)14 and 21.

3.3.8 Embedding and Sectioning of Tibias and Kidneys

At P14, tibias of mice were dissected and placed in Cal-Ex, a decalcifying and fixing solution (Fisher C5511-1D) overnight, while kidneys were dissected, and once renal capsules were removed, were fixed in Bouin's fixative (Polysciences, Inc. 16045) overnight. Tibias and kidneys were placed into 70% ethanol in water. Tissues were processed and dehydrated through a series of ethanol washes and embedded in paraffin wax. Paraffin blocks were sectioned at 10μm and 7μm for tibias and kidneys, respectively.

3.3.9 Skeletal Preparations

Alizarin red and alcian blue staining was performed using standard protocols (Kingsley Lab Protocol, Ryan Roundtree, Version 1.1, 3/31/2003). Briefly, mice were eviscerated and fixed in 95% Ethanol for 1-2 days, and stained with alcian blue (Acros Organics 33864-99-2) for 14 days. After alcian blue staining, skeletons were fixed with 95% ethanol for an additional 1-2 days and cleared with potassium hydroxide for approximately 2-5 days, or until tissue was cleared. Skeletons were then stained with 1% alizarin red (Acros Organics 130-22-3) in potassium hydroxide for 1-2 days or until completely stained. Once staining was complete, skeletons were placed into glycerol for imaging and long-term storage. Skeletal preparations were then imaged (Leica M165C) and measured using Image J software.

3.3.10 Hematoxylin and Eosin Staining

Tibia and kidney sections at P14 were stained using standard hematoxylin and eosin staining methods. Briefly, sections were de-paraffinized and rehydrated through a series of ethanol rinses. Sections were then stained with Hematoxylin (Sigma HHS32) and Eosin (Sigma HT110216) before being dehydrated and mounted with Permanent Mounting Media (Fisher, SP15-500). Sections were imaged using a light microscope (Nikon 80i) attached to a Nikon DS-Fi1 camera.

3.3.11 Safranin O and Fast Green Staining

P14 tibia sections were stained using Safranin O and Fast Green Staining (American MasterTech, KTSFO). Briefly, sections were de-paraffinized and rinsed in 100% ethanol. Slides were stained with Weigert's Hematoxylin, 0.2% Fast Green, and Safranin O in separate steps.

After staining, sections were dehydrated in 100% Ethanol, cleared in Xylene and mounted using Permanent Mounting Media (Fisher SP15-500).

3.4 Results

3.4.1 THM2 localizes to the primary cilia

To determine the subcellular localization of THM2, we used a custom-made antibody, generated by Proteintech that recognizes an amino acid sequence in exon 22 of THM2. Since *Thm2* is a paralog of an established ciliary protein, *Thm1*[20], and both are orthologous to the IFT139 flagellar protein in *Chlamydomonas reinhardtii*[20], ciliary localization was investigated. Immunofluorescence staining for THM2 in retinal pigment epithelial (RPE) cells revealed localization throughout the axoneme of the primary cilium (Figure 3.1).

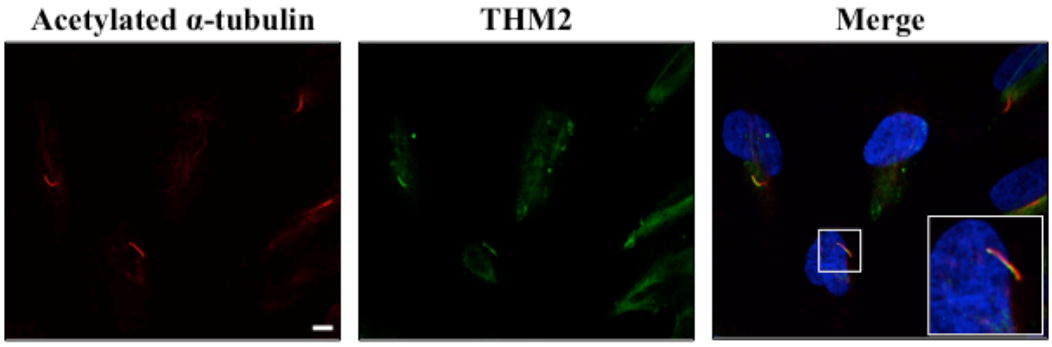

Figure 3.1. THM2 localizes to the primary cilium. Immunofluorescence staining of THM2 (green) and acetylated α-tubulin (red) in RPE cells. Scale bar equals 5μm.

3.4.2 In vitro loss of Thm2 does not affect cilia structure

In vitro and *in vivo* loss of *Thm1* results in short cilia with a bulb-like tip due to a decrease in retrograde IFT trafficking[20]. To examine the role of *Thm2* in cilia structure, we infected human embryonic kidney (293T) cells with lentivirus containing a shRNA targeted against *Thm2*. Clones were selected and expanded to generate clonal *Thm2* knockdown cell lines. Protein level analysis revealed clone, 2-1, showed the most efficient knockdown (Figure 3.2A). Cilia length was analyzed in EV 2-5 and *Thm2* knockdown 2-1 clonal cell lines. The primary cilia axoneme was stained for ARL13B (Figure 3.2B) and axoneme lengths were blindly measured using Metamorph software. Histograms of measured cilia lengths revealed no significant differences in cilia length distribution between *Thm2* knockdown and control cell lines (Figure 3.2C), suggesting THM2 loss alone does not affect ciliogenesis.

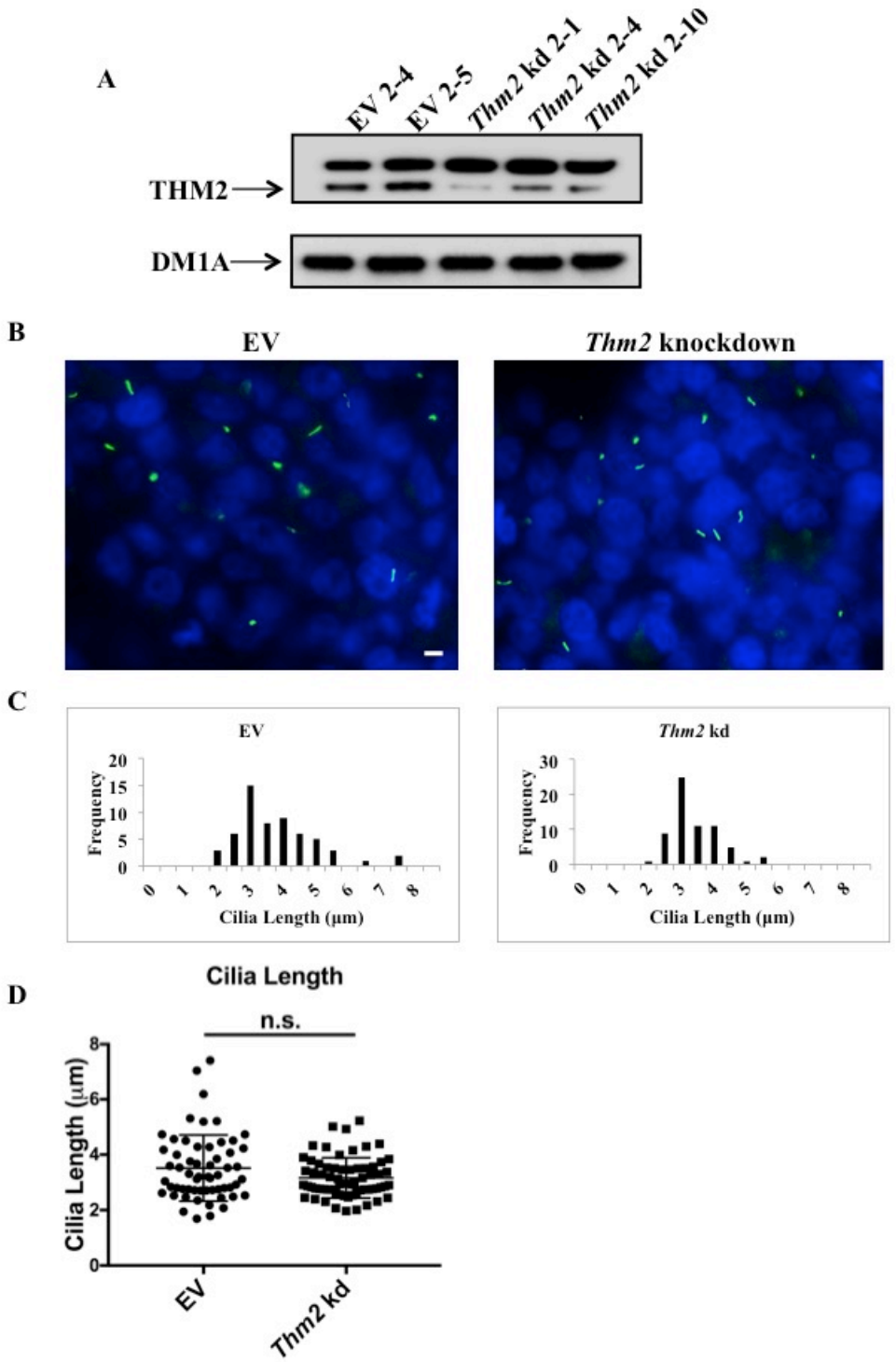

Figure 3.2. *Thm2* is dispensable for ciliogenesis. (A) Western blot analysis of clonally expanded *Thm2* knockdown clones, clone 2-1 showed the greatest decrease in THM2 expression and was used for cilia length analysis. Empty vector clone 2-5 was used for control measurements. (B) Immunofluorescence staining for primary cilia labeled with ARL13b (green) in control and *Thm2* knockdown cell lines and (C) Histogram distribution plots of primary cilia lengths in EV and *Thm2* knockdown cell lines indicate loss of *Thm2* does not affect ciliogenesis. Scale bar equals 10µm.

3.4.3 Generation of Thm2 knockout mouse model

To determine a role for *Thm2 in vivo*, we created the first *Thm2* knockout mouse model (*Thm2*$^{-/-}$). To generate this mouse model, a *Thm2* knockout mouse construct from the Knockout Mouse Project (KOMP) was used. Prior to my joining the lab, other lab members used a mouse harboring a flippase recombinase (FLP) to excise a LacZ neo construct flanked by flippase recombinase target (FRT) sites. Therefore, the mouse model I began to work with contained lox P sites flanking exon 6 (Figure 3.3A). Mice containing the KOMP allele were mated with mice expressing Cre recombinase driven by the cytomegalovirus promoter (CMV). This caused exon 6 to be excised, which created a premature stop codon, and *Thm2* null allele. To genotype these mice, primers were designed to flank exon 6 and revealed the presence of a WT band at 1,086bp and a recombined band at approximately 400bp. At times, the PCR reaction favored the amplification of the recombined (*Thm2*$^{-/-}$) allele. To ensure the presence or absence of a WT allele, a separate genotyping assay was used. If the WT allele was present, the genotyping assay revealed a band at 461bp (Figure 3.3B). Western blot analysis of P14 testis confirmed the loss of THM2 protein in the *Thm2* knockout mouse compared to the WT mouse (Figure 3.3C).

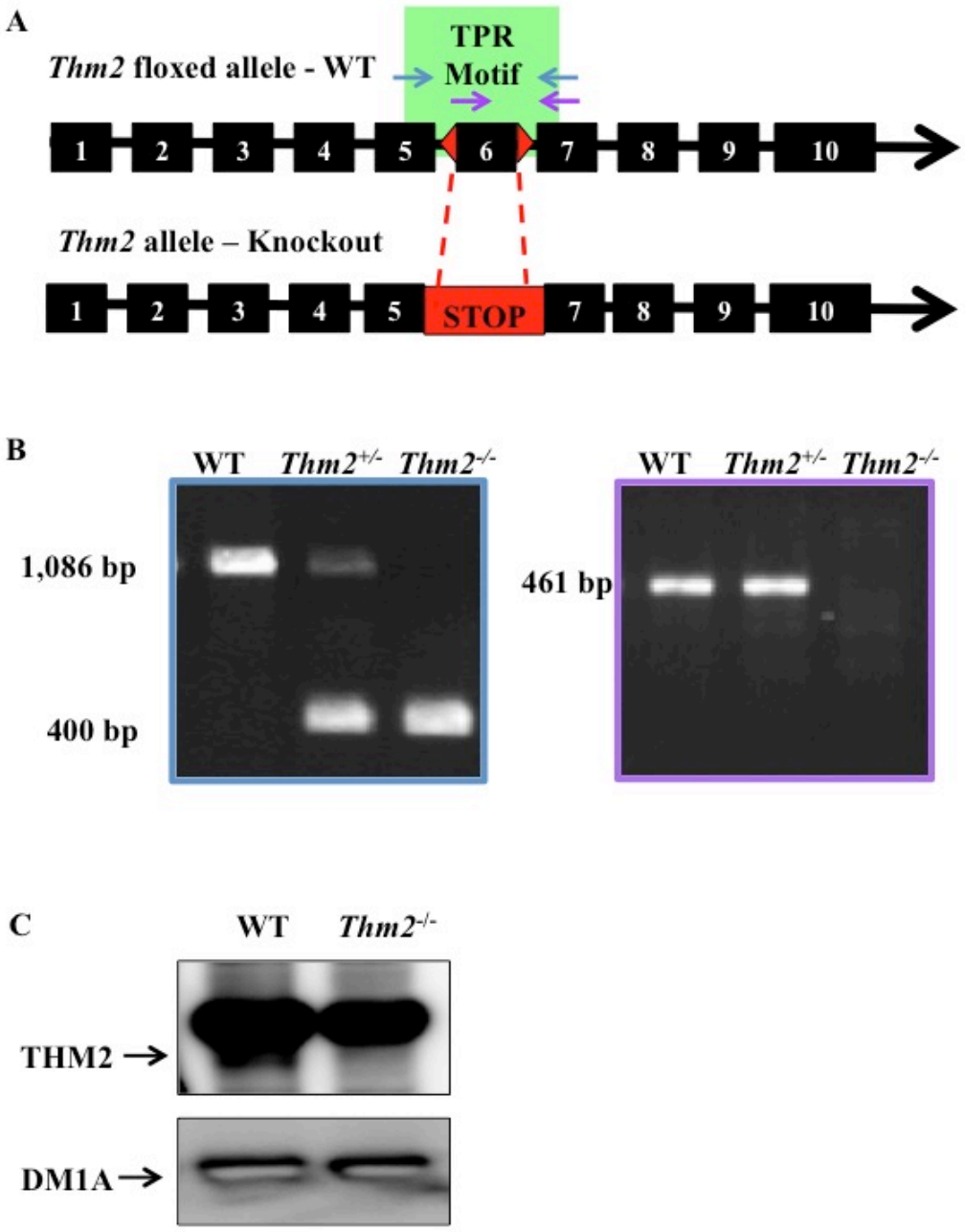

Figure 3.3. *Thm2*$^{-/-}$ mouse was generated using KOMP construct. (A) Schematic diagram of the KOMP construct in genomic DNA of *Thm2*. Exons are represented by black boxes and introns by the black line. Lox P sites surrounding exon 6 are depicted as red triangles. Genomic primers are indicated in blue (WT and recombination band) and purple (WT band). Once exon 6 is spliced out, a premature stop codon is created. (B) Representative images of genotyping results including WT, *Thm2*$^{+/-}$, and *Thm2*$^{-/-}$ mouse using primers indicated in blue and the confirmation of a WT band in the WT and *Thm2*$^{+/-}$ mice using primers indicated in purple. (C) THM2 western blot analysis of P14 testis extracts confirms loss of THM2.

3.4.4 Thm2$^{-/-}$; Thm1$^{aln/+}$ mice are smaller than control littermates

Since many mouse models harboring mutations in ciliary genes are embryonic lethal[20,21,66,67], we hypothesized that loss of *Thm2* would cause embryonic lethality. Unexpectedly, *Thm2* knockout mice survived into adulthood with seemingly normal health. Since paralogs can share redundant functions[127,128], a null allele of *Thm1 (aln)* was introduced. At P14, *Thm2$^{-/-}$;Thm1$^{aln/+}$* mice backcrossed five generations onto a C57BL6/J background were significantly smaller than their control littermates with a decrease in total body weight and crown to rump length (Figure 3.4A-C). To determine whether *Thm2$^{-/-}$; Thm1$^{aln/+}$* mice would maintain the smaller size at weaning age, we followed their development to P21 at which the size differences persisted with *Thm2$^{-/-}$; Thm1$^{aln/+}$* mice being significantly smaller than their control littermates (Figure 3.4D-F).

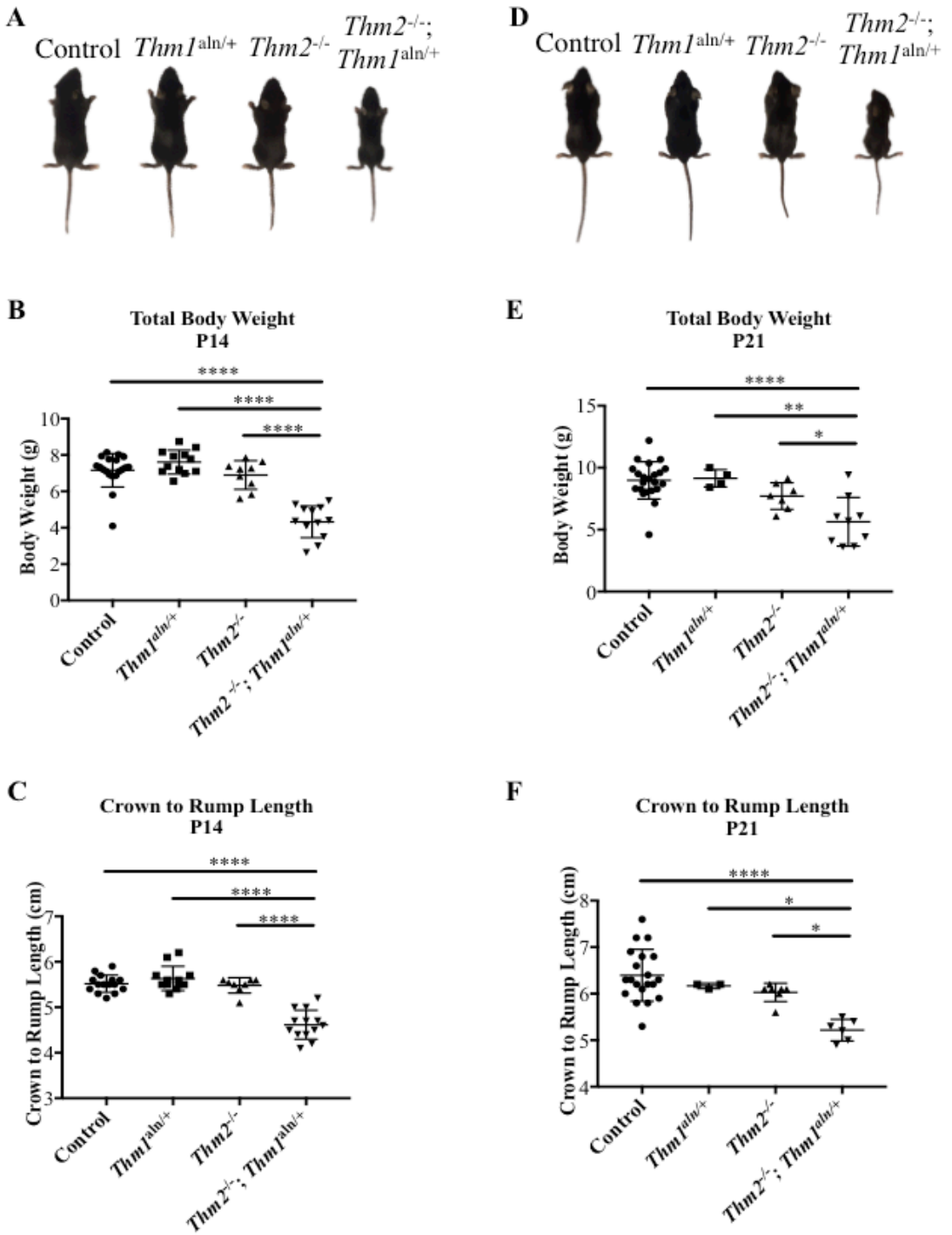

Figure 3.4. Five generations on a C57BL6/J background, *Thm2*$^{-/-}$; *Thm1*$^{aln/+}$ mice exhibit decreased total body weight and length. (A) Image of Control, *Thm1*$^{aln/+}$, *Thm2*$^{-/-}$, and *Thm2*$^{-/-}$; *Thm1*$^{aln/+}$ littermates at P14. (B) Total body weights and (C) crown to rump lengths of P14 Control, *Thm1*$^{aln/+}$, *Thm2*$^{-/-}$, and *Thm2*$^{-/-}$; *Thm1*$^{aln/+}$ mice. (D) Image of Control, *Thm1*$^{aln/+}$, *Thm2*$^{-/-}$, and *Thm2*$^{-/-}$; *Thm1*$^{aln/+}$ mice at P21. (E) Total body weights and (F) crown to rump lengths of P21 Control, *Thm1*$^{aln/+}$, *Thm2*$^{-/-}$, and *Thm2*$^{-/-}$; *Thm1*$^{aln/+}$ littermates. Results indicate *Thm2*$^{-/-}$; *Thm1*$^{aln/+}$ mice are smaller than littermates at p14 and p21. Error bars represent mean ± standard deviation. ****p≤0.0001, **p≤0.01, *p≤0.05

3.4.5 Thm2$^{-/-}$; Thm1$^{aln/+}$ mice exhibit shortened endochondral bone lengths

Since mutations in ciliary genes have been shown to play a role in the development of the endochondral skeleton[20,31,79,81], and *Thm2*$^{-/-}$*; Thm1*$^{aln/+}$ mice were smaller than control littermates at P14 and P21, we investigated the skeleton of *Thm2*$^{-/-}$*; Thm1*$^{aln/+}$ mice. More specifically, mutations in *THM1* have been identified in patients with Jeune Syndrome which is a skeletal disorder affecting bones that are formed through endochondrial ossification, such as the tibia, femur, humerus, radius, ulna, and ribs. To further characterize the nature of the skeletal defects in *Thm2*$^{-/-}$*;Thm1*$^{aln/+}$ mice, skeletal preparations were performed using alizarin red and alcian blue to stain the bone and cartilage, respectively, and bone lengths were measured using Image J software (Figure 3.5A). At P14, *Thm2*$^{-/-}$*;Thm1*$^{aln/+}$ mice exhibited shorter bones, including the tibia, femur, humerus, radius and ulna compared to control littermates. Furthermore, the sternum and diameter of *Thm2*$^{-/-}$*, Thm1*$^{aln/+}$ ribcages were smaller than control littermates. Interestingly, the skulls of *Thm2*$^{-/-}$*; Thm1*$^{aln/+}$ mice were also shorter when measured from the tip of the nose to the back of the head, suggesting that skull bone development, which occurs through intramembranous ossification instead of endochondral ossification, may also be affected (Figure 3.5B). These data indicate that *Thm2* and *Thm1* function in skeletal development in mice backcrossed five generations on a C57BL6/J background.

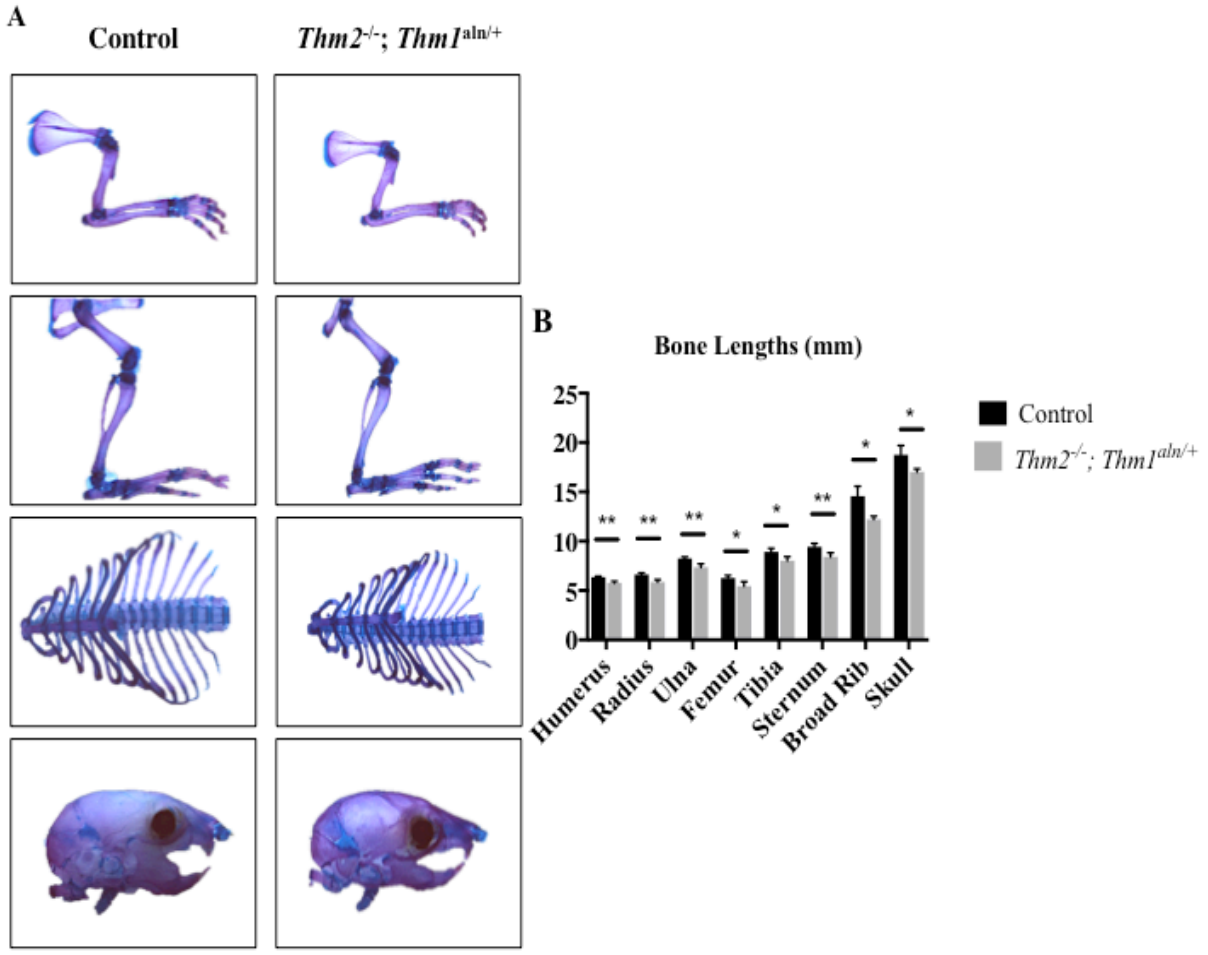

Figure 3.5. Bones of *Thm2*$^{-/-}$; *Thm1*$^{aln/+}$ mice are shorter than control mice (A) Representative images showing P14 skeletal preparations of control and *Thm2*$^{-/-}$;*Thm1*$^{aln/+}$ littermates using alizarin red to stain bone and alcian blue to stain cartilage. (B) Graph showing lengths of control and *Thm2*$^{-/-}$; *Thm1*$^{aln/+}$ bones at P14 shows shorter bones in *Thm2*$^{-/-}$; *Thm1*$^{aln/+}$ mice compared to littermate controls. Error bars represent mean ± standard deviation. **p≤0.01, *p≤0.05

3.4.6 Growth plates of Thm2$^{-/-}$;Thm1$^{aln/+}$ mice appear abnormal

Deletion of *Ift80* and *Ift88* have resulted in abnormal growth plate organization[79,81]. To examine the decreased endochondral bone length defects in *Thm2$^{-/-}$; Thm1$^{aln/+}$* mice at the cellular level, we investigated the growth plate organization at P14 (Figure 3.6A). Broadly, the growth plate can be divided into two major regions, the proliferative zone and the hypertrophic zone[72]. When compared to control littermates, histological analysis of growth plates of *Thm2$^{-/-}$; Thm1$^{aln/+}$* mice appear to exhibit an abnormal staining pattern. Trends indicate *Thm2$^{-/-}$; Thm1$^{aln/+}$* growth plates exhibited an increase in the proliferation zone length, and a decrease in the hypertrophic zone. Similar results were obtained when growth plate sections were stained with Safranin O and fast green, which stain the cartilage and bone, respectively (Figure 3.6B).

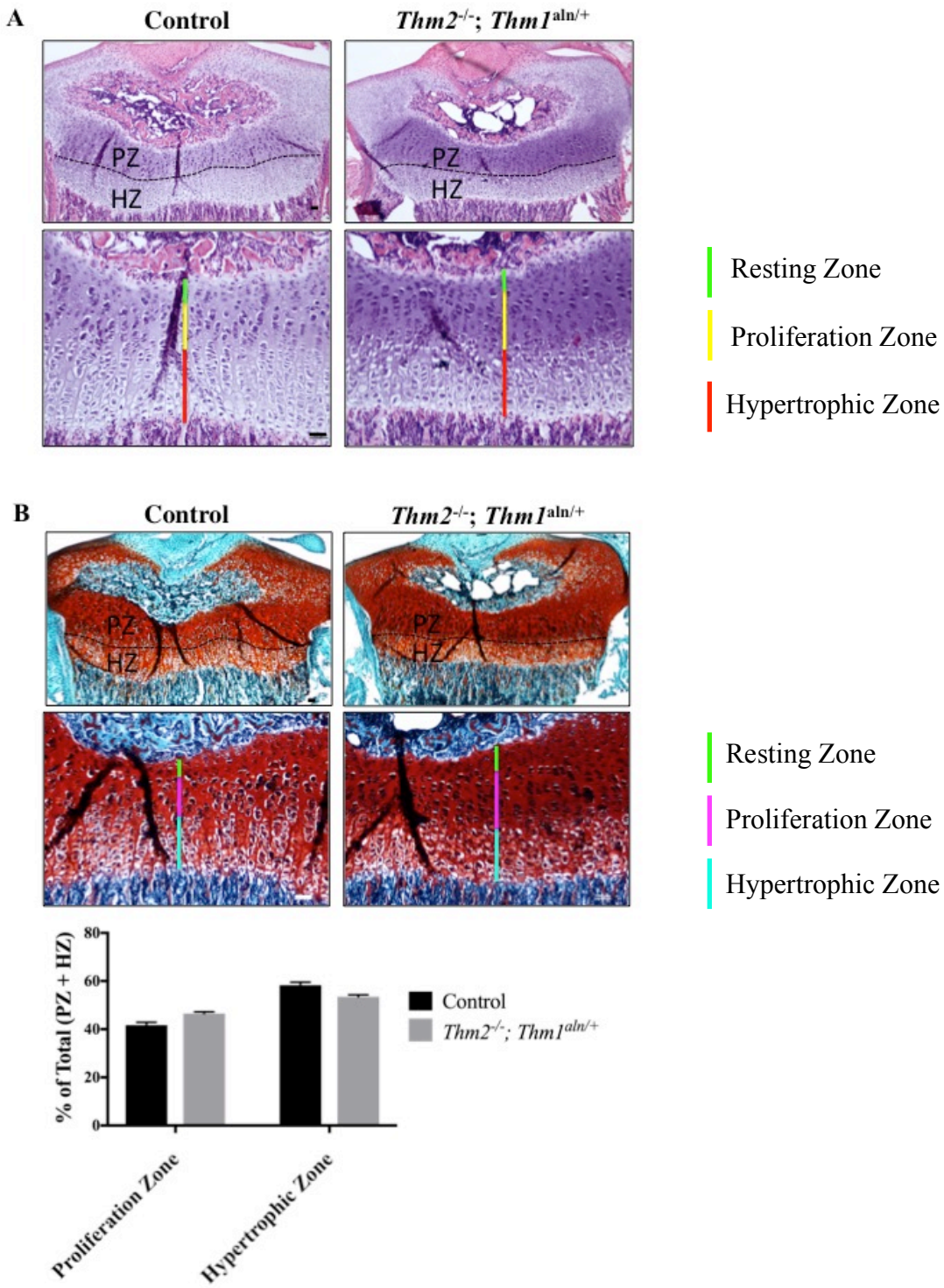

Figure 3.6. Growth plates of *Thm2*$^{-/-}$; *Thm1*$^{aln/+}$ mice appear abnormal. (A) Hematoxylin and eosin staining of Control and *Thm2*$^{-/-}$; *Thm1*$^{aln/+}$ growth plates at P14. (B) Control and *Thm2*$^{-/-}$; *Thm1*$^{aln/+}$ growth plates stained with Safranin O and Fast Green at P14. PZ-Proliferation Zone, HZ-Hypertrophic zone and black dotted line separates the two regions. (C) Quantification indicates a trend of increased proliferation zone length and decreased hypertrophic zone length, suggesting abnormal growth plate morphology. Scale bars equal 100μm.

3.4.7 Thm2$^{-/-}$; Thm1$^{aln/+}$ kidneys are not cystic

Since renal cysts are among the most common clinical manifestations of ciliopathies[129], we analyzed the kidneys of *Thm2$^{-/-}$; Thm1$^{aln/+}$* mice at P14. Histological analysis revealed normal morphology of the *Thm2$^{-/-}$; Thm1$^{aln/+}$* mice, similar to the morphology observed in control kidneys (Figure 3.7A). Although total kidney weights are smaller in *Thm2$^{-/-}$; Thm1$^{aln/+}$* mice (Figure 3.7B), kidney weight/body weight ratio of *Thm2$^{-/-}$; Thm1$^{aln/+}$* mice are not significantly different from those of control littermates (Figure 3.7C).

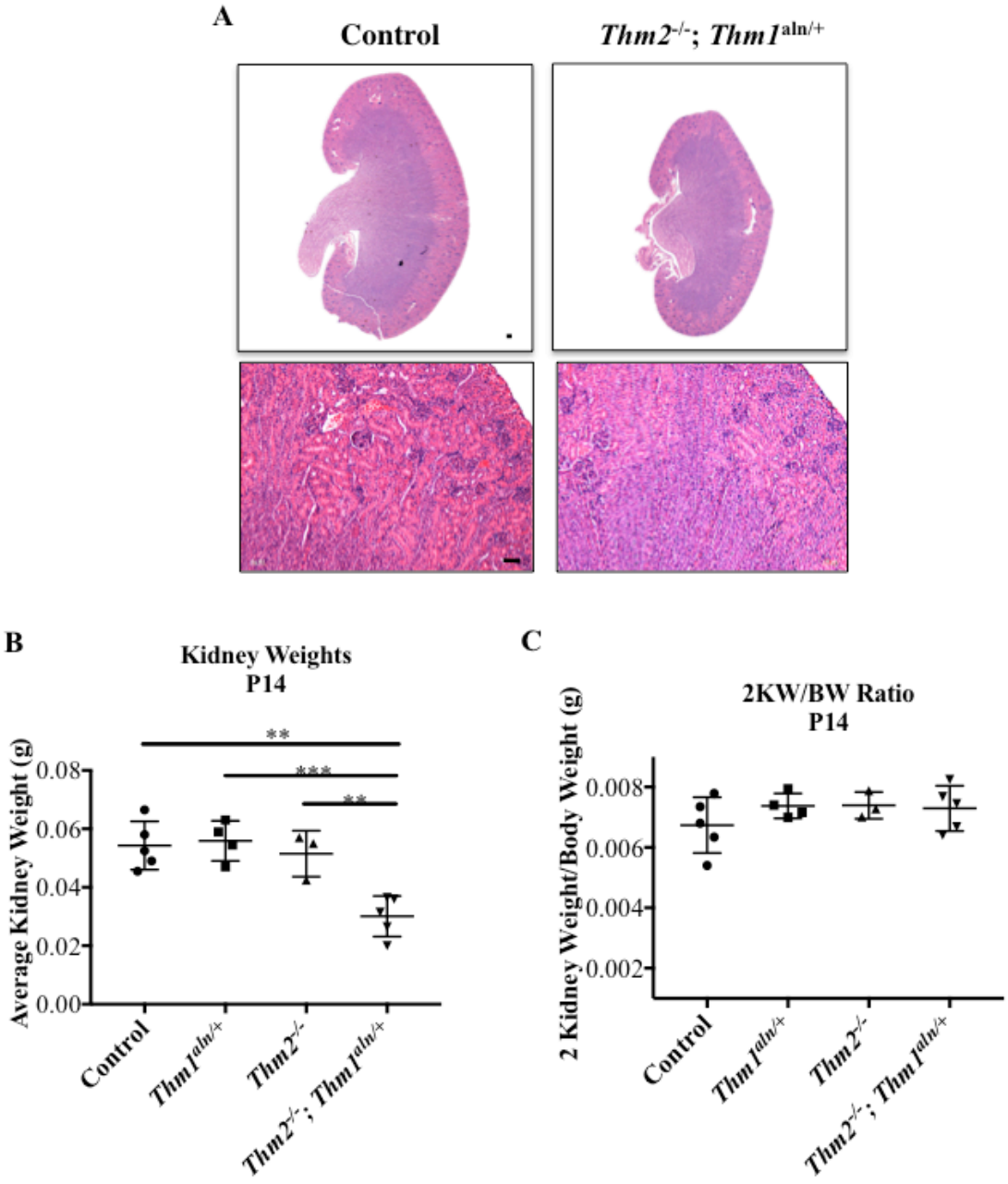

Figure 3.7. Kidneys of *Thm2*$^{-/-}$; *Thm1*$^{aln/+}$ mice are not cystic. (A) Histological analysis of control and *Thm2*$^{-/-}$; *Thm1*$^{aln/+}$ kidneys. (B) Average kidney weights and (C) Kidney weight to body weight ratios of Control, *Thm1*$^{aln/+}$, *Thm2*$^{-/-}$ and *Thm2*$^{-/-}$; *Thm1*$^{aln/+}$ mice are not statistically different. Scale bars equal 100μm. Error bars represent mean ± standard deviation. **p≤0.01, ***p≤0.001

3.5 Discussion

In these studies, we establish *Thm2* as a novel ciliary protein and generate the first known *in vitro and in vivo* models of *Thm2* deficiency. *In vitro* knockdown of *Thm2* results in normal cilia length while the *in vivo* model shows *Thm2,* together with *Thm1,* is essential for skeletal development. These data expand our knowledge of the ciliary proteome, and more specifically increase our knowledge of ciliary proteins involved in skeletal development. Previously, analysis of IFT-A embryonic mutants, *Thm1*[20,31], *Ift140*[67] and *Ift144*[66], revealed defects in skeletal development including polydactyly and abnormal rib morphology. Interestingly, hypomorphic mutation of *Ift80*[79] and conditional deletion of *Ift88*[81], two *Ift* Complex B genes, led to polydactyly and shortened long bones. To our knowledge, this is the first *Ift-null* mouse model surviving embryogenesis and exhibiting post-natal skeletal abnormalities.

Mutations in *THM1*[43] have been identified in patients with Jeune Syndrome (JATD), which is characterized by skeletal abnormalities[64]. Our data suggest *Thm2*$^{-/-}$*; Thm1*$^{aln/+}$ mice may serve as a model to study Jeune Syndrome and abnormalities in endochondral ossification. The most consequential skeletal abnormality of JATD is narrowing of the thoracic cavity, which often results in respiratory insufficiency[64]. Other skeletal abnormalities include polydactyly and shortening of the long bones[64]. In *Thm2*$^{-/-}$*; Thm1*$^{aln/+}$ mice, alcian blue and alizarin red skeletal stains at P14 revealed narrowing of the thoracic cavity and shortening of the long bones. To date, polydactyly has not been observed in any of the *Thm2*$^{-/-}$*; Thm1*$^{aln/+}$ mice. Furthermore, Jeune Syndrome patients exhibit varying degrees of skeletal severity[65]. Approximately 60-80% of patients die during the neonatal-infantile period of life[64], but some patients are able to survive into adulthood[65]. Thus, *Thm2*$^{-/-}$*; Thm1*$^{aln/+}$ mice provide a novel model to study skeletal defects similar to those seen in the human disease.

Analysis of P14 tibia growth plates in *Thm2*$^{-/-}$; *Thm1*$^{aln/+}$ mice appear to exhibit an increased proliferation zone and a decreased hypertrophic zone. In the growth plate, PTHrP is expressed from the perichondral cells and chondrocytes where it is able to promote proliferation of chondrocytes within the growth plate[72]. Once the level of PTHrP is below a certain threshold, pre-hypertrophic and early hypertrophic cells produce *Ihh* which affects a variety of skeletal processes including increased chondrocyte proliferation within the growth plate, stimulation of the production of PTHrP, and differentiation of perichondral cells to osteoblasts of the bone collar[72]. Endochondral growth plates of *Ihh*-null mice exhibit a decrease in Hh signaling and proliferation as measured by BrdU incorporation, as well as a decrease in proliferation zone length at E14.5[74]. In contrast, conditional deletion of Suppressor of Fused (Sufu), a negative regulator of Hh signaling[73], using a Col2a1-Cre recombinase resulted in increased *Ptch1,* a target of Hh signaling, accompanied by an increase in the proliferative zone and a decrease in the hypertrophic zone in the growth plate of E16.5 tibia explants[73]. An additional study revealed loss of *Sufu* in mice resulted in hypoplasia of the scapula, radius, ulna, and humerus at E14.5, compared to control littermates[130]. Therefore, these results suggest that, in the absence of Hh signaling, chondrocytes undergo premature hypertrophy[69] while the inappropriate activation of Hh signaling causes chondrocytes to stay in the proliferation zone. These data suggest Hh signaling in bone development is a tightly regulated process with both increases and decreases in signaling resulting in skeletal abnormalities.

We hypothesize that because *Thm2* and *Thm1*[20] localize to the primary cilium and primary cilia are necessary for Hh signaling[12], the abnormalities in growth plates of *Thm2*$^{-/-}$; *Thm1*$^{aln/+}$ mice are due to abnormalities in Hh signaling. Since paralogs, such as the *Gli* transcription factors, can have redundant functions[127,128] and loss of *Thm1* has previously been

shown to result in increased Hh signaling[20], we hypothesize that like *Thm1*, loss of *Thm2* may also increase Hh signaling, leading to an increase in the proliferation zone or decrease in the differentiation (proliferative to hypertrophic zone) of chondrocytes in the growth plate of *Thm2*$^{-/-}$ *; Thm1*$^{aln/+}$ mice. However, further molecular studies are needed to support this hypothesis.

Interestingly, i*n vitro* knockdown of *Thm2* in 293T cells resulted in normal cilia lengths and the kidneys of P14 *Thm2*$^{-/-}$*; Thm1*$^{aln/+}$ mice appear normal. In contrast, loss of *Thm1* during late embryogenesis results in shortened primary cilia with a bulb-like tip and cystic kidneys at six weeks of age[26]. This suggests *Thm1* and *Thm2* share unique and redundant functions which may vary by tissue type.

Taken together, the first *in vivo* model of *Thm2* loss has revealed a role for *Thm2,* together with *Thm1,* in skeletal development. We show the shorter length of *Thm2*$^{-/-}$*; Thm1*$^{aln/+}$ bones is accompanied by an expansion of the proliferative zone of growth plates and a reduction of the hypertrophic zone of growth plates of P14 tibias. Further studies investigating the molecular mechanisms underlying the growth plate abnormalities will expand our knowledge of roles of individual ciliary proteins and their role in signaling and endochondral ossification.

Chapter Four: Novel Role of *Thm2* and *Thm1* in Spermatogenesis

4.1 Abstract

Primary cilia are antenna-like appendages extending from the surface of almost all vertebrate cells. Mutations in ciliary genes result in pleiotropic disorders collectively termed ciliopathies. The clinical manifestations of ciliopathies can include obesity, cystic kidney disease, skeletal abnormalities, and infertility. *Thm1* encodes an intraflagellar transport (IFT) Complex A protein and negative regulator of Hedgehog signaling. In mouse, early embryonic loss of *Thm1* causes peri-natal lethality, while post-natal loss results in cystic kidney disease and obesity. Here, we investigate the role of a novel gene and paralog of *Thm1, Thm2*. Using CRISPR/Cas9 genome editing, we generated a *Thm2* knockout mouse on a mixed FVB/C57BL6/J background. *Thm2*-null mice reached adulthood with normal body weights, skeletal patterning, kidneys, lungs, and hearts at three months of age. Since paralogs can have redundant functions, we combined a null allele of *Thm1 (alien),* with *Thm2* deletion. $Thm2^{-/-};Thm1^{aln/+}$ mice on this mixed FVB/C57BL6/J background survived into adulthood with seemingly normal health. However, $Thm2^{-/-};Thm1^{aln/+}$ male mice exhibited a 44% reduction in fertility compared to their control littermates. $Thm2^{-/-};Thm1^{aln/+}$ male mice showed reduced sperm count, abnormal sperm morphology and impaired sperm motility. Further, $Thm2^{-/-};Thm1^{aln/+}$ male mice showed abnormal testis morphology, including a thin germinal epithelium, suggesting defects in early spermatogenesis. These findings establish novel roles for *Thm2* and *Thm1* in spermatogenesis and expand our knowledge of the ciliary proteome.

4.2 Introduction

Infertility is a global issue affecting approximately 15% of couples[82]. Although medical intervention can be helpful for couples struggling with infertility, the median out-of-pocket cost for reproductive assistance is $5,338, placing a significant financial burden on families, and even discouraging some from seeking assistance[131]. Both male and female factors contribute to infertility cases, with female factors accounting for approximately 50%, male factors for 20-30%, and a combination of male and female factors for the remaining 20-30% of cases[82]. Male infertility can be caused by a variety of factors influencing sperm development, ultimately leading to decreased sperm production and/or poor sperm quality[42]. Multiple cell types within the testis participate in spermatogenesis, including germ cells, Sertoli cells, and Leydig cells[90]. Germ cells mature within the germinal epithelium of the seminiferous tubules, where another cell type, Sertoli cells, are found[90]. Sertoli cells support the process of spermatogenesis and function with Leydig cells, which are situated in the interstitium, between seminiferous tubules[90]. Leydig cells are integral to the hypothalamus-pituitary-gonadal signaling process, which controls the amount of sex steroids produced by the testis, such as testosterone, which act to regulate spermatogenesis[90]. Therefore, the mechanisms underlying male infertility can be complex, costly, and difficult to manage, highlighting the need for further research.

Ciliopathies are a group of diseases that occur due to mutations in ciliary genes, and provide a connection between genetic disorders and infertility[47,85]. Cilia depend on intraflagellar transport (IFT) for the trafficking of protein cargo along the microtubule-based ciliary axoneme[11]. Anterograde IFT, which transports cargo from the base to the tip of the cilium, is mediated largely by IFT Complex-B proteins and the kinesin motor[11]. Retrograde IFT, which returns cargo from the tip to the base of the cilium, is mediated by IFT Complex A proteins and

the cytoplasmic dynein motor[11]. IFT-A proteins also mediate the ciliary entry of membrane receptors in mammalian cells[108]. Cilia can be divided broadly into two categories - non-motile (primary) and motile cilia[40]. Non-motile cilia contain an axoneme with a 9+0 microtubule organization while motile cilia contain an axoneme with a 9+2 microtubule organization[40] along with axonemal dynein motor proteins which allow for the beating motion of the motile ciliary axoneme[39]. Two ciliopathies have been associated with male infertility, primary cilia dyskinesia (PCD), a disorder of motile cilia[85], and Bardet-Biedl Syndrome (BBS), a disorder of primary cilia[47].

The sperm flagellum shares many structural similarities with motile cilia[85]. Therefore, mutations resulting in abnormal ciliary beating patterns, such as those in PCD, affect the motility of sperm flagellum, often resulting in infertility[85]. In contrast, infertility in BBS patients is attributed to hypogonadism[47] which leads to immature testis, almost always resulting in infertility[88]. BBS is classified as a hypogonadotrophic hypogonadism which is caused by decreases in the hormones of the hypothalamic-hypophyseal pathway, including gonadotrophin releasing hormone (GnRH), follicular stimulating hormone (FSH) and luteinizing hormone (LH), or growth hormone (GH)[88]. Furthermore, primary cilia are known to mediate Hh signaling[14] and evidence of Hh is found in germ cells[91], Sertoli cells[92], and Leydig cells[92] throughout the testis. Confirming the importance of Hh signaling in the testis, mouse mutants of the Hh signaling ligand in the testis, Desert Hedgehog (*Dhh)*[15], lack mature sperm and are infertile[92].

Mutant mouse models generated from loss of ciliary proteins have revealed the roles of specific ciliary genes in spermatogenesis. Global loss of *Bbs4* resulted in infertility and sperm lacking a flagellum, even though primary and motile cilia were generated throughout the body[89]. Other mouse models revealed the role of anterograde IFT and motor trafficking components.

Hypomorphic loss of *Ift88*^{Tg737Rpw} resulted in abnormal sperm morphology, including the absence of sperm tails in some cases, low sperm counts and male infertility[97]. Interestingly, conditional deletion *of Ift20* in male germ cells resulted in infertility at two to three months of age, but reduced fertility at six weeks of age[98]. *Ift20* mutant sperm exhibited a variety of phenotypes including the complete absence of the tail, irregularly shaped sperm heads, or the presence of a tail with a bend or kink [98]. Further, loss of the molecular motor, *Kif3a,* in germ cells resulted in male infertility, with decreased epididymal sperm amounts, and abnormal sperm morphology of the head and tail[99].

While the roles of anterograde trafficking components in spermatogenesis have been studied, the function of proteins involved in retrograde IFT is unknown. Mutations in *THM1,* an IFT Complex A gene[20], have been identified in patients with BBS[43]. Loss of *Thm1* in mouse causes developmental defects[20], cystic kidney disease[26], and obesity[32]. *Thm1* has a paralog, *Thm2,* which is uncharacterized. To investigate the *in vivo* function of THM2, we generated a novel mouse model of *Thm2* loss using CRISPR/Cas9 genome editing and discovered novel roles for *Thm2,* and *Thm1,* in sperm development.

4.3 Methods

4.3.1 Generation of Thm2 knockout (Thm2$^{-/-}$) mouse

In collaboration with Dr. Jay Vivian at the University of Kansas Medical Center Transgenic and Gene Targeting Facility (KUMC TGIF), *Thm2*-null mice were generated using Clustered Regularly Interspaced Short Palindromic Repeats (CRISPR)/Cas9 genomic engineering. Dr. Shondra Miller at the Washington University Genome Engineering and iPSC

Center (GEiC) identified, created, and validated guide RNA's (gRNA's) for functionality and efficiency to cut DNA at specific target sites *in vitro*. Two gRNA's that cut genomic DNA 30% of the time were selected. Dr. Melissa Larson, of KUMC TGIF, performed pro-nuclear injections on F1 embryos with FVB oocyte donors and C57BL6/J males. In total, 317 embryos were injected with 20ng/μl of each of the gRNA's and 50ng/μl of the Cas9 RNA and 198 embryos were injected with 10ng/μl of each of the gRNA's and 50ng/μl of the Cas9 gRNA. A total of 42 founders were born from these injections. When mutations due to non-homologous end joining (NHEJ) in genomic DNA were confirmed via sequencing, founders were crossed to wild-type (WT) FVB mice to expand the lines.

4.3.2 Genotyping of NHEJ events following CRISPR/Cas9 genome editing

Multiple PCR reactions were designed to characterize the mutations generated by NHEJ following CRISPR/Cas9 genome editing. Two sets of genotyping primers were designed around the gRNA in exon 4 while one set of genotyping primers was designed to flank the entire region between exon 4 and intron 8. The first primer set surrounding exon 4 included F-Thm2ex4p-5' TAC TAC GCC AGC CTC TTC CT 3' and R-Thm2ex4p-5' CCC TCC TGT ACC TCT TTG GA 3' and was expected to produce a WT band of 107bp. The second primer set surrounding exon 4 included F-Thm2ex4r-5' TGT CTG AAG CCA ACA GAG AGG 3' and R–Thm2ex4r-5' GTT CAA GGC CAC CTT TGC T 3' and was expected to produce a WT band of 1,000bp. PCR amplicons with a lower molecular weight indicate evidence of NHEJ in exon 4. Primers designed to detect a mutant band with the large deletion flank exon 4 and intron 8 and include, F-Thm2ex4b-5' GGA GAG CAG CTT GAA GGA AA 3' and R-Thm2ex4b-5' GTC ACG GCT GGT GTG ATT C. A PCR amplicon was expected at 216bp, only in the event of NHEJ. To

detect the presence of a WT allele, a separate PCR reaction using primers within exon 6, F-WT-5'AAC TTC CTG CCC GCT TTA GT 3' and R-WT-5' GTG TCA GAT ACC CTG GAA CCA GAG 3' were used. In the presence of a WT allele, this PCR reaction yields an amplicon of approximately 461bp.

4.3.3 Sequencing of Thm2 knockout mouse

PCR products obtained using primers from above were ran on an agarose gel, excised, and DNA was extracted using the Qiaex II DNA extraction kit (Qiagen, 20021). Samples were sent to Genewiz for sequencing analysis. Sequencing results were then analyzed to determine the presence or absence of stop codons resulting from NHEJ events.

4.3.4 Skeletal Preparations

At three months of age, alizarin red and alcian blue staining was performed using standard protocols (Kingsley Lab Protocol, Ryan Roundtree, Version 1.1, 3/31/2003). Briefly, mice were eviscerated and fixed in 95% ethanol for 1-2 days. They were then stained with alcian blue (Acros Organics 33864-99-2) for 14 days and fixed with 95% ethanol for an additional 1-2 days. Potassium hydroxide was used for approximately 2-5 days, or until tissue was cleared. Skeletons were then stained with 1% alizarin red (Acros Organics 130-22-3) in potassium hydroxide for 1-2 days, or until completely stained. Once staining was complete, skeletons were placed into glycerol for long-term storage and imaged.

4.3.5 Histological Analysis

When mice were three months of age, hearts, lungs, and kidneys were placed in Bouin's fixative (Polysciences, Inc. 16045) overnight and placed in 70% ethanol in water. Testis were placed in either Bouin's fixative (Polysciences, Inc. 16045) or 4% paraformaldehyde (PFA) overnight, cut in half, and placed again overnight in 4% PFA or Bouin's fixative before being placed in 70% ethanol in PBS or 70% ethanol in water, respectively. Tissues were processed and dehydrated through a series of ethanol washes and embedded in paraffin wax. Paraffin blocks were sectioned at 7μm. Histological staining was then performed using standard hematoxylin and eosin staining methods. Briefly, sections were de-paraffinized and rehydrated through a series of ethanol rinses. Sections were then stained with Hematoxylin (Sigma HHS32) and Eosin (Sigma HT110216) and mounted with Permanent Mounting Media (Fisher, SP15-500). Stained sections were imaged using a Nikon 80i light microscope attached to a Nikon DS-Fil camera.

4.3.6 Fertility testing

Control and *Thm2*$^{-/-}$*; Thm1*$^{aln/+}$ mice from the same litter were weaned and housed together until at least 7-8 weeks of age. Control and *Thm2*$^{-/-}$*; Thm1*$^{aln/+}$ male mice were then placed in separate cages with females for one month. Pregnancies were recorded to determine percent fertility.

4.3.7 Sperm count and morphology analysis

Sperm from control and *Thm2*$^{-/-}$*; Thm1*$^{aln/+}$ mice was collected from the caudal epididymis of 12-week-old mice after swim up. Briefly, caudal epididymides and vas deferens were isolated, cut with a razor blade and placed in PBS at 37°C for 10 minutes. Sperm were then

counted using a hemocytometer. For morphological analysis, sperm were placed in 4% PFA after swim up and imaged using Nikon TE2000 inverted microscope attached to a Photometrics CoolSnap HQ cooled cCD camera.

4.3.8 Live imaging of sperm

Sperm were imaged in an enclosed imaging chamber made using a glass slide, coverslip, and petroleum jelly sealant. Caudal epididymis and vas deferens were dissected and sperm was allowed to swim out in PBS for 10 minutes and imaged immediately after. Live sperm were imaged using a Nikon TE2000 inverted microscope (10x objective lens) and a Photometrics CoolSnap HQ2 cooled CCD camera, which were controlled by Nikon Elements Advanced Research 4.50.00. Images were captured using a 100ms exposure at approximately 6 frames per second. Movies were edited and sped up 2x in iMovie software.

4.4 Results

4.4.1 Generation of Thm2 null mice using CRISPR/Cas9 genome editing

To determine a role for *Thm2 in vivo,* we generated a *Thm2*-null mouse using CRISPR/Cas9 genome editing. Two gRNA's were designed to target exon 4 and intron 8 (Figure 4.1A). Through this targeting approach, two types of deleterious gene rearrangements could result through non-homologous end joining (NHEJ): one generating deletions in exon 4 only, and the other generating large deletions encompassing exon 4 through intron 8. Genotyping primers were designed to flank the gRNA in exon 4 as well as the entire region between exon 4 and intron 8. In the presence of a WT allele, the first primer set (purple) was expected to produce an

amplicon of approximately 107 bp, and the second primer set (red) was expected to produce an amplicon of approximately 1,000bp (Figure 4.1A). Any mutations or insertions in exon 4 would cause the amplicon to deviate from the expected size. Therefore, amplicons detected at smaller, or larger, base pair sizes were used to indicate mutations caused by NHEJ in exon 4. In contrast, the primers flanking exon 4 and intron 8 were not expected to produce a PCR amplicon in the presence of a WT allele because the distance between the two primers is too large to be amplified (4,664bp) with a regular Taq polymerase. However, in the event that NHEJ occurred and the genomic region encompassing exon 4 and intron 8 is deleted, band sizes were estimated to be approximately 216bp. Representative results for founders harboring the large deletion between exon 4 and intron 8 are shown (Figure 4.1B). Genotyping results indicated that mutations in exon 4 alone were found in approximately 43% of the founders while mutations spanning exon 4 to intron 8 were found in approximately 40% of the founders (Figure 4.1C). As expected, mice harboring a mutation spanning exon 4 to intron 8 resulted in a PCR amplicon of approximately 200bp (not less than 100bp, but not more than 300bp). Sequencing results of multiple founders confirmed mutations in exon 4 alone and loss of the entire genomic region between exon 4 and intron 8. We chose to expand a line harboring a mutation deleting the entire region between exon 4 and intron 8, which created a stop codon in exon 4. Using the PCR primers spanning exon 4 and intron 8, a PCR amplicon of 198bp is generated (blue arrows). Using the PCR primers located near exon 6 (orange arrows), a WT amplicon of 461bp is generated (Figure 4.1D). The large deletion results in complete loss of the first predicted tetratricopeptide (TPR) motif. In the event that aberrant splicing takes place from exon 3 to exon 9, approximately 176 codons (13.4% of the total protein) and 20kDa of protein would be lost.

This did not occur. Western blot analysis of P14 kidney and testis reveal the complete loss of THM2 protein (Figure 4.1E).

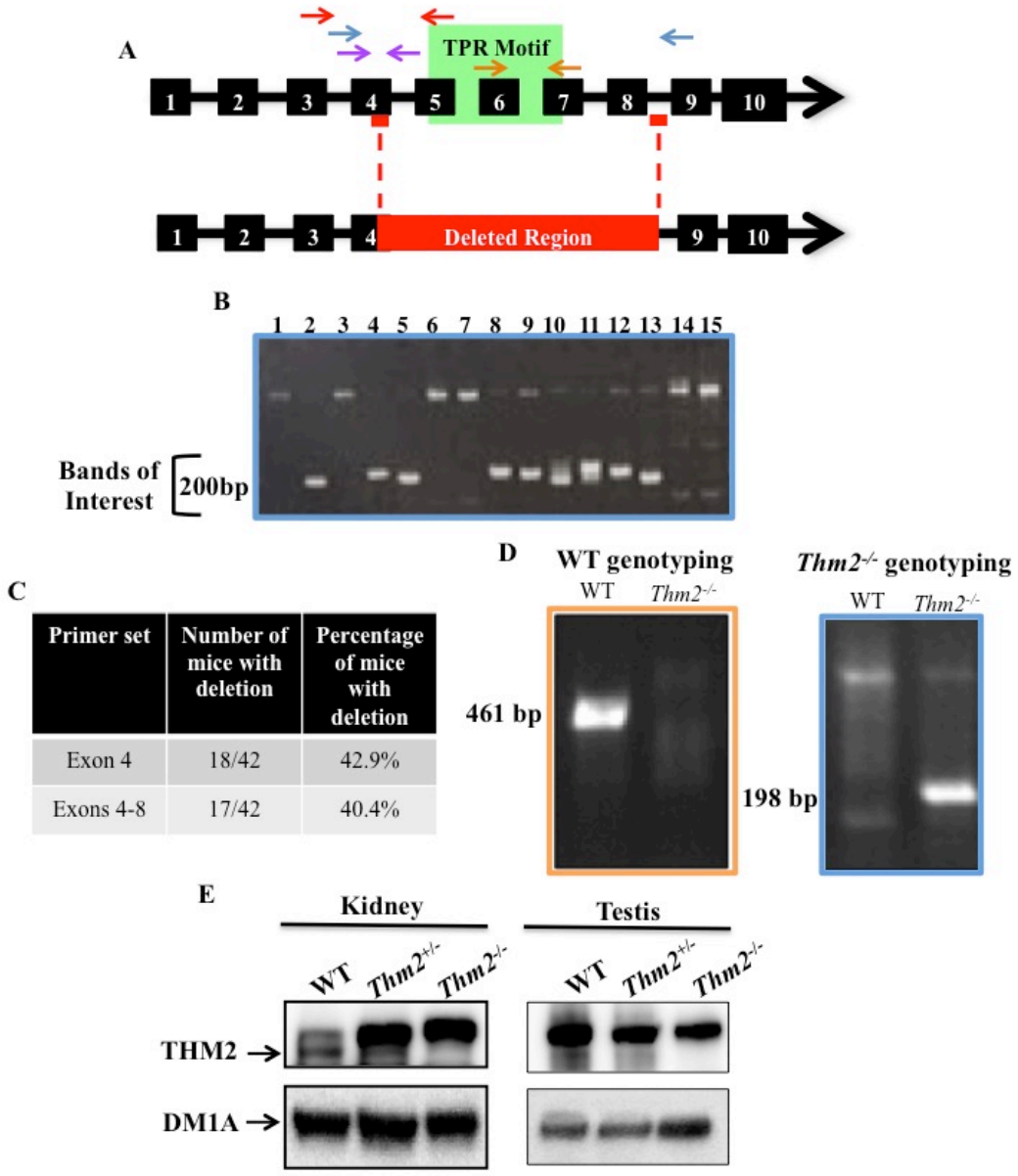

Primer set	Number of mice with deletion	Percentage of mice with deletion
Exon 4	18/42	42.9%
Exons 4-8	17/42	40.4%

Figure 4.1. Generation of *Thm2* null mouse using CRISPR/Cas9 Genome Editing. (A) Two guide RNA's were generated to target exon 4 and intron 8 (red horizontal lines). Primers designed to detect mutations occurring in exon 4 are in purple and red. Primers used to detect mutations deleting the region between exon 4 and intron 8 are in blue. Primers used to detect the presence of a WT band are in orange. (B) Representative image of genotyping results generated from founders harboring mutations deleting the region between exon 4 and intron 8. (C) Genotyping results indicated gRNA's created deletions in exon 4 and from exon 4 to intron 8 approximately 43% and 40% of the time, respectively. (D) Sequencing analysis revealed a founder line harboring a mutation deleting exon 4 to intron 8 which created a stop codon in exon 4. This line resulted in a WT band of 461bp and a mutant band at 198bp. (E) Western blot analysis of P14 kidney and testis revealed the complete loss of *Thm2* in *Thm2*$^{-/-}$ mice.

4.4.2 Thm2 knockout mice appear healthy at three months of age

Loss of many intraflagellar transport proteins, including THM1[20], results in embryonic lethality[21,66,67]. However, not surprisingly, *Thm2*$^{-/-}$ mice survived into adulthood with seemingly normal health, similar to the *Thm2* knockout mouse described in Chapter 3. At three months of age, *Thm2*$^{-/-}$ mice on a mixed FVB/C57BL6/J background were characterized by normal body weight (Figure 4.2A) and normal skeletal patterning (Figure 4.2B). Histological analysis of heart, kidney, and lungs of *Thm2*$^{-/-}$ did not reveal any abnormalities (Figure 4.2C), suggesting *Thm2*$^{-/-}$ mice are healthy at three months of age.

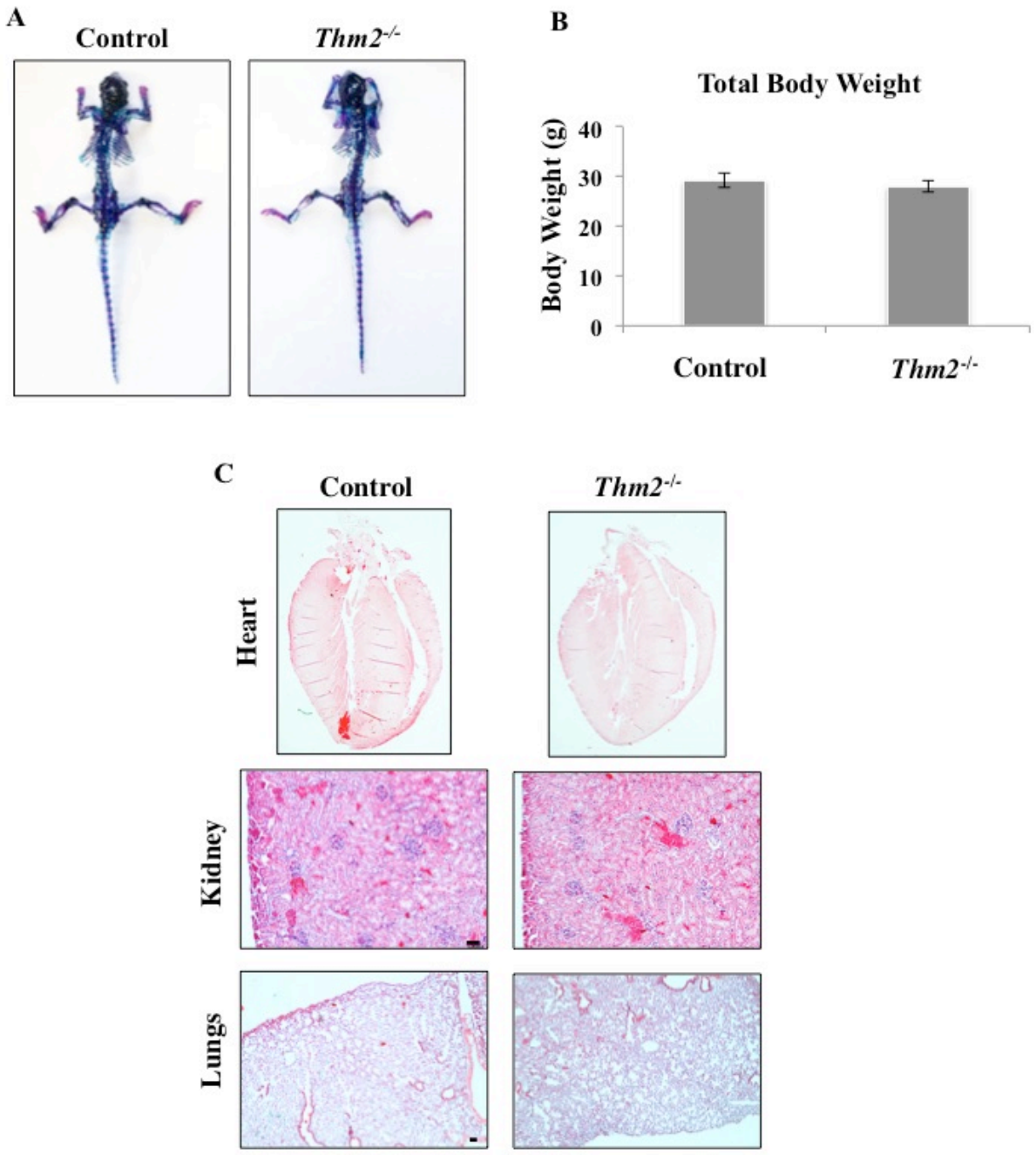

Figure 4.2. *Thm2* null mice are seemingly healthy at three months of age. *Thm2*$^{-/-}$ mice exhibit (A) similar skeletal patterning and (B) body weights. (C) Histological analysis of *Thm2* null mice heart, kidneys, and lungs at three months of age shows normal morphology. Scale bar equals 100μm.

4.4.3 Thm2$^{-/-}$; Thm1$^{aln/+}$ mice are characterized by decreased fertility

Since *Thm2* and *Thm1* are paralogs[20] and paralogs can have redundant functions[127,128], we combined a null allele (*aln)* of *Thm1* with *Thm2* deletion. While setting up breeding cages, we noticed that several *Thm2$^{-/-}$; Thm1$^{aln/+}$* male mice produced vaginal plugs in females, but these matings did not result in pregnancies. Thus, to examine *Thm2$^{-/-}$; Thm1$^{aln/+}$* male fertility more systematically, ≥ 7 week-old *Thm2$^{-/-}$; Thm1$^{aln/+}$* male mice and littermate controls were placed with females and resulting pregnancies were monitored over a one-month period. All control males tested were able to father litters with females. In contrast, five of nine *Thm2$^{-/-}$; Thm1$^{aln/+}$* males fathered litters with females, indicating a decrease in fertility (Figure 4.3A).

4.4.4 Thm2$^{-/-}$; Thm1$^{aln/+}$ mice exhibit decreased sperm counts and abnormal morphology and motility

To determine the mechanisms underlying the decrease in fertility, sperm from the caudal epididymis were counted and morphology was analyzed. Sperm counts revealed significantly lower sperm numbers in the *Thm2$^{-/-}$; Thm1$^{aln/+}$* males compared to control males (Figure 4.3B). Furthermore, sperm morphology of *Thm2$^{-/-}$; Thm1$^{aln/+}$* males exhibited abnormalities. The sperm tails of *Thm2$^{-/-}$; Thm1$^{aln/+}$* mice showed three different morphologies: (1) normal (2) bent, and (3) retroflexed, with the tail flipped back towards the head (Figure 4.3C). Retroflexed sperm were infrequently observed in control mice, and sperm with bent tails were observed to a greater extent in *Thm2$^{-/-}$; Thm1$^{aln/+}$* male mice. Further, while control sperm exhibited normal waveform beat of the tail, propelling the sperm forward, *Thm2$^{-/-}$; Thm1$^{aln/+}$* sperm showed impaired motility. Retroflexed mutant sperm showed abnormal twitching movement or circular movement

(Movie 4.1). These results suggest low sperm count and abnormal sperm morphology leading to defective motility result in the inability of some *Thm2*$^{-/-}$; *Thm1*$^{aln/+}$ males to impregnate females.

A

Genotype	Total Males	Fertile Males	Percentage of Fertile Males
Control	9	9	100%
Thm2$^{-/-}$*;Thm1*$^{aln/+}$	9	5	56%

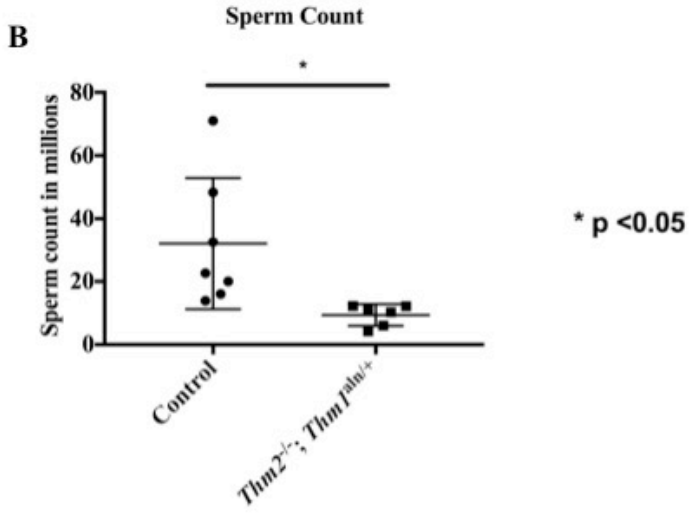

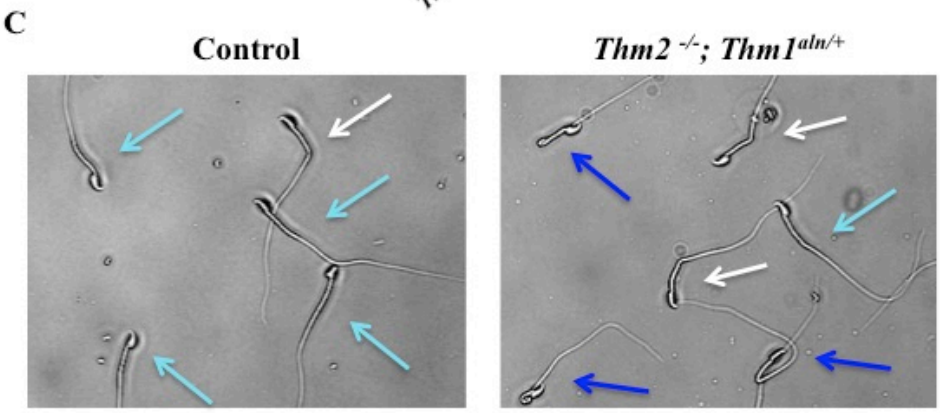

Figure 4.3. *Thm2*$^{-/-}$*; Thm1*$^{aln/+}$ mice exhibit decreased fertility, low sperm counts, and abnormal morphology. (A) Table summarizing data from fertility matings indicates decreased fertility in *Thm2*$^{-/-}$*; Thm1*$^{aln/+}$ mice. (B) Sperm counts from caudal epididymides of *Thm2*$^{-/-}$*; Thm1*$^{aln/+}$ mice were lower than control littermates. (C) Light microscopy of sperm in control and *Thm2*$^{-/-}$*; Thm1*$^{aln/+}$ mice show three different sperm morphology categories (1) Normal flagellum (light blue arrow), (2) Bent flagellum (white arrow), and (3) retroflexed flagellum (dark blue arrow). Error bars represent mean plus standard deviation.*p≤0.05

Control

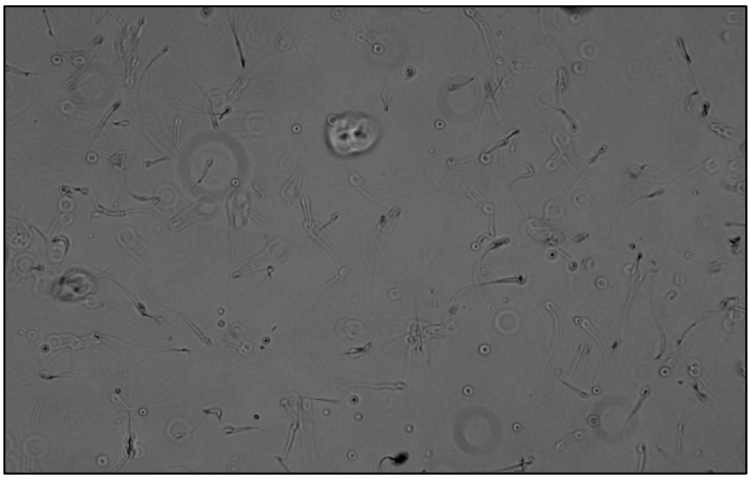

***Thm2*$^{-/-}$*; Thm1*$^{aln/+}$**

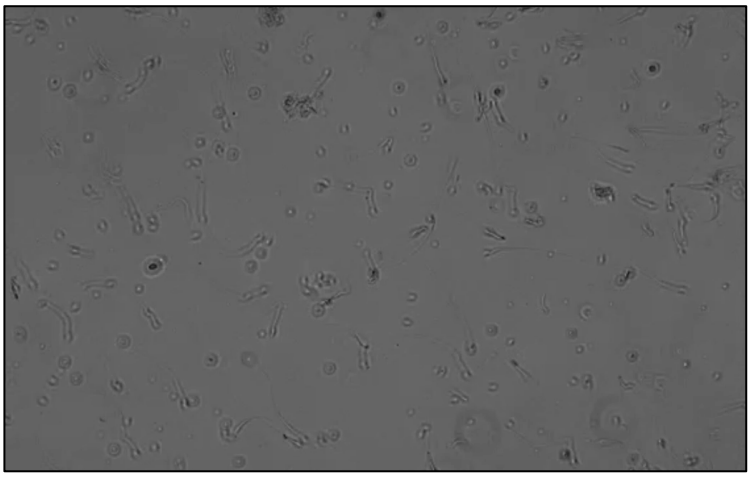

Movie 4.1. *Thm2*$^{-/-}$*; Thm1*$^{aln/+}$ sperm exhibit decreased motility and abnormal beating pattern. Live imaging analysis of control and *Thm2*$^{-/-}$*; Thm1*$^{aln/+}$ sperm shows abnormal flagellar beating movement in *Thm2*$^{-/-}$*; Thm1*$^{aln/+}$ mice.

4.4.5 Testis of Thm2$^{-/-}$; Thm1$^{aln/+}$ mice are abnormal

Since *Thm2$^{-/-}$; Thm1$^{aln/+}$* male mice exhibited low sperm counts, and sperm with abnormal morphology, we investigated the morphology of the testis. Spermatogenesis occurs within the seminiferous tubules of the testis and is dependent on multiple cell types[90]. Leydig cells are found in the interstitium, between seminiferous tubules[92], and respond to hormones necessary to produce testosterone, which aid in the process of spermatogenesis[90]. Sertoli cells are located within the seminiferous tubules and support the maturation of male germ cells[90]. Male germ cells mature as they move towards the lumen of the seminiferous tubules[90]. Histological analysis of *Thm2$^{-/-}$; Thm1$^{aln/+}$* testes revealed a spectrum of abnormalities, ranging from mild to severe. At the mild end of the spectrum, approximately half of the seminiferous tubules exhibit a decrease in sperm in the lumen. In the middle of the spectrum, *Thm2$^{-/-}$; Thm1$^{aln/+}$* mice exhibit less sperm in the lumen of seminiferous tubules, and a thin germinal epithelium, suggesting impaired maturation of the germ cells. At the severe end of the spectrum, *Thm2$^{-/-}$; Thm1$^{aln/+}$* testis are characterized by seminiferous tubules with a thin germinal epithelium, the presence of vacuole-like structures, a nearly complete absence of flagella in the lumen, and increased amounts of interstitium between the seminiferous tubules (Figure 4.4), revealing the defects can involve cells outside the seminiferous tubules.

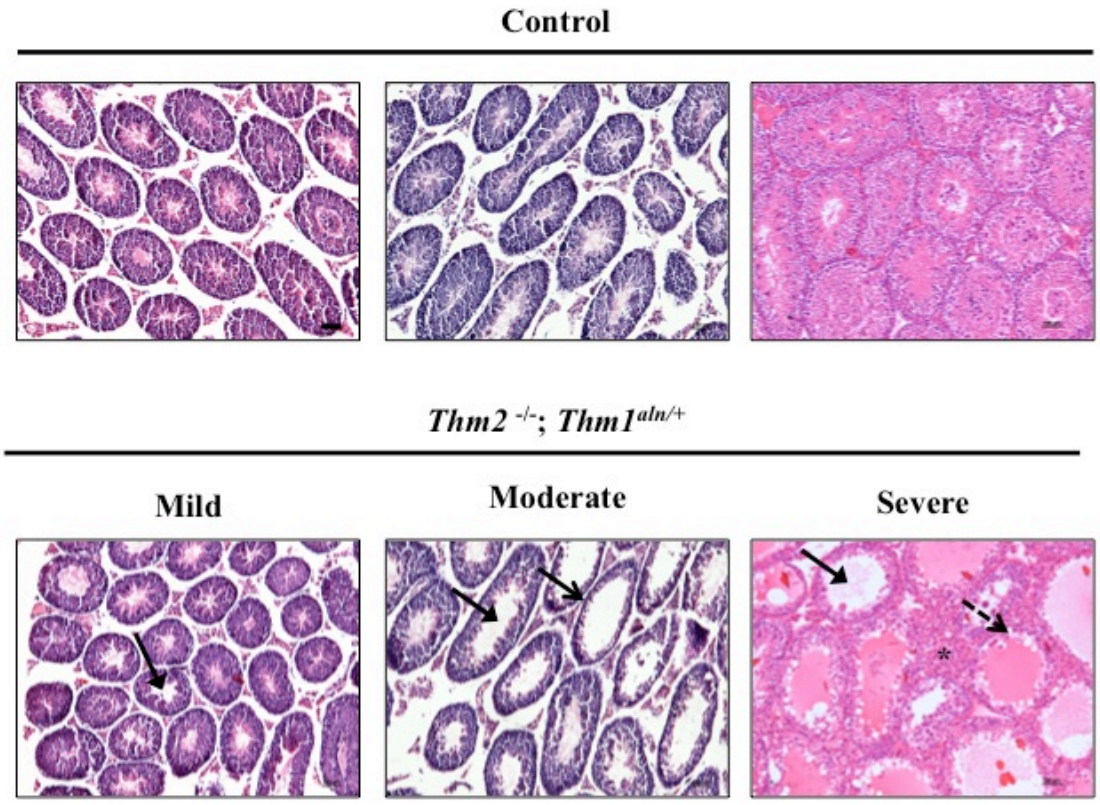

Figure 4.4. Histological analysis reveals abnormal testis morphology of *Thm2*$^{-/-}$; *Thm1*$^{aln/+}$ mice. Hematoxylin and Eosin staining of ≥12 week testis ranging from mild to severe abnormalities in 3 mutant mice with age-matched controls. Mild *Thm2*$^{-/-}$; *Thm1*$^{aln/+}$ testes exhibit a decrease in the amount of flagella in the lumens of the seminiferous tubules. Moderate abnormalities exhibit a significant decrease in the flagella in the lumens and a decrease in the germinal epithelium. Severe abnormalities exhibit a nearly complete loss of flagella within the lumen of the seminiferous tubule, increased interstitium, and vacuole-like structures. Solid black arrow with block arrowhead indicates the lumen of seminiferous tubules with little to no sperm flagella. Solid black arrow denotes narrow germinal epithelium. Dashed line black arrow with block arrowhead indicates vacuole-like structures in seminiferous tubules. Asterisk denotes increased interstitium.

4.4.6 Thm2$^{-/-}$; Thm1$^{aln/+}$ kidneys are normal

Loss of many ciliary proteins, including THM1, results in cystic kidney disease[26,27,132,133], underscoring the importance of primary cilia in kidney development, and renal tubular integrity. To investigate the role of *Thm2* in kidney tubular development, we examined kidney morphology at 12 weeks of age in *Thm2*$^{-/-}$*; Thm1*$^{aln/+}$ and control mice. Histological analysis revealed kidneys with normal morphology (Figure 4.5).

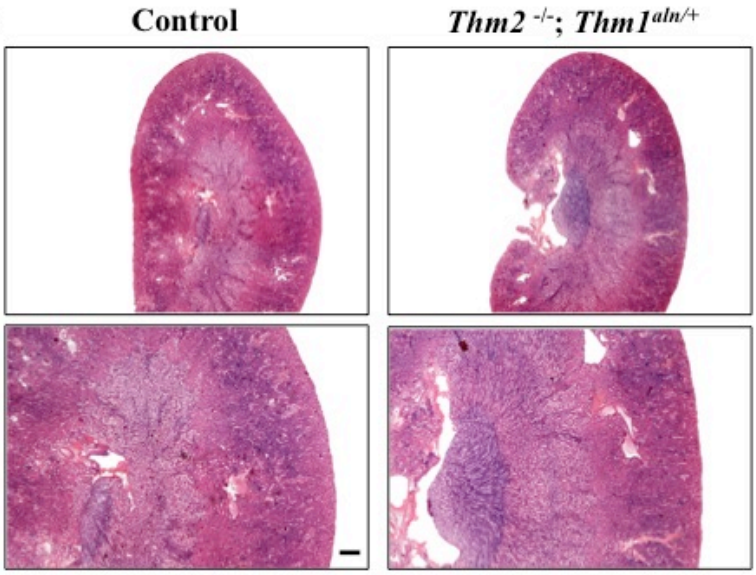

Figure 4.5. Histological analysis reveals normal kidney morphology of *Thm2*$^{-/-}$; *Thm1*$^{aln/+}$ mice. (A) Hematoxylin and Eosin staining of kidneys of ≥ 12 week old control and *Thm2*$^{-/-}$; *Thm1*$^{aln/+}$ mice. Staining indicates the absence of cystic kidneys in *Thm2*$^{-/-}$; *Thm1*$^{aln/+}$ mice. Scale bar equals 500um.

4.5 Discussion

In this study, we generate a novel *in vivo* model of *Thm2* loss using CRISPR/Cas9 genome editing. Using two gRNA's, we target exon 4 and intron 8 to create a large deletion between exon 4 and intron 8, which results in a stop codon in exon 4. Loss of THM2 alone does not result in obvious abnormalities at three months of age with normal body weight, skeletal patterning, and kidney, lung, and heart histology. However, loss of *Thm2* together with one allele of *Thm1 (alien),* causes abnormal testis and sperm morphology, low sperm count, defective sperm motility, and decreased fertility. To our knowledge, this is the first characterization of the role of an IFT Complex A protein (THM1) in male fertility.

Previously, roles for IFT Complex B proteins, IFT88 and IFT20, in male fertility have been shown[97,98]. Complete infertility was reported in hypomorphic $Ift88^{Tg737Rpw}$ mutants, although age of mice was not specified[97], while germ line specific loss of *Ift20,* using the *Stra8*-iCre, decreased male fertility at six weeks of age and caused complete infertility at two to three months of age[98]. $Thm2^{-/-}; Thm1^{aln/+}$ male mice of greater than 7 weeks of age exhibited a 44% decrease in fertility compared to control littermates. Furthermore, similarities were observed between the two IFT Complex B mutants, including abnormal sperm morphology and decreased sperm count[97,98]. In both the *Ift20* and the *Ift88* mutants, several sperm flagella were completely absent, with some *Ift88* mutant mice exhibiting short sperm tails, and *some Ift20* mutant mice exhibiting sperm tails with a bend[97,98]. Unlike IFT Complex B mutants, $Thm2^{-/-}; Thm1^{aln/+}$ male mice appeared to maintain the flagellar structure on all sperm heads. However, many sperm flagella were characterized by abnormal morphology, with bent or retroflexed sperm tails. Additionally, $Thm2^{-/-}; Thm1^{aln/+}$sperm showed impaired motility. Sperm with retroflexed tails

showed a twitching motion or circular movement, in contrast to the waveform displayed by control sperm.

Mutations in *THM1* have been identified in patients with BBS[43]. BBS is characterized by a myriad of phenotypic abnormalities, including male hypogonadism[47]. Almost all male BBS patients exhibit infertility and testes which fail to mature[88]. Hypogonadism in BBS patients is attributed to abnormalities of the hypothalamic-hypophyseal axis[88], which produces hormones that regulate the amount of steroid hormones, such as testosterone[90,93]. Testosterone is important in the development of male gonads and in spermatogenesis[90]. Deletion of *Bbs2, Bbs3, and Bbs4* in mice results in male infertility and the complete absence of flagella within the seminiferous tubules of the testis, demonstrating the importance of BBS proteins in spermatogenesis[89,134,135].

Luteinizing hormone (LH) is an important regulator of the hypothalamic-hypophyseal axis and of Leydig cell function. Loss of the LH receptor in mice resulted in a decrease in testis size along with smaller seminiferous tubules and fewer, underdeveloped, Leydig cells[136]. Additionally, spermatogenesis was halted at the round spermatid stage[136]. Further studies of $Thm2^{-/-}; Thm1^{aln/+}$ male mice are necessary to determine the status of hypothalamic-hypophyseal signaling, and can include measuring levels of serum testosterone, gonadotrophin releasing hormone, follicular stimulating hormone, and luteinizing hormone.

Spermatogenesis occurs in the germinal epithelium of seminiferous tubules where male germ cells mature before being released into the lumen of the tubule[90]. Within the testis, multiple cell types, such as Sertoli cells, Leydig cells, and germ cells, participate in the process of spermatogenesis[90]. Since the loss of *Thm2* and *Thm1* is not specific to a certain cell type, we cannot rule out the role of Sertoli cells, Leydig cells, nor germ cells in the phenotypes observed in $Thm2^{-/-}; Thm1^{aln/+}$ male mice. Conditional loss of Sertoli cells in mice at P50 resulted in a

severe decrease in Leydig cell number and germ cell number[137]. Interestingly, testis morphology remained intact and basal levels of testosterone were maintained, suggesting that even after the loss of a substantial number of Leydig cells, remaining Leydig cells were able to sustain baseline testosterone levels[137]. Thus, further studies are needed to discern which cell types are affected in *Thm2*$^{-/-}$*; Thm1*$^{aln/+}$ male mice.

Although BBS is characterized as a disorder of the primary cilium[47], primary cilia are not found in the seminiferous tubules, but are found on the surface of immature Leydig cells[95]. Primary cilia mediate Hh signaling[14] and loss of *Thm1* results in an increase in Hh signaling[20]. Since evidence of Hh signaling is found throughout spermatogenesis[91], in Sertoli cells[92], and Leydig cells[92], misregulation of Hh signaling may contribute to the abnormalities and decreased fertility observed in the *Thm2*$^{-/-}$*; Thm1*$^{aln/+}$ male mice**.** *Dhh* null mice are characterized by a significant loss of germ cells[92], underscoring the importance of Hh signaling in spermatogenesis. Since loss of *Thm1* has been shown to increase Hh signaling, the abnormalities in testis structure and spermatogenesis in *Thm2*$^{-/-}$*; Thm1*$^{aln/+}$ male mice may be attributed to defects in Hh signaling.

In contrast to other ciliary mutants affecting spermatogenesis[89,97,99,134], *Thm2*$^{-/-}$*; Thm1*$^{aln/+}$ adult male mice are not completely infertile, but rather exhibit a decrease in fertility. 44% of *Thm2*$^{-/-}$*; Thm1*$^{aln/+}$ male mice are infertile, suggesting variability in the phenotype. Furthermore, the testis morphology of *Thm2*$^{-/-}$*; Thm1*$^{aln/+}$ mice also exhibits variability, with some mutants exhibiting relatively mild defects, including a decrease in sperm in approximately half of the seminiferous tubules, and others exhibiting severe abnormalities, including a thin germinal epithelium, presence of vacuoles within the seminiferous tubules, and increased interstitium. Since the genetic background of mice can affect phenotype[92], this variability may be attributed to

the mixed FVB/C57BL6/J background. Backcrossing the mutations ten generations onto either a pure C57BL6/J or FVB background may render the *Thm2*$^{-/-}$*; Thm1*$^{aln/+}$ male mice completely infertile, and decrease the variability of the testis phenotype.

Finally, although loss of *Thm1* results in cystic kidney disease[26], and a clinical manifestation of BBS is renal cystic disease[33], histological analysis of *Thm2*$^{-/-}$*; Thm1*$^{aln/+}$ kidneys reveals normal kidneys at three months of age, suggesting *Thm2* and *Thm1* may have unique and redundant functions in cilia structure and signaling which are specific to different tissues.

In summary, we generated a novel model of *Thm2* loss using CRISPR/Cas9 genome editing and established a role for *Thm2* and *Thm1* in male fertility on a mixed FVB/C57BL6/J background. *Thm2*$^{-/-}$*; Thm1*$^{aln/+}$ male mice mated to females after 7 weeks of age exhibited decreased fertility, with only 56% of males exhibiting fertility, compared to 100% of control males. Light microscopy analysis of epididymal sperm revealed significantly lower amounts in *Thm2*$^{-/-}$*; Thm1*$^{aln/+}$ male mice compared to control mice, and abnormal morphology. Furthermore, histological analysis of *Thm2*$^{-/-}$*; Thm1*$^{aln/+}$ testis revealed abnormalities ranging from mild to severe defects. We propose defects in testis development, caused by misregulated Sertoli and Leydig cell signaling, may underlie spermatogenesis abnormalities. To our knowledge, this has not been reported in other IFT mutant models. Further studies are necessary to determine the contribution of different cell types and signaling pathways resulting in decreased fertility, and abnormal testis and sperm morphology of *Thm2*$^{-/-}$*; Thm1*$^{aln/+}$ male mice. Overall, this study elucidates both unique and redundant functions of *Thm2* and *Thm1,* increases our knowledge of the ciliary proteome, and specifically establishes a role for *Thm2,* together with *Thm1,* in male fertility.

Chapter Five: Summary, Conclusions, Future Directions, and Significance

5.1. Summary and Conclusions

5.1.1 Establishing novel roles for Thm1 and Thm2

To expand our knowledge of *Thm1* and determine the function of a novel gene, *Thm2,* we generated a *Thm1* knockdown 3T3-L1 pre-adipocyte cell line, a *Thm2* knockdown 293T renal embryonic cell line, and two *Thm2* knockout mouse models – one using a Knockout Mouse Project (KOMP) construct and the other using CRISPR/Cas9 genome editing. Earlier studies of post-natal loss of *Thm1* resulted in obesity, which could be attributed to hyperphagia and dysregulation of the POMC appetite-controlling neuropeptide, prior to the onset of obesity[32]. Using a *Thm1* knockdown 3T3-L1 mouse pre-adipocyte cell line, we established that deficiency of *Thm1* increased adipogenesis and insulin sensitivity, providing an additional mechanism underlying *Thm1*-deficient obesity. Previous studies have revealed different roles for different ciliary proteins in adipogenesis. Knockdown of the IFT Complex B protein, *Ift88,* a subunit of the anterograde molecular motor, *Kif3a,* or *Alms1* resulted in a decrease in adipogenesis, with a corresponding decrease in markers of pro-adipogenic signaling, such as PPARγ[59,60]. In contrast, loss of *Bbs10 or Bbs12* resulted in increased adipogenesis with increased PPARγ levels[58]. These results suggest ciliary proteins may work in concert to intricately regulate adipogenesis. Our data show loss of *Thm1* results in an increase in adipogenesis and pro-adipogenic markers such as PPARγ and CEBPα, similar to loss of *Bbs10* or *Bbs12,* but in contrast to loss of *Ift88, Kif3a,* and *Alms1*.

Additionally, this work reveals that the novel ciliary gene, *Thm2,* together with *Thm1,* is essential in skeletal and sperm development. While loss of *Thm2* alone resulted in seemingly normal mice, additional loss of one allele of *Thm1 (alien)* revealed skeletal and sperm defects that were influenced by mouse strain background. An overt $Thm2^{-/-}; Thm1^{aln/+}$ phenotype was not

obvious on a mixed FVB/C57BL6/J background, but after backcrossing the colony five generations onto a C57BL6/J background, *Thm2*$^{-/-}$*; Thm1*$^{aln/+}$ mice were significantly smaller than their littermates at post-natal day (P) 14 and P21, with shorter long bones and tibia growth plates that showed expanded chondrocytic proliferation zones and shortened hypertrophic zones. This growth plate phenotype is similar to that of mouse mutants of *Sufu,* a negative regulator of Hh signaling[73]. The altered tibia growth plates indicate THM2 and THM1 function in development of bone derived through endochondral ossification. In contrast to other IFT-A mouse mutants, complete loss of *Thm2,* and one allele of *Thm1,* does not result in embryonic lethality. In the human population, mutations in ciliary IFT-A genes, *IFT144*[64,66]*, IFT140*[64,67]*,* and *THM1*[43] have been identified in patients with Jeune Syndrome. Hypomorphic loss of *Ift144* and *Ift140* resulted in embryonic lethality in the mouse[66,67], whereas patients with Jeune syndrome are born but, often, do not live past the early years of life[64]. Thus, *Thm2*$^{-/-}$*; Thm1*$^{aln/+}$ mice provide a novel post-natal model to study molecular and cellular mechanisms underlying skeletal defects of Jeune Syndrome.

Using a second *Thm2* knockout mouse model, we confirmed that *Thm2* knockout mice do not show an obvious phenotype. After introducing a null allele of *Thm1 (alien)*[20]*,* and maintaining the line on a mixed FVB/C57BL6/J background, we also confirmed that *Thm2*$^{-/-}$*; Thm1*$^{aln/+}$mice reach adulthood and appear normal. However, when male mice of at least seven weeks of age were mated to females, only 56% of *Thm2*$^{-/-}$*; Thm1*$^{aln/+}$ male mice were able to father litters, indicating a decrease in fertility. Similarly, germ-line specific *Ift20* null mice exhibited a 62.5% decrease in fertility when mated at 6 weeks of age. These mice were completely infertile at 2-3 months of age[98], suggesting that age exacerbates the infertility. Loss of IFT88 and IFT20 resulted in abnormal spermatogenesis, with many sperm heads exhibiting a

complete loss of flagella[97,98]. Interestingly, some *Ift20* mutant sperm have flagella present, but exhibit a bend in the morphology[98]. In contrast, all *Thm2*$^{-/-}$*;Thm1*$^{aln/+}$ sperm appear to maintain the presence of a flagellum, but many are irregularly shaped with a bend or retroflexed position, and have impaired motility.

Interestingly, histological analysis of *Thm2*$^{-/-}$*; Thm1*$^{aln/+}$ testis revealed variability in the severity of abnormalities. Mild testis abnormalities of *Thm2*$^{-/-}$*; Thm1*$^{aln/+}$ mutants include decreased sperm flagella in approximately half of the seminiferous tubules. In contrast, severe testis abnormalities of *Thm2*$^{-/-}$*; Thm1*$^{aln/+}$ testis include nearly complete absence of sperm tails in the lumen of seminiferous tubules, vacuoles, decreased width of germinal epithelium, and an expanded interstitium. These abnormalities reflect defects in testis development. Mutations in *THM1* have been found in patients with Bardet-Biedl Syndrome (BBS)[43] which is characterized by various phenotypic abnormalities, including hypogonadism, resulting in infertility[47]. Therefore, we hypothesize defects in Leydig cell and Sertoli cell signaling may cause the abnormalities observed in *Thm2*$^{-/-}$*; Thm1*$^{aln/+}$ sperm. To our knowledge, this mechanism has not been reported in prior IFT mutant models. Thus, the *Thm2*$^{-/-}$*; Thm1*$^{aln/+}$ mice may provide a novel model to study molecular and cellular mechanisms underlying male infertility of BBS.

Taken together, our studies establish novel roles for *Thm1* and *Thm2* in adipogenesis, skeletal development, and spermatogenesis and contribute valuable *in vitro* and *in vivo* models, to study molecular mechanisms underlying the clinical abnormalities of ciliopathies. Further, our studies elucidate novel genetic interactions between *Thm1* and *Thm2*.

5.1.2 Unique and redundant functions of Thm1 and Thm2

A BLAST search revealed mouse THM1 and THM2 proteins share 58% and 55% homology, respectively, with *Chlamydomonas reinhardtii* IFT139, leading us to hypothesize these paralogs share equal function of IFT139 in mammals. However, our studies indicate that THM1 plays a broader and more identifiable role in organ systems throughout the body, and in ciliogenesis[20,26,28,32]. In mouse, early embryonic loss of *Thm1* resulted in peri-natal lethality, and forebrain, skeletal, and neural tube patterning defects, while perinatal deletion of *Thm1* resulted in cystic kidney disease and obesity[20,26,28,31,32]. Further, our *in vitro* data demonstrate a direct role for *Thm1* in the regulation of adipogenesis. In contrast, *Thm2* loss alone does not affect embryogenesis nor post-natal development on a mixed FVB/C57BL6/J background, or on a C57/BL6/J background at the 5th generation. Additionally, while deficiency of *Thm1* impairs retrograde IFT, causing shortened primary cilia with a bulb-like structure at the distal tip[32], *Thm2* knockdown reveals normal cilia length. Interestingly, deletion of *Thm2,* together with additional loss of one allele of *Thm1* impairs skeletal and sperm development, revealing that loss of *Thm2* is sensitive to *Thm1* dosage and therefore that the functions of THM2 and THM1 in bone and sperm development are interdependent.

Our data also reveal that the unique and redundant functions of *Thm1* and *Thm2* vary with tissue type. Based on our studies, *Thm2* functions to a larger extent in development of the skeleton and sperm than in other tissues, such as the kidney. Other paralogs, such as the *Gli* transcription factors and Hh signaling ligands also show tissue specificity. For example, *Gli2* is involved in neural tube patterning while *Gli3* functions in limb patterning[15]. Furthermore, *Shh* is essential for embryogenesis and post-natal tissue maintenance, while *Dhh* functions in spermatogenesis, and *Ihh* functions in bone development[15]. However, the complete loss of *Thm1,*

together with loss of *Thm2* may reveal additional roles for *Thm2* in other tissue types, including the kidney, hypothalamus, and/or adipose tissue.

5.1.3 Genetic modifiers of Thm1- and Thm2-null phenotypes

Our studies have revealed that the phenotypes of *Thm2*$^{-/-}$*; Thm1*$^{aln/+}$ mice are influenced by genetic modifiers. Indeed, different mouse strains have been shown to modify the phenotype. For instance, loss of IL-10 results in colitis on a C3H/HeJBir background, but not on a C57/BL6/J background[138]. Additionally, loss of *Dhh* on a 129/Sv background halts spermatogenesis at an earlier stage compared to loss on a 129/Sv/C57BL6/J background[92]. Our investigations show that on a mixed FVB/C57BL6/J background, *Thm2*$^{-/-}$*; Thm1*$^{aln/+}$ mice exhibit little evidence of skeletal defects. However, *Thm2*$^{-/-}$*; Thm1*$^{aln/+}$ mice five generations onto a C57BL6/J background show a marked decrease in body weight and crown-to-rump length compared to control littermates. These results suggest genetic modifiers on the C57BL6/J background render the skeletal phenotype more severe. The differences observed are intriguing because in the human population, the severities of phenotypes, even within the same ciliopathy, are appreciable. For instance, most patients with Jeune Syndrome die during infancy (60-80%)[64], but some are able to survive into adulthood[65].

Only two of fourteen *Thm2*$^{-/-}$*; Thm1*$^{aln/+}$ males five generations on a C57BL6/J background were mated to females. One has completed fertility testing and although he was placed in the same cage with four females for one month, none of them became pregnant, suggesting that fertility defects of *Thm2*$^{-/-}$*; Thm1*$^{aln/+}$ mice on a FVB/C57/BL6/J mixed background may also occur on a pure C57BL6/J background. Furthermore, the severity of the testis phenotype of the *Thm2*$^{-/-}$*; Thm1*$^{aln/+}$ mice varies on the FVB/C57BL/J background, with

some testes appearing only mildly affected, while others appear severely disrupted and include the absence of flagella in the lumens of seminiferous tubules, decreased germinal epithelium, the presence of vacuoles, and increased interstitium. In an attempt to explain the variability observed between backgrounds and on a mixed background, I hypothesize that polymorphisms in other ciliary genes present in different mouse strains contribute to the severity of the disease phenotype.

Finally, our data suggest that *Thm1* and *Thm2* may both serve as genetic modifiers. Neither $Thm2^{-/-}$ nor $Thm1^{aln/+}$ mice show phenotypes, while combining these alleles results in skeletal and sperm defects. This suggests that mutation of one allele of *Thm1* or both alleles of *Thm2* may serve to modify disease severity of ciliopathies.

5.2 Future Directions

5.2.1 Furthering knowledge of Thm1 and Thm2 in adipogenesis

In chapter two, we showed that loss of *Thm1* in pre-adipocytes results in an increase in adipogenesis *in vitro*. Future directions include validating this increased adipogenesis *in vivo*. Using the *Thm1* floxed mouse allele, *Thm1* can be specifically deleted in the pre-adipocytes of mice with a tissue specific Cre recombinase, PdgfRα-Cre[139]. The adipocytes and fat pads of *Thm1* conditional knockout mice can then be assessed for abnormal size and morphology, and analyzed for insulin sensitivity. Furthermore, a role for *Thm2* has not yet been identified in adipogenesis. *In vivo* and *in vitro* experiments can be used to determine if *Thm2* functions in adipogenesis. *In vitro, Thm1;Thm2* double knockdown cell lines can be generated to measure the extent of adipogenesis and insulin sensitivity. Additionally, *Thm1;Thm2* double knockout mice can be generated to validate *in vitro* results. Since loss of *Thm2* does not affect normal

development, null alleles for *Thm2* can be utilized, but since loss of *Thm1* results in perinatal lethality[20], conditional deletion of *Thm1* in pre-adipocytes is necessary. The results of these experiments will allow *Thm2* to be included or excluded, from the list of genes that regulate adipogenesis.

5.2.2 Furthering knowledge of Thm1 and Thm2 in skeletal development

In chapter three, we showed that loss of *Thm2,* in addition to one allele of *Thm1* results in skeletal abnormalities when mice have been backcrossed five generations onto a C57BL6/J background. To fully understand the mechanisms underlying the abnormalities observed, cilia structure and Hedgehog (Hh) signaling status should be investigated. Given the role of THM1 as a negative regulator of Hh signaling and that reducing alleles of *Thm1* together with deletion of *Thm2* generates phenotypes, we hypothesize that THM2 also functions as a negative regulator of Hh signaling. If Hh signaling is upregulated in $Thm2^{-/-}; Thm1^{aln/+}$ mice, as hypothesized, genetic downregulation, or pharmacological treatment, of Hh signaling can be performed to determine a causative role for this pathway in the skeletal defects observed.

Additional analysis of $Thm2^{-/-}; Thm1^{aln/+}$ mice, just after birth, and as adults would help establish a timeline to answer the question of when skeletal defects initiate and terminate. To obtain the most informational data, daily weights can be recorded for the first week after birth, when $Thm2^{-/-}; Thm1^{aln/+}$ skeletal abnormalities become apparent, and then continued on a weekly basis. This would provide data on individual size progression, which would help to identify when skeletal abnormalities manifest, and how progression of skeletal development occurs. Preliminary studies have revealed $Thm2^{-/-}; Thm1^{aln/+}$ mice are indistinguishable from control littermates, and $Thm2^{-/-}; Thm1^{aln/+}$ mice beyond weaning remain smaller than control littermates

at 2 months of age (Figure 5.1). Furthermore, using a conditional allele of *Thm1, Thm1* and *Thm2* double knockout mice could be generated to further understand the gene dosage effects of *Thm1* and *Thm2* in the skeletal phenotype.

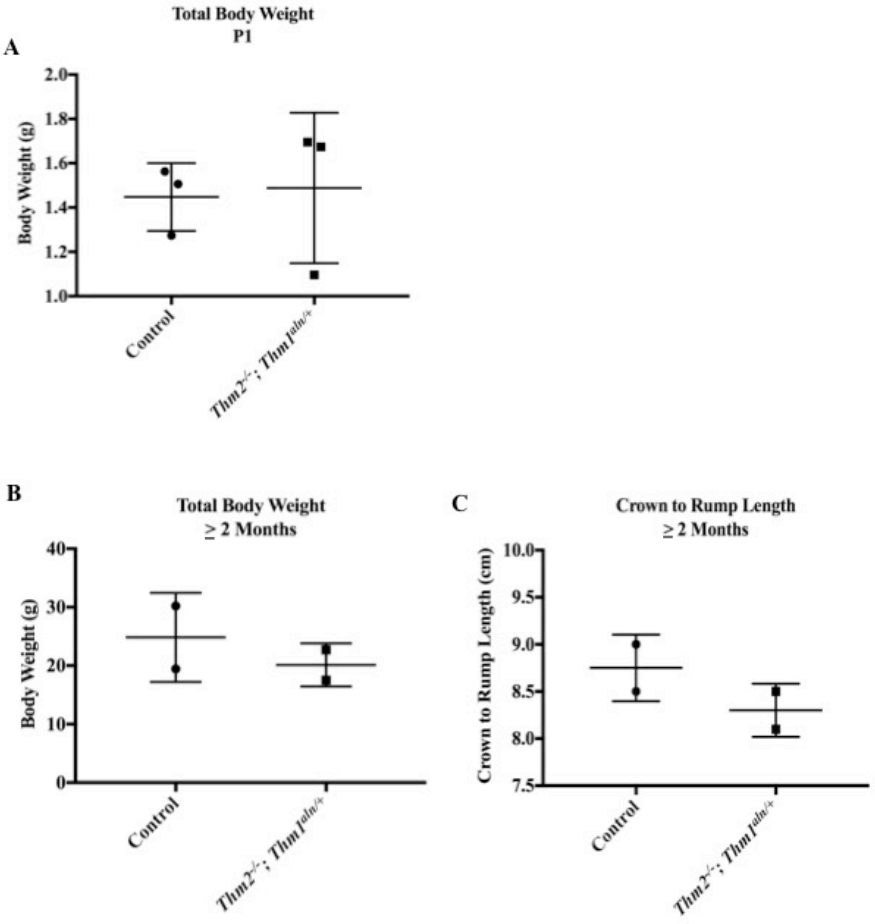

Figure 5.1. Additional skeletal timepoints. (A) Preliminary analysis of *Thm2*$^{-/-}$*; Thm1*$^{aln/+}$ mice at P1. (B-C) Preliminary analysis of control and *Thm2*$^{-/-}$*; Thm1*$^{aln/+}$ mice at ≥ 2 months of age including (B) Body weights and (C) crown to rump lengths. Error bars represent mean ± standard deviation.

5.2.3 Furthering knowledge of Thm1 and Thm2 in spermatogenesis

In chapter four, our data showed loss of *Thm2,* in addition to one allele of *Thm1,* results in a decrease in male fertility on a mixed FVB/C57BL6/J background. To understand the molecular mechanisms resulting in the decreased fertility, future experiments include analyzing the primary cilia length on cells in the testis, and determining Hh signaling status in the testis. Since multiple cell types within the testis contribute to the development of sperm, future investigations include determining the individual contributions of male germ cells, Sertoli cells, and Leydig cells in the $Thm2^{-/-}$; $Thm1^{aln/+}$ spermatogenesis phenotype. In order to do this, a *Thm1* conditional knockout mouse can be used in combination with cell-type specific Cre recombinase expression. Cell specific Cre recombinases previously established include, stimulated by retinoic acid gene 8 (Stra8-iCre) for germ cells[98], the anti-Mullerian hormone (AMH-Cre) for Sertoli cells[140], and Cytochrome P(450) 17alpha-hydroxylast/17, 20-lyase (Cyp17iCre) for Leydig cells[141]. Another experiment that can be used to determine the role of Sertoli cells in spermatogenesis utilizes the 15P-1 Sertoli cell-derived line[94]. Previously, these cells have been shown to support spermatogenesis through meiosis when co-cultured with testicular cells[94]. Co-culturing of control and *Thm2;Thm1* double knockdown 15P-1 cell lines with germ cells from wild type mice would determine if defects in spermatogenesis in $Thm2^{-/-}$; $Thm1^{aln/+}$ mice are due to abnormal Sertoli cell signaling.

Mutations in *THM1* have been found in patients with Bardet-Biedl Syndrome[43], which results in hypogonadotrophic hypogonadism[88]. This is characterized by abnormalities in the hypophyseal-testicular signaling axis[88], important for the development of the testis[90]. Circulating hormone levels of this pathway, such as gonadotrophin releasing hormone (GnRH), luteinizing hormone (LH), follicular stimulating hormone (FSH)[88], can be measured to determine the status

of this signaling pathway. Deviations of hormone levels in *Thm2*$^{-/-}$*; Thm1*$^{aln/+}$ mice compared to control mice would indicate possible molecular mechanisms by which the testis and sperm abnormalities occur. Additionally, using a *Thm1* conditional allele, with a Cre recombinase specific to the germ cells, Leydig cells, or Sertoli cells, *Thm1;Thm2* double knockout mice can be created to determine if the complete loss of *Thm1* exacerbates the infertility.

5.2.4 Potential interactions of Thm1 and Thm2 with genes encoding signaling molecules that localize to the primary cilium

Loss of *Thm1* results in renal cysts, which are also present in patients with Autosomal Dominant Polycystic Kidney Disease (ADPKD)[26]. Mutations in *PKD1* and *PKD2* are responsible for ADPKD. *PKD1* and *PKD2* encode the proteins Polycystin-1 (PC1) and Polycystin-2 (PC2) which localize to the primary cilium[142] and form a complex responsible for sensing signals[143]. Previously, loss of PC1 or PC2 together with proteins required for anterograde trafficking, IFT20 and KIF3A, decreased the cystogenic potential of kidneys compared to loss of PC1 or PC2 alone[143]. Furthermore, loss of one allele of *Kif3a* in addition to one allele of *Pkd1* rescued the skeletal defects observed in *Pkd1* heterozygote mice[121]. These results suggest that signaling proteins, such as PC1 and PC2, may interact with IFT proteins within primary cilia. Further studies investigating the interacting partners of *Thm1* and *Thm2* are necessary to determine the extent and nature of these genetic interactions.

6.2.5 Establishing roles of Thm1 and Thm2 in other tissue types

Loss of *Thm1* has resulted in peri-natal lethality, embryonic defects, obesity and cystic kidney disease. However, loss of *Thm2* and one allele of *Thm1* does not appear to have an effect

on kidney morphology or maintenance of body weight. To determine if *Thm2* functions in other tissue types throughout the body, complete double knockouts can be generated to fully characterize the role of *Thm2* during embryogenesis. Some preliminary data that I generated support a role for *Thm2* in forebrain development with *Thm1;Thm2* double knockout mice exhibiting smaller forebrains than *Thm1* knockout mice alone. Histological analysis reveals abnormal architecture in the telencephalon and diencephalon regions of the forebrain of $Thm2^{-/-}$; $Thm1^{aln/aln}$ mice (Figure 5.2). This suggests that *Thm2* likely functions during embryogenesis, which can be revealed with loss of *Thm1*. Similarly, potential roles for *Thm2* in obesity and cystic kidney disease can be elucidated using a conditional knockout of *Thm1* and determining the phenotype of the *Thm2;Thm1* double knockout mice in comparison to *Thm1* conditional knockout mice alone. Based on our data in skeletal development and spermatogenesis, and preliminary embryonic forebrain analysis, we hypothesize loss of *Thm1* and *Thm2* will exacerbate the *Thm1* knockout phenotypes, if *Thm2* functions in that tissue type.

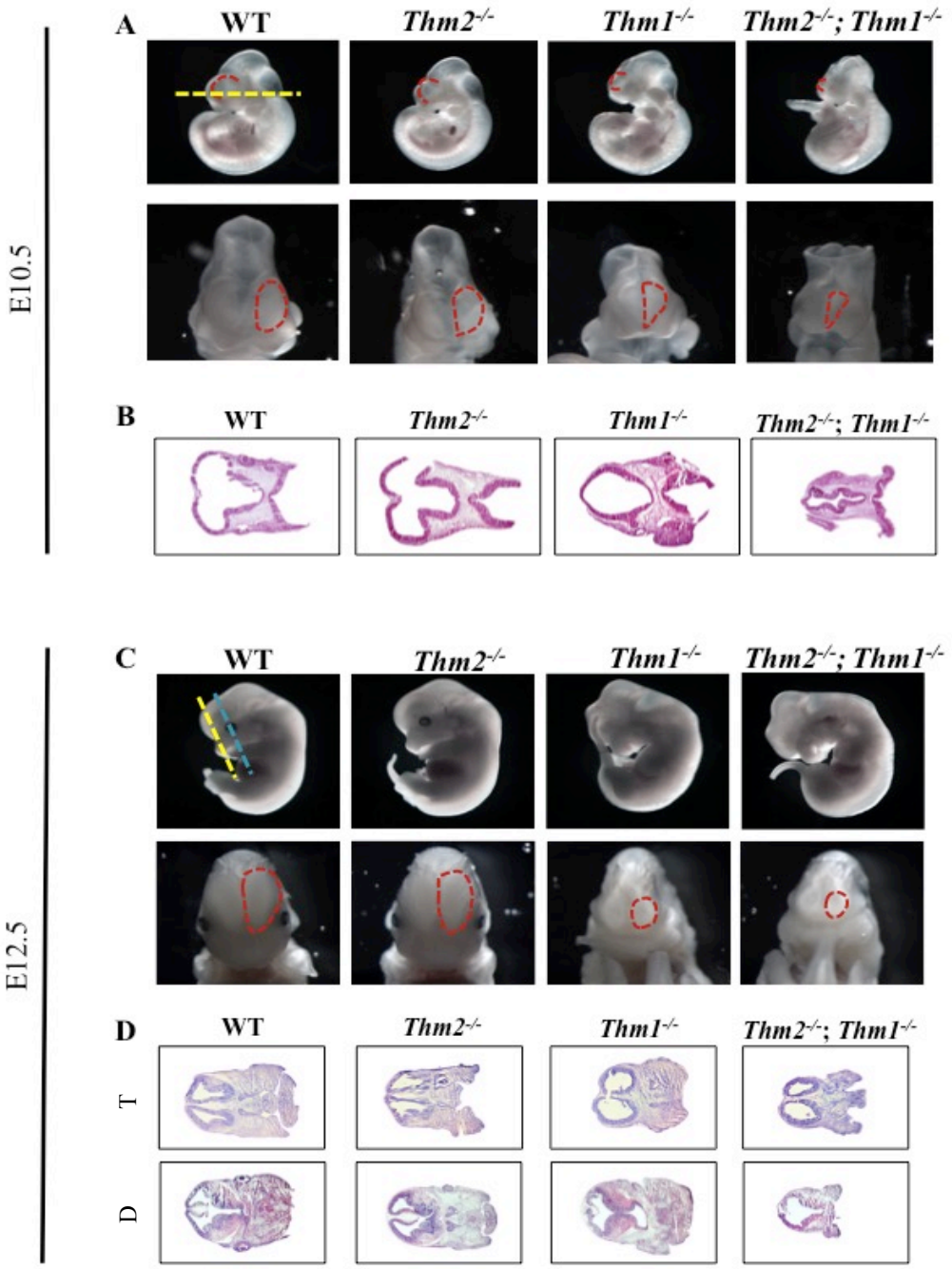

Figure 5.2. Embryonic Forebrain Abnormalities. Preliminary analysis of embryonic forebrains at (A) E10.5 and (C) E12.5 of control and *Thm2*$^{-/-}$*; Thm1*$^{aln/aln}$ mice. (B) Histological analysis of forebrain and (D) telencephalon (T) (dotted yellow line) and diencephalon (dotted blue line) regions. Telencephalons are outlined in red dotted lines.

5.2.6 Examining the function of Thm2 within the primary cilium

While we know THM2 localizes to the primary cilium, we do not understand the function of THM2 within this organelle. Since IFT139 and THM1 are IFT-A proteins[20], we hypothesize that THM2 is also an IFT Complex A protein. To determine this, experiments can be performed as described[20]. Briefly, IFT88-GFP can be expressed in a control cell line, *Thm2* knockdown cells lines, and *Thm2;Thm1* double knockdown cell lines. Live imaging can then be used to determine the trafficking of IFT88-GFP tagged particles. Since loss of THM2 alone does not result in cilia differences, I do not expect an accumulation of IFT88-GFP tagged particles at the tip of the cilia. However, I hypothesize *Thm2;Thm1* double knockdown cell lines will show further accumulation of IFT88-GFP at the ciliary tip compared to *Thm1* knockdown cell lines alone, which would indicate *Thm2* is an IFT Complex A protein, responsible for retrograde trafficking.

5.2.7 Investigating functional similarities and differences between Thm1 and Thm2 and Chlamydomonas reinhardtii IFT139

In order to determine the functional relationships between mammalian *Thm1* and *Thm2* and *Chlamydomonas reinhardtii IFT139,* the mutant strain of IFT139 can be utilized. Loss of *Chlamydomonas reinhardtii* IFT139 resulted in a bulge at the tip of the flagellum and a decrease in trafficking velocity from the tip to the base[37]. Rescue experiments can be performed by separately and jointly expressing mammalian *Thm1* and *Thm2* in the IFT139 mutant strain. Since loss of *Thm1* results in ciliary abnormalities[20], but loss of *Thm2* does not, I hypothesize that sole expression of THM1 or joint expression of THM1 and THM2 will be needed to rescue the phenotype. If THM1 is able to rescue the phenotype of IFT139 mutants alone, this suggests

THM1 shares many functional similarities with *Chlamydomonas reinhardtii* IFT139 in ciliogenesis. However, if both THM1 and THM2 are needed to rescue the phenotype of *Chlamydomonas reinhardtii* IFT139 mutants, this suggests that THM1 and THM2 work together to fulfill the functions of *Chlamydomonas reinhardtii* IFT139 in flagellar/ciliary assembly. These studies will elucidate the functional similarities between *Thm1* and IFT139 and *Thm2* and IFT139, which will enable further understanding of the roles of THM1 and THM2 in flagella/cilia assembly, furthering our knowledge of protein relationships in the ciliary proteome.

5.3 Significance of this work

Since the beginning of this century, ciliary research has increased significantly, yet a complete understanding of the ciliary proteome and its function has not yet been achieved. Our studies focused on two paralogs, *Thm1* and *Thm2*. Previously, it has been shown that *Thm1* loss results in embryonic lethality, embryonic skeletal and forebrain abnormalities, post-natal kidney cysts, obesity, and increased Hh signaling[20,26,28,31,32]. In contrast, a role for *Thm2* had not been studied. By establishing a direct role for *Thm1* in adipogenesis and insulin sensitivity, and a role for the novel ciliary gene, *Thm2,* together with *Thm1,* in skeletal and sperm development, our studies have contributed to the body of knowledge surrounding ciliary proteins (Figure 5.3). In the process, we have developed novel *in vitro* and *in vivo* models of *Thm1* and *Thm2* loss, which can be used to study the molecular underpinnings not only of adipogenesis, skeletal development, and spermatogenesis, but also of other processes regulated by cilia, including regulation of appetite, and maintenance of renal tubules and of the retina. By determining the function of ciliary genes and their interactions, novel molecular mechanisms and therapeutic targets can be identified toward treating the clinical manifestation of cilia dysfunction.

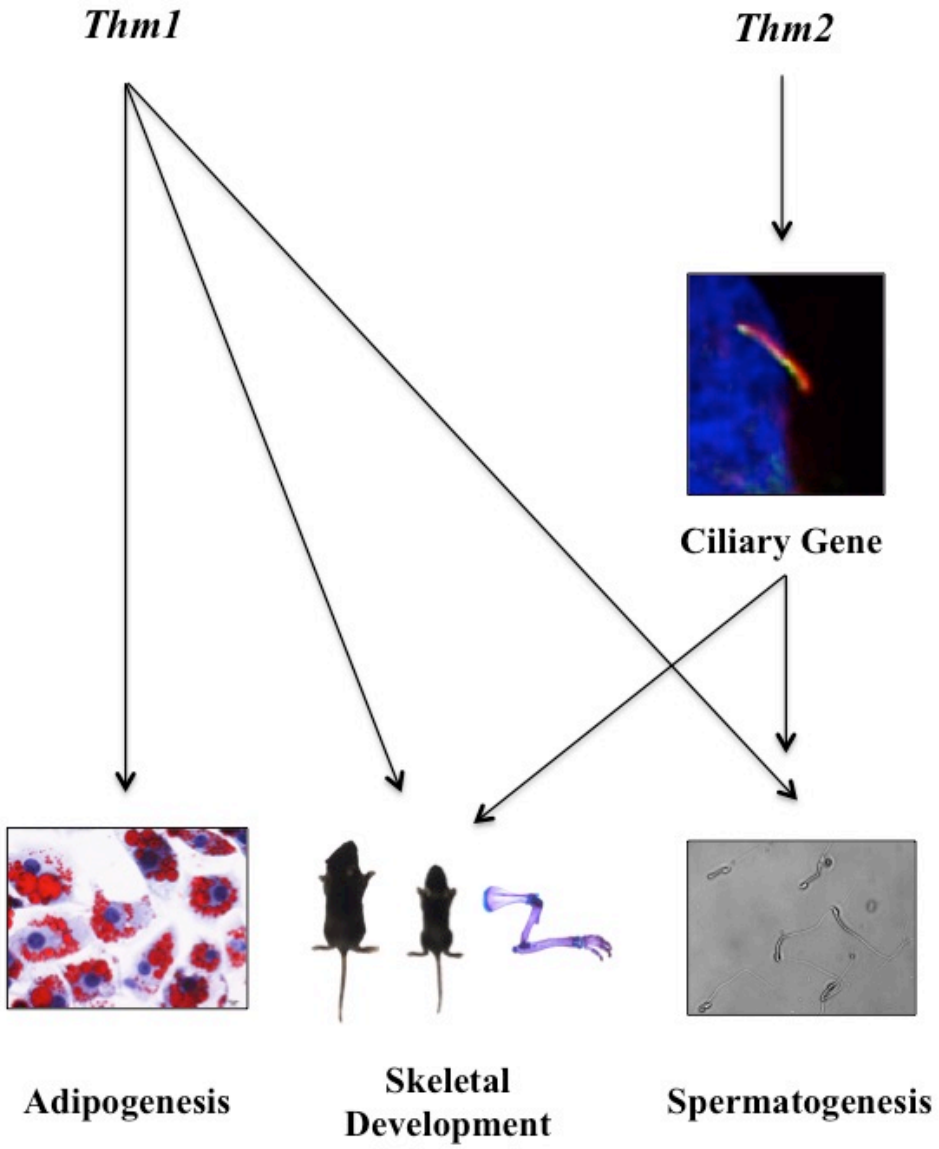

Figure 5.3. Summary of findings. Our studies of *Thm1* and *Thm2* expand our knowledge of *Thm1* in adipogenesis and insulin sensitivity and establish *Thm2* as a ciliary protein necessary for skeletal development and spermatogenesis, together with *Thm1*.

References

1. Plotnikova, O.V., Pugacheva, E.N. & Golemis, E.A. Primary cilia and the cell cycle. *Methods Cell Biol* **94**, 137-60 (2009).
2. Bisgrove, B.W. & Yost, H.J. The roles of cilia in developmental disorders and disease. *Development* **133**, 4131-43 (2006).
3. Utrilla, J.C. *et al.* Comparative study of the primary cilia in thyrocytes of adult mammals. *J Anat* **227**, 550-60 (2015).
4. Guemez-Gamboa, A., Coufal, N.G. & Gleeson, J.G. Primary cilia in the developing and mature brain. *Neuron* **82**, 511-21 (2014).
5. Malicki, J.J. & Johnson, C.A. The Cilium: Cellular Antenna and Central Processing Unit. *Trends Cell Biol* (2016).
6. Szymanska, K. & Johnson, C.A. The transition zone: an essential functional compartment of cilia. *Cilia* **1**, 10 (2012).
7. Jin, H. *et al.* The conserved Bardet-Biedl syndrome proteins assemble a coat that traffics membrane proteins to cilia. *Cell* **141**, 1208-19 (2010).
8. Lechtreck, K.F. IFT-Cargo Interactions and Protein Transport in Cilia. *Trends Biochem Sci* **40**, 765-78 (2015).
9. Hsiao, Y.C., Tuz, K. & Ferland, R.J. Trafficking in and to the primary cilium. *Cilia* **1**, 4 (2012).
10. Tran, P.V. & Lechtreck, K.F. An age of enlightenment for cilia: The FASEB summer research conference on the "Biology of Cilia and Flagella". *Dev Biol* **409**, 319-28 (2016).
11. Keeling, J., Tsiokas, L. & Maskey, D. Cellular Mechanisms of Ciliary Length Control. *Cells* **5**(2016).
12. Goetz, S.C. & Anderson, K.V. The primary cilium: a signalling centre during vertebrate development. *Nat Rev Genet* **11**, 331-44 (2010).
13. Veland, I.R., Awan, A., Pedersen, L.B., Yoder, B.K. & Christensen, S.T. Primary cilia and signaling pathways in mammalian development, health and disease. *Nephron Physiol* **111**, p39-53 (2009).
14. Goetz, S.C., Ocbina, P.J. & Anderson, K.V. The primary cilium as a Hedgehog signal transduction machine. *Methods Cell Biol* **94**, 199-222 (2009).
15. Wong, S.Y. & Reiter, J.F. The primary cilium at the crossroads of mammalian hedgehog signaling. *Curr Top Dev Biol* **85**, 225-60 (2008).
16. Niewiadomski, P. *et al.* Gli protein activity is controlled by multisite phosphorylation in vertebrate Hedgehog signaling. *Cell Rep* **6**, 168-81 (2014).
17. Huangfu, D. *et al.* Hedgehog signalling in the mouse requires intraflagellar transport proteins. *Nature* **426**, 83-7 (2003).
18. Liu, A., Wang, B. & Niswander, L.A. Mouse intraflagellar transport proteins regulate both the activator and repressor functions of Gli transcription factors. *Development* **132**, 3103-11 (2005).
19. Houde, C. *et al.* Hippi is essential for node cilia assembly and Sonic hedgehog signaling. *Dev Biol* **300**, 523-33 (2006).
20. Tran, P.V. *et al.* THM1 negatively modulates mouse sonic hedgehog signal transduction and affects retrograde intraflagellar transport in cilia. *Nat Genet* **40**, 403-10 (2008).

21. Qin, J., Lin, Y., Norman, R.X., Ko, H.W. & Eggenschwiler, J.T. Intraflagellar transport protein 122 antagonizes Sonic Hedgehog signaling and controls ciliary localization of pathway components. *Proc Natl Acad Sci U S A* **108**, 1456-61 (2011).
22. Fu, W., Wang, L., Kim, S., Li, J. & Dynlacht, B.D. Role for the IFT-A Complex in Selective Transport to the Primary Cilium. *Cell Rep* **17**, 1505-1517 (2016).
23. Liem, K.F., Jr. *et al.* The IFT-A complex regulates Shh signaling through cilia structure and membrane protein trafficking. *J Cell Biol* **197**, 789-800 (2012).
24. Gerdes, J.M. *et al.* Disruption of the basal body compromises proteasomal function and perturbs intracellular Wnt response. *Nat Genet* **39**, 1350-60 (2007).
25. Corbit, K.C. *et al.* Kif3a constrains beta-catenin-dependent Wnt signalling through dual ciliary and non-ciliary mechanisms. *Nat Cell Biol* **10**, 70-6 (2008).
26. Tran, P.V. *et al.* Downregulating hedgehog signaling reduces renal cystogenic potential of mouse models. *J Am Soc Nephrol* **25**, 2201-12 (2014).
27. Jonassen, J.A., San Agustin, J., Follit, J.A. & Pazour, G.J. Deletion of IFT20 in the mouse kidney causes misorientation of the mitotic spindle and cystic kidney disease. *J Cell Biol* **183**, 377-84 (2008).
28. Stottmann, R.W., Tran, P.V., Turbe-Doan, A. & Beier, D.R. Ttc21b is required to restrict sonic hedgehog activity in the developing mouse forebrain. *Dev Biol* **335**, 166-78 (2009).
29. Ocbina, P.J., Tuson, M. & Anderson, K.V. Primary cilia are not required for normal canonical Wnt signaling in the mouse embryo. *PLoS One* **4**, e6839 (2009).
30. Christensen, S.T. & Ott, C.M. Cell signaling. A ciliary signaling switch. *Science* **317**, 330-1 (2007).
31. Herron, B.J. *et al.* Efficient generation and mapping of recessive developmental mutations using ENU mutagenesis. *Nat Genet* **30**, 185-9 (2002).
32. Jacobs, D.T. *et al.* Dysfunction of intraflagellar transport-A causes hyperphagia-induced obesity and metabolic syndrome. *Dis Model Mech* **9**, 789-98 (2016).
33. Volta, F. & Gerdes, J.M. The role of primary cilia in obesity and diabetes. *Ann N Y Acad Sci* (2016).
34. Huynh Cong, E. *et al.* A homozygous missense mutation in the ciliary gene TTC21B causes familial FSGS. *J Am Soc Nephrol* **25**, 2435-43 (2014).
35. Iomini, C., Li, L., Esparza, J.M. & Dutcher, S.K. Retrograde intraflagellar transport mutants identify complex A proteins with multiple genetic interactions in Chlamydomonas reinhardtii. *Genetics* **183**, 885-96 (2009).
36. Behal, R.H. *et al.* Subunit interactions and organization of the Chlamydomonas reinhardtii intraflagellar transport complex A proteins. *J Biol Chem* **287**, 11689-703 (2012).
37. Piperno, G. *et al.* Distinct mutants of retrograde intraflagellar transport (IFT) share similar morphological and molecular defects. *J Cell Biol* **143**, 1591-601 (1998).
38. Tobin, J.L. & Beales, P.L. The nonmotile ciliopathies. *Genet Med* **11**, 386-402 (2009).
39. Mitchison, H.M. & Valente, E.M. Motile and non-motile cilia in human pathology: from function to phenotypes. *J Pathol* **241**, 294-309 (2017).
40. Brown, J.M. & Witman, G.B. Cilia and Diseases. *Bioscience* **64**, 1126-1137 (2014).
41. Krakow, D. & Rimoin, D.L. The skeletal dysplasias. *Genet Med* **12**, 327-41 (2010).
42. Kumar, N. & Singh, A.K. Trends of male factor infertility, an important cause of infertility: A review of literature. *J Hum Reprod Sci* **8**, 191-6 (2015).

43. Davis, E.E. *et al.* TTC21B contributes both causal and modifying alleles across the ciliopathy spectrum. *Nat Genet* **43**, 189-96 (2011).
44. O'Neill, S. & O'Driscoll, L. Metabolic syndrome: a closer look at the growing epidemic and its associated pathologies. *Obes Rev* **16**, 1-12 (2015).
45. Cornier, M.A. *et al.* The metabolic syndrome. *Endocr Rev* **29**, 777-822 (2008).
46. Lusk, J.L. Economics and obesity policy. *Int J Obes (Lond)* (2017).
47. Priya, S., Nampoothiri, S., Sen, P. & Sripriya, S. Bardet-Biedl syndrome: Genetics, molecular pathophysiology, and disease management. *Indian J Ophthalmol* **64**, 620-627 (2016).
48. Suspitsin, E.N. & Imyanitov, E.N. Bardet-Biedl Syndrome. *Mol Syndromol* **7**, 62-71 (2016).
49. Collin, G.B. *et al.* Mutations in ALMS1 cause obesity, type 2 diabetes and neurosensory degeneration in Alstrom syndrome. *Nat Genet* **31**, 74-8 (2002).
50. Khan, S.A. *et al.* Genetics of human Bardet-Biedl syndrome, an updates. *Clin Genet* **90**, 3-15 (2016).
51. Katsanis, N. *et al.* Triallelic inheritance in Bardet-Biedl syndrome, a Mendelian recessive disorder. *Science* **293**, 2256-9 (2001).
52. Marshall, J.D. *et al.* Alstrom Syndrome: Mutation Spectrum of ALMS1. *Hum Mutat* **36**, 660-8 (2015).
53. Collin, G.B. *et al.* Alms1-disrupted mice recapitulate human Alstrom syndrome. *Hum Mol Genet* **14**, 2323-33 (2005).
54. Seo, S. *et al.* Requirement of Bardet-Biedl syndrome proteins for leptin receptor signaling. *Hum Mol Genet* **18**, 1323-31 (2009).
55. Berbari, N.F. *et al.* Leptin resistance is a secondary consequence of the obesity in ciliopathy mutant mice. *Proc Natl Acad Sci U S A* **110**, 7796-801 (2013).
56. Gerdes, J.M. *et al.* Ciliary dysfunction impairs beta-cell insulin secretion and promotes development of type 2 diabetes in rodents. *Nat Commun* **5**, 5308 (2014).
57. Marion, V. *et al.* BBS-induced ciliary defect enhances adipogenesis, causing paradoxical higher-insulin sensitivity, glucose usage, and decreased inflammatory response. *Cell Metab* **16**, 363-77 (2012).
58. Marion, V. *et al.* Transient ciliogenesis involving Bardet-Biedl syndrome proteins is a fundamental characteristic of adipogenic differentiation. *Proc Natl Acad Sci U S A* **106**, 1820-5 (2009).
59. Zhu, D., Shi, S., Wang, H. & Liao, K. Growth arrest induces primary-cilium formation and sensitizes IGF-1-receptor signaling during differentiation induction of 3T3-L1 preadipocytes. *J Cell Sci* **122**, 2760-8 (2009).
60. Huang-Doran, I. & Semple, R.K. Knockdown of the Alstrom syndrome-associated gene Alms1 in 3T3-L1 preadipocytes impairs adipogenesis but has no effect on cell-autonomous insulin action. *Int J Obes (Lond)* **34**, 1554-8 (2010).
61. Yuan, X. & Yang, S. Primary Cilia and Intraflagellar Transport Proteins in Bone and Cartilage. *J Dent Res* **95**, 1341-1349 (2016).
62. McInerney-Leo, A.M. *et al.* Short-rib polydactyly and Jeune syndromes are caused by mutations in WDR60. *Am J Hum Genet* **93**, 515-23 (2013).
63. Poyner, S.E. & Bradshaw, W.T. Jeune syndrome: considerations for management of asphyxiating thoracic dystrophy. *Neonatal Netw* **32**, 342-52 (2013).

64. Drera, B., Ferrari, D., Cavalli, P. & Poggiani, C. A case of neonatal Jeune syndrome expanding the phenotype. *Clin Case Rep* **2**, 156-8 (2014).
65. de Vries, J. *et al.* Jeune syndrome: description of 13 cases and a proposal for follow-up protocol. *Eur J Pediatr* **169**, 77-88 (2010).
66. Ashe, A. *et al.* Mutations in mouse Ift144 model the craniofacial, limb and rib defects in skeletal ciliopathies. *Hum Mol Genet* **21**, 1808-23 (2012).
67. Miller, K.A. *et al.* Cauli: a mouse strain with an Ift140 mutation that results in a skeletal ciliopathy modelling Jeune syndrome. *PLoS Genet* **9**, e1003746 (2013).
68. Waters, A.M. & Beales, P.L. Ciliopathies: an expanding disease spectrum. *Pediatr Nephrol* **26**, 1039-56 (2011).
69. Yang, J., Andre, P., Ye, L. & Yang, Y.Z. The Hedgehog signalling pathway in bone formation. *Int J Oral Sci* **7**, 73-9 (2015).
70. Muthialu, N., Mussa, S., Owens, C.M., Bulstrode, N. & Elliott, M.J. One-stage sequential bilateral thoracic expansion for asphyxiating thoracic dystrophy (Jeune syndrome). *Eur J Cardiothorac Surg* **46**, 643-7 (2014).
71. Mackie, E.J., Tatarczuch, L. & Mirams, M. The skeleton: a multi-functional complex organ: the growth plate chondrocyte and endochondral ossification. *J Endocrinol* **211**, 109-21 (2011).
72. Kronenberg, H.M. Developmental regulation of the growth plate. *Nature* **423**, 332-6 (2003).
73. Hsu, S.H. *et al.* Suppressor of fused (Sufu) mediates the effect of parathyroid hormone-like hormone (Pthlh) on chondrocyte differentiation in the growth plate. *J Biol Chem* **287**, 36222-8 (2012).
74. St-Jacques, B., Hammerschmidt, M. & McMahon, A.P. Indian hedgehog signaling regulates proliferation and differentiation of chondrocytes and is essential for bone formation. *Genes Dev* **13**, 2072-86 (1999).
75. Thompson, C.L., Chapple, J.P. & Knight, M.M. Primary cilia disassembly down-regulates mechanosensitive hedgehog signalling: a feedback mechanism controlling ADAMTS-5 expression in chondrocytes. *Osteoarthritis Cartilage* **22**, 490-8 (2014).
76. Shao, Y.Y., Wang, L., Welter, J.F. & Ballock, R.T. Primary cilia modulate Ihh signal transduction in response to hydrostatic loading of growth plate chondrocytes. *Bone* **50**, 79-84 (2012).
77. Yuan, X., Serra, R.A. & Yang, S. Function and regulation of primary cilia and intraflagellar transport proteins in the skeleton. *Ann N Y Acad Sci* **1335**, 78-99 (2015).
78. Song, B., Haycraft, C.J., Seo, H.S., Yoder, B.K. & Serra, R. Development of the post-natal growth plate requires intraflagellar transport proteins. *Dev Biol* **305**, 202-16 (2007).
79. Rix, S., Calmont, A., Scambler, P.J. & Beales, P.L. An Ift80 mouse model of short rib polydactyly syndromes shows defects in hedgehog signalling without loss or malformation of cilia. *Hum Mol Genet* **20**, 1306-14 (2011).
80. Yuan, X. & Yang, S. Deletion of IFT80 Impairs Epiphyseal and Articular Cartilage Formation Due to Disruption of Chondrocyte Differentiation. *PLoS One* **10**, e0130618 (2015).
81. Haycraft, C.J. *et al.* Intraflagellar transport is essential for endochondral bone formation. *Development* **134**, 307-16 (2007).
82. Agarwal, A., Mulgund, A., Hamada, A. & Chyatte, M.R. A unique view on male infertility around the globe. *Reprod Biol Endocrinol* **13**, 37 (2015).

83. Bieniek, J.M. & Lo, K.C. Recent advances in understanding & managing male infertility. *F1000Res* **5**, 2756 (2016).
84. Ferlin, A., Arredi, B. & Foresta, C. Genetic causes of male infertility. *Reprod Toxicol* **22**, 133-41 (2006).
85. Lucas, J.S. *et al.* Diagnosis and management of primary ciliary dyskinesia. *Arch Dis Child* **99**, 850-6 (2014).
86. Knowles, M.R., Daniels, L.A., Davis, S.D., Zariwala, M.A. & Leigh, M.W. Primary ciliary dyskinesia. Recent advances in diagnostics, genetics, and characterization of clinical disease. *Am J Respir Crit Care Med* **188**, 913-22 (2013).
87. Isidori, A.M., Giannetta, E. & Lenzi, A. Male hypogonadism. *Pituitary* **11**, 171-80 (2008).
88. Nistal, M., Paniagua, R., Gonzalez-Peramato, P. & Reyes-Mugica, M. Perspectives in Pediatric Pathology, Chapter 18. Hypogonadotropic Hypogonadisms. Pediatric and Pubertal Presentations. *Pediatr Dev Pathol* **19**, 291-309 (2016).
89. Mykytyn, K. *et al.* Bardet-Biedl syndrome type 4 (BBS4)-null mice implicate Bbs4 in flagella formation but not global cilia assembly. *Proc Natl Acad Sci U S A* **101**, 8664-9 (2004).
90. Holstein, A.F., Schulze, W. & Davidoff, M. Understanding spermatogenesis is a prerequisite for treatment. *Reprod Biol Endocrinol* **1**, 107 (2003).
91. Szczepny, A., Hime, G.R. & Loveland, K.L. Expression of hedgehog signalling components in adult mouse testis. *Dev Dyn* **235**, 3063-70 (2006).
92. Bitgood, M.J., Shen, L. & McMahon, A.P. Sertoli cell signaling by Desert hedgehog regulates the male germline. *Curr Biol* **6**, 298-304 (1996).
93. Meccariello, R., Fasano, S., Pierantoni, R. & Cobellis, G. Modulators of hypothalamic-pituitary-gonadal axis for the control of spermatogenesis and sperm quality in vertebrates. *Front Endocrinol (Lausanne)* **5**, 135 (2014).
94. Rassoulzadegan, M. *et al.* Transmeiotic differentiation of male germ cells in culture. *Cell* **75**, 997-1006 (1993).
95. Nygaard, M.B., Almstrup, K., Lindbaek, L., Christensen, S.T. & Svingen, T. Cell context-specific expression of primary cilia in the human testis and ciliary coordination of Hedgehog signalling in mouse Leydig cells. *Sci Rep* **5**, 10364 (2015).
96. Yao, H.H., Whoriskey, W. & Capel, B. Desert Hedgehog/Patched 1 signaling specifies fetal Leydig cell fate in testis organogenesis. *Genes Dev* **16**, 1433-40 (2002).
97. San Agustin, J.T., Pazour, G.J. & Witman, G.B. Intraflagellar transport is essential for mammalian spermiogenesis but is absent in mature sperm. *Mol Biol Cell* **26**, 4358-72 (2015).
98. Zhang, Z. *et al.* Intraflagellar transport protein IFT20 is essential for male fertility and spermiogenesis in mice. *Mol Biol Cell* (2016).
99. Lehti, M.S., Kotaja, N. & Sironen, A. KIF3A is essential for sperm tail formation and manchette function. *Mol Cell Endocrinol* **377**, 44-55 (2013).
100. Kierszenbaum, A.L. *et al.* GMAP210 and IFT88 are present in the spermatid golgi apparatus and participate in the development of the acrosome-acroplaxome complex, head-tail coupling apparatus and tail. *Dev Dyn* **240**, 723-36 (2011).
101. Stephens, J.M. The fat controller: adipocyte development. *PLoS Biol* **10**, e1001436 (2012).

102. Christodoulides, C., Lagathu, C., Sethi, J.K. & Vidal-Puig, A. Adipogenesis and WNT signalling. *Trends Endocrinol Metab* **20**, 16-24 (2009).
103. Kim, J.Y. *et al.* Obesity-associated improvements in metabolic profile through expansion of adipose tissue. *J Clin Invest* **117**, 2621-37 (2007).
104. Hildebrandt, F., Benzing, T. & Katsanis, N. Ciliopathies. *N Engl J Med* **364**, 1533-43 (2011).
105. Guo, D.F. & Rahmouni, K. Molecular basis of the obesity associated with Bardet-Biedl syndrome. *Trends Endocrinol Metab* **22**, 286-93 (2011).
106. Girard, D. & Petrovsky, N. Alstrom syndrome: insights into the pathogenesis of metabolic disorders. *Nat Rev Endocrinol* **7**, 77-88 (2011).
107. Qin, H., Diener, D.R., Geimer, S., Cole, D.G. & Rosenbaum, J.L. Intraflagellar transport (IFT) cargo: IFT transports flagellar precursors to the tip and turnover products to the cell body. *J Cell Biol* **164**, 255-66 (2004).
108. Mukhopadhyay, S. *et al.* TULP3 bridges the IFT-A complex and membrane phosphoinositides to promote trafficking of G protein-coupled receptors into primary cilia. *Genes Dev* **24**, 2180-93 (2010).
109. Nachury, M.V. *et al.* A core complex of BBS proteins cooperates with the GTPase Rab8 to promote ciliary membrane biogenesis. *Cell* **129**, 1201-13 (2007).
110. Scheidecker, S. *et al.* Exome sequencing of Bardet-Biedl syndrome patient identifies a null mutation in the BBSome subunit BBIP1 (BBS18). *J Med Genet* **51**, 132-6 (2014).
111. Zhang, Q., Yu, D., Seo, S., Stone, E.M. & Sheffield, V.C. Intrinsic protein-protein interaction-mediated and chaperonin-assisted sequential assembly of stable bardet-biedl syndrome protein complex, the BBSome. *J Biol Chem* **287**, 20625-35 (2012).
112. Seo, S. *et al.* BBS6, BBS10, and BBS12 form a complex with CCT/TRiC family chaperonins and mediate BBSome assembly. *Proc Natl Acad Sci U S A* **107**, 1488-93 (2010).
113. Lechtreck, K.F. *et al.* The Chlamydomonas reinhardtii BBSome is an IFT cargo required for export of specific signaling proteins from flagella. *J Cell Biol* **187**, 1117-32 (2009).
114. Su, X. *et al.* Bardet-Biedl syndrome proteins 1 and 3 regulate the ciliary trafficking of polycystic kidney disease 1 protein. *Hum Mol Genet* **23**, 5441-51 (2014).
115. Xu, Q. *et al.* BBS4 and BBS5 show functional redundancy in the BBSome to regulate the degradative sorting of ciliary sensory receptors. *Sci Rep* **5**, 11855 (2015).
116. Lindstrand, A. *et al.* Recurrent CNVs and SNVs at the NPHP1 locus contribute pathogenic alleles to Bardet-Biedl syndrome. *Am J Hum Genet* **94**, 745-54 (2014).
117. Heon, E. *et al.* Mutations in C8ORF37 cause Bardet Biedl syndrome (BBS21). *Hum Mol Genet* **25**, 2283-2294 (2016).
118. Schaefer, E. *et al.* Identification of a novel mutation confirms the implication of IFT172 (BBS20) in Bardet-Biedl syndrome. *J Hum Genet* **61**, 447-50 (2016).
119. Bujakowska, K.M. *et al.* Mutations in IFT172 cause isolated retinal degeneration and Bardet-Biedl syndrome. *Hum Mol Genet* **24**, 230-42 (2015).
120. Forcioli-Conti, N., Lacas-Gervais, S., Dani, C. & Peraldi, P. The primary cilium undergoes dynamic size modifications during adipocyte differentiation of human adipose stem cells. *Biochem Biophys Res Commun* **458**, 117-22 (2015).
121. Qiu, N., Cao, L., David, V., Quarles, L.D. & Xiao, Z. Kif3a deficiency reverses the skeletal abnormalities in Pkd1 deficient mice by restoring the balance between osteogenesis and adipogenesis. *PLoS One* **5**, e15240 (2010).

122. Heydet, D. *et al.* A truncating mutation of Alms1 reduces the number of hypothalamic neuronal cilia in obese mice. *Dev Neurobiol* **73**, 1-13 (2013).
123. Starks, R.D. *et al.* Regulation of Insulin Receptor Trafficking by Bardet Biedl Syndrome Proteins. *PLoS Genet* **11**, e1005311 (2015).
124. Dalbay, M.T., Thorpe, S.D., Connelly, J.T., Chapple, J.P. & Knight, M.M. Adipogenic Differentiation of hMSCs is Mediated by Recruitment of IGF-1r Onto the Primary Cilium Associated With Cilia Elongation. *Stem Cells* **33**, 1952-61 (2015).
125. Pospisilik, J.A. *et al.* Drosophila genome-wide obesity screen reveals hedgehog as a determinant of brown versus white adipose cell fate. *Cell* **140**, 148-60 (2010).
126. Benzinou, M. *et al.* Bardet-Biedl syndrome gene variants are associated with both childhood and adult common obesity in French Caucasians. *Diabetes* **55**, 2876-82 (2006).
127. Park, H.L. *et al.* Mouse Gli1 mutants are viable but have defects in SHH signaling in combination with a Gli2 mutation. *Development* **127**, 1593-605 (2000).
128. Abbasi, A.A., Goode, D.K., Amir, S. & Grzeschik, K.H. Evolution and functional diversification of the GLI family of transcription factors in vertebrates. *Evol Bioinform Online* **5**, 5-13 (2009).
129. Quinlan, R.J., Tobin, J.L. & Beales, P.L. Modeling ciliopathies: Primary cilia in development and disease. *Curr Top Dev Biol* **84**, 249-310 (2008).
130. Zhulyn, O. & Hui, C.C. Sufu and Kif7 in limb patterning and development. *Dev Dyn* **244**, 468-78 (2015).
131. Wu, A.K., Odisho, A.Y., Washington, S.L., 3rd, Katz, P.P. & Smith, J.F. Out-of-pocket fertility patient expense: data from a multicenter prospective infertility cohort. *J Urol* **191**, 427-32 (2014).
132. Lin, F. *et al.* Kidney-specific inactivation of the KIF3A subunit of kinesin-II inhibits renal ciliogenesis and produces polycystic kidney disease. *Proc Natl Acad Sci U S A* **100**, 5286-91 (2003).
133. Shibazaki, S. *et al.* Cyst formation and activation of the extracellular regulated kinase pathway after kidney specific inactivation of Pkd1. *Hum Mol Genet* **17**, 1505-16 (2008).
134. Nishimura, D.Y. *et al.* Bbs2-null mice have neurosensory deficits, a defect in social dominance, and retinopathy associated with mislocalization of rhodopsin. *Proc Natl Acad Sci U S A* **101**, 16588-93 (2004).
135. Zhang, Q. *et al.* Bardet-Biedl syndrome 3 (Bbs3) knockout mouse model reveals common BBS-associated phenotypes and Bbs3 unique phenotypes. *Proc Natl Acad Sci U S A* **108**, 20678-83 (2011).
136. Lei, Z.M. *et al.* Targeted disruption of luteinizing hormone/human chorionic gonadotropin receptor gene. *Mol Endocrinol* **15**, 184-200 (2001).
137. Rebourcet, D. *et al.* Sertoli cells maintain Leydig cell number and peritubular myoid cell activity in the adult mouse testis. *PLoS One* **9**, e105687 (2014).
138. Beckwith, J., Cong, Y., Sundberg, J.P., Elson, C.O. & Leiter, E.H. Cdcs1, a major colitogenic locus in mice, regulates innate and adaptive immune response to enteric bacterial antigens. *Gastroenterology* **129**, 1473-84 (2005).
139. Jeffery, E. *et al.* Characterization of Cre recombinase models for the study of adipose tissue. *Adipocyte* **3**, 206-11 (2014).
140. Lecureuil, C., Fontaine, I., Crepieux, P. & Guillou, F. Sertoli and granulosa cell-specific Cre recombinase activity in transgenic mice. *Genesis* **33**, 114-8 (2002).

141. Bridges, P.J. *et al.* Generation of Cyp17iCre transgenic mice and their application to conditionally delete estrogen receptor alpha (Esr1) from the ovary and testis. *Genesis* **46**, 499-505 (2008).
142. Rangan, G.K., Tchan, M.C., Tong, A., Wong, A.T. & Nankivell, B.J. Recent advances in autosomal-dominant polycystic kidney disease. *Intern Med J* **46**, 883-92 (2016).
143. Ma, M., Tian, X., Igarashi, P., Pazour, G.J. & Somlo, S. Loss of cilia suppresses cyst growth in genetic models of autosomal dominant polycystic kidney disease. *Nat Genet* **45**, 1004-12 (2013).